U.PORTO

DOUTORAMENTO
BIOLOGIA BÁSICA E APLICADA

Resistance of ferroportin to hepcidin binding causes pulmonary iron overload and restrictive lung disease

Joana Matos das Neves

D
2017

U.PORTO

Joana Matos das Neves. Resistance of ferroportin to hepcidin binding causes pulmonary iron overload and restrictive lung disease

D.ICBAS 2017

Resistance of ferroportin to hepcidin binding causes pulmonary iron overload and restrictive lung disease

Joana Matos das Neves

SEDE ADMINISTRATIVA

INSTITUTO DE CIÊNCIAS BIOMÉDICAS ABEL SALAZAR
FACULDADE DE CIÊNCIAS
FACULDADE DE MEDICINA

Joana Matos das Neves

Resistance of ferroportin to hepcidin binding causes pulmonary iron overload and restrictive lung disease

Tese de Candidatura ao grau de Doutor em Biologia Básica e Aplicada submetida ao Instituto de Ciências Biomédicas Abel Salazar da Universidade do Porto.

Orientador – Doutora Martina U. Muckenthaler
Categoria – Professor
Afiliação – University of Heidelberg, Germany

Co-orientador – Doutora Maria da Graça Porto
Categoria – Professora Catedrática
Afiliação – Instituto de Ciências Biomédicas Abel Salazar, Universidade do Porto, Portugal

This work was supported by Fundação para a Ciência e a Tecnologia by means of a PhD fellowship (SFRH / BD / 51702 / 2011) awarded to Joana Matos das Neves through the Graduate Program in Areas of Basic and Applied Biology (GABBA), Universidade do Porto, Portugal. The work was also supported with funding from Deutsches Zentrum für Lungenforschung (DZL).

Aos meus pais,

Acknowledgements

First of all, I want to thank my supervisor Prof. Dr. Martina Muckenthaler. I am very grateful for the opportunity to join your laboratory, where I had a wonderful environment to develop my PhD project. Thank you for all our scientific discussions and for believing in me. Thank you for your guidance and for simultaneously giving me the freedom I needed to follow my own ideas, which allowed me to grow as a scientist.

I thank Prof. Dr. Graça Porto for accepting me as her student. Thank you for your interest in my work, for your support and for being always available to help me.

I would like to thank the current and former members of the Muckenthaler group. Thank you for the friendly work environment and for the lovely time we spent together inside and outside the lab. A very special acknowledgement to Dr. Sandro Altamura. Thank you for all the guidance and mentoring during this period of my life. Thank you for everything you taught me and for all the support - my PhD will always be connected to you. A big “thank you” goes to my friend and colleague Ana Rita da Silva. We have gone through our PhDs in parallel, always being there for each other, both inside and outside the lab. Thank you for the unforgettable moments we spent together in Heidelberg. I also thank Milene Costa da Silva, my GABBA and lab colleague, with whom I shared a desk every single day of my PhD.

I would like to express my gratitude to my collaborators, Prof. Dr. Christian Mühlfeld, Dr. Christina Brandenberger, Dr. Simone Kraut and Prof. Dr. Norbert Weissmann for their contribution to this work.

I am extremely grateful to the GABBA program for this amazing opportunity. I thank all the professors and the current and former directors: Prof. Dr. António Amorim and Prof. Dr. Alexandre do Carmo. A special “thank you” to my colleagues and friends of the 15th edition of the GABBA program, with whom I had the privilege to share the beginning of this journey.

I would like to thank all my friends outside the lab. A special “obrigada” to my Portuguese friends here in Heidelberg that made this new city feel like home. A big thanks to my Portuguese friends back in Portugal – thank you for not letting the distance affect our friendship. It warms my heart to know that we can still count on each other after all these years.

I want to thank my family, especially my parents who were **always** there for me. Despite living in different countries, you made sure I would never feel alone. Thank you for all the hours we spent on skype and for all the packages/letters/postcards we exchanged throughout the years – those small gifts were crucial to fight my home sickness. I know that I can always count on you and I know I wouldn’t have made it without your love and support. Obrigada!

Finally, I thank Roman Teimer. Thank you for all the support and advice. Thank you for cheering me up when things went wrong and for celebrating with me when things worked out. Thank you for your patience, for your silliness, and for your love. Thank you for accepting me exactly as I am and for making me believe in myself. Obrigada!

Abstract

Emerging evidence suggests that pulmonary iron accumulation is implicated in a spectrum of chronic and acute lung diseases, such as cystic fibrosis and pulmonary alveolar proteinosis. In patients with chronic obstructive pulmonary disease, iron deposits in alveolar macrophages and the percentage of iron loaded macrophages is associated with increased disease severity. On the other hand thalassemia major, a disease characterized by transfusional iron overload, has been associated with impaired lung function. However, the mechanism(s) involved in pulmonary iron deposition and its role in the *in vivo* pathogenesis of lung diseases remained unknown.

The supply of iron to the lung depends on its systemic plasma availability, which is controlled by the hepcidin/ferroportin regulatory axis. The work presented here aims to understand whether a disruption in the hepcidin/ferroportin regulatory system and the subsequent increase in systemic iron levels affect lung iron homeostasis and function. To achieve this goal, we took advantage of a murine disease model of hereditary hemochromatosis type 4 ($Slc40a1^{C326S}$), hallmarked by a C326S amino acid substitution in ferroportin that impairs hepcidin binding.

We show that resistance of ferroportin to hepcidin binding causes pulmonary iron accumulation in defined lung cell types. The increase in pulmonary iron levels correlates with an increase in lipid peroxidation, suggesting that iron-mediated oxidative stress could contribute to the pathogenesis of lung diseases. Measurements of lung function in aged $Slc40a1^{C326S/C326S}$ mice revealed classical signs of restrictive lung disease, such as a decrease in total lung capacity and lung compliance. Furthermore, $Slc40a1^{C326S/C326S}$ mice show a severe decrease in blood oxygen saturation when compared to wild-type animals. Taken together, these findings implicate iron overload in lung pathology, which is so far not considered a classical iron-related disorder.

Resumo

A acumulação de ferro nos pulmões está associada a um largo espectro de doenças respiratórias, tais como a fibrose quística e a proteinose alveolar pulmonar. Em pacientes com doença pulmonar crónica obstrutiva, a deposição de ferro foi detectada em macrófagos alveolares e a percentagem de macrófagos com acumulação de ferro foi associada ao grau de severidade da doença. Por outro lado, pacientes com formas severas de talassemia (uma doença caracterizada por elevados níveis sistémicos de ferro) apresentam frequentemente alterações da função pulmonar. No entanto, o(s) mecanismo(s) envolvido(s) na acumulação de ferro nos pulmões e o papel do ferro na patologia de doenças respiratórias ainda não é conhecido.

O fornecimento de ferro às células do pulmão depende da sua disponibilidade sistémica na corrente sanguínea, a qual é controlada pela sistema regulatório hepcidina/ferroportina. O trabalho apresentado nesta tese teve como objectivo perceber como é que uma disrupção no sistema hepcidina/ferroportina e o consequente aumento nos níveis sistémicos de ferro afectam a homeostase de ferro no pulmão e a função pulmonar. Para atingir este objectivo, analisámos um ratinho modelo da doença hemocromatose hereditária tipo 4 ($Slc40a1^{C326S}$), que é caracterizado pela substituição de uma cisteína por uma serina na posição 326 da ferroportina. Esta mutação na ferroportina impede a ligação da hepcidina.

Nesta tese mostramos que uma disrupção no sistema regulatório hepcidina/ferroportina causa acumulação de ferro no pulmão, a qual é restricta a tipos celulares específicos. O aumento dos níveis de ferro neste orgão está associado a um aumento na peroxidação de lípidos, o que sugere que o stress oxidativo mediado por ferro pode contribuir para a patogénese de doenças pulmonares. Testes de função pulmonar em ratinhos $Slc40a1^{C326S/C326S}$ com 9 meses revelaram sinais característicos de doença pulmonar restritiva, tal como uma diminuição da capacidade pulmonar total e da *compliance* pulmonar. Além disso, ratinhos $Slc40a1^{C326S/C326S}$ apresentam uma redução severa na saturação de oxigénio no sangue. Em conclusão, estes resultados revelam uma contribuição do aumento dos níveis de ferro na etiopatogenia de doenças pulmonares, as quais até agora não têm sido consideradas doenças tipicamente associadas a alterações na homeostase do ferro.

List of abbreviations

AM – Alveolar macrophage

AT1 – Alveolar epithelial type 1 cell

AT2 – Alveolar epithelial type 2 cell

Bach1 – Btb And Cnc Homology 1

BAL – Bronchoalveolar lavage

BMDM – Bone marrow-derived macrophages

BMP – Bone morphogenic proteins

Ccl – C-C motif chemokine ligand

CCSP – Club cell secretory protein

CD – Cluster of differentiation

cDNA – Complementary DNA

CO_2 – Carbon dioxide

COPD – Chronic obstructive pulmonary disease

Cxcl – C-X-C motif chemokine ligand

DAB – 3,3-diaminobenzidinetetrahydrochloride

DcytB – Duodenal cytochrome B

DMT1 – Divalent metal transporter 1

DNA – Deoxyribonucleic acid

dNTP – Deoxynucleotide triphosphate

ECM – Extracellular matrix

EDTA – Ethylenediaminetetraacetic acid

ELISA – Enzyme-linked immunosorbent assay

EPO – Erythropoietin

ERFE – Erythropherrone

FeNTA – Iron-nitrilotriacetate

FPN – Ferroportin

FtH – Ferritin heavy chain

FtL – Ferritin light chain

g – Gram

GDF-15 – Growth differentiation factor 15

GM-CSF – Granulocyte-macrophage colony-stimulating factor

GM-R – Granulocyte-macrophage colony-stimulating factor receptor

$Hamp^{-/-}$ – Hepcidin knock out

HBSS – Hank's balanced salt solution

HFE – Human hemochromatosis protein

HH – Hereditary hemochromatosis

HIF – Hypoxia inducible factor

HJV – Hemojuvelin

HO – Heme oxygenase

HRG-1 – Mammalian homologue heme responsive gene 1

IL – Interleukin

IRE – Iron-responsive element

IRIDA – Iron-refractory iron deficiency anemia

IRP – Iron regulatory protein

JAK – Janus kinase

LIP – Labile Iron Pool

LPS – Lipopolysaccharide

MAPK – Mitogen-activated protein kinases

M-CSF – Macrophage colony-stimulating factor

mRNA – Messenger RNA

Nrf2 – Nuclear Factor Erythroid 2-like

NTBI – Non-transferrin-bound iron

O_2 – Oxygen

PBS – Phosphate-buffered saline

PCR – Polymerase chain reaction

PHD – Prolyl hydroxylases

PI3K – Phosphatidylinositol 3-Kinase

PNEC – Pulmonary neuroendocrine cell

Ppia – Peptidylprolyl isomerase A

ppm – parts per million

proSP-C – Prosurfactant protein C

pVHL – von Hippel-Lindau tumor suppressor

qRT-PCR – Quantitative reverse transcription-polymerase chain reaction

RNA – Ribonucleic acid

ROS – Reactive oxygen species

RPL19 – Ribosomal protein L19

SEM – Standard error of the mean

SiglecF – Sialic acid-binding immunoglobulin-like lectin F

SMA – Smooth muscle actin

SMAD – Mothers against decapentaplegic homolog

sMAF – Small Maf proteins

SMC – Smooth muscle cells

SP – Surfactant protein

STAT – Signal transduction and activator of transcription

STEAP3 – Six Transmembrane Epithelial Antigen of the Prostate 3

TBARS – Thiobarbituric acid reactive substances

$Tf\text{-}Fe_2$ – Diferic transferrin

TfR1 – Transferrin receptor 1

TfR2 – Transferrin receptor 2

TGF-β – Transforming growth factor β

TLR – Toll-like receptor

TMPRSS6 – Transmembrane protease, serine 6

TNF – Tumor necrosis factor

TWSG1 – Twisted gastrulation homolog 1

UTR – Untranslated regions

WT – wild-type

ZIP – Zrt/IRT-like protein

Table of Contents

Chapter I

General Introduction

1. Mammalian Iron Homeostasis

1.1 Biological role of iron

Iron is one of the most abundant elements in the crust of the Earth and it plays a key role in the biology of almost all living organisms. It has the remarkable ability to exist in multiple oxidation states, ranging from -2 to +6; the divalent ferrous (Fe^{2+}) and the trivalent ferric (Fe^{3+}) being the most common species [1]. By readily accepting and donating electrons, iron acts as an important co-factor for enzymes and proteins involved in fundamental metabolic processes, such as DNA synthesis (e.g. ribonucleotide reductase), oxygen transport (e.g. hemoglobin), and mitochondrial respiration (e.g. cytochromes) [1]. However, this ability to fluctuate between different oxidation states also explains why free iron is very reactive and potentially toxic. Iron catalyzes the formation of reactive oxygen species (ROS) through “Fenton-type” reactions [2]. These highly reactive radicals can damage lipids, proteins, and nucleic acids, leading to cellular damage and tissue injury [3].

The binding of iron to proteins and prostethic groups counteracts its chemical reactivity and potentially deleterious effects. Nevertheless, iron levels must be strictly controlled in order to meet the cellular and systemic metabolic needs while preventing detrimental iron overload.

1.2 Iron distribution

The average adult human body contains 3-4 grams (g) of iron. Even though all cells contain small amounts of iron in iron-containing proteins, most of the body’s iron is present in the hemoglobin of erythrocytes (2-3 g). Iron is delivered to tissues and cells through the bloodstream, which contains 2-4 mg of iron bound to the iron-transport protein transferrin (reviewed in [4]).

1.3 Iron absorption, utilization, storage, and recycling

Iron absorption

Dietary iron is mainly found in the form of ferric iron (Fe^{3+}) or associated with heme groups and is absorbed by duodenal enterocytes. Since there is no regulated pathway to excrete iron from the organism, the control of intestinal iron absorption is crucial to maintain adequate body iron levels (reviewed in [5]). Inorganic Fe^{3+} needs to be reduced to Fe^{2+} by the membrane-associated ferrireductase duodenal cytochrome B (DcytB) before being transported to the cytosol via the divalent metal transporter 1 (DMT1) expressed in the brush-border membrane of enterocytes

(Figure 1.1) [6, 7]. Heme iron is absorbed by an independent mechanism that is not clearly known yet. Subsequently, iron is released intracellularly from heme by heme oxygenase (HO) 1 [8]. Cytosolic iron can be used for metabolic processes or exported into the bloodstream via the only known cellular iron exporter ferroportin expressed in the basolateral membrane of enterocytes (Figure 1.1) [9, 10]. The export of iron via ferroportin is coupled with the reoxidation of Fe^{2+} to Fe^{3+}, a process that is catalyzed by hephaestin, a trans-membrane ferroxidase [11]. Ferric iron is then loaded onto the glycoprotein transferrin, which has two high-affinity sites for Fe^{3+} [12]. By maintaining iron in a chemically inert form, iron binding to transferrin prevents the generation of reactive radicals and allows its delivery to every cell of the organism.

Cellular iron uptake, utilization, and storage

Cells take up transferrin bound iron via transferrin receptor 1 (TfR1). The binding of diferic transferrin (Tf-Fe_2) to TfR1 triggers the endocytosis of the Tf-Fe_2/TfR1 complex via clathrin-coated vesicles [13]. The acidification of endosomes leads to conformational changes in TfR1 and transferrin and the subsequent release of iron [14]. Upon reduction of ferric iron to ferrous iron by metalloreductase Six Transmembrane Epithelial Antigen of the Prostate 3 (STEAP3), iron is transported to the cytosol via DMT1 [15, 16]. Transferrin and TfR1 are recycled to the cell surface and can be reutilized [13].

Iron trafficking within the cells is still poorly understood but it is known that most of the intracellular iron is directed towards the mitochondria where it is used for Fe-S cluster biogenesis and heme synthesis [17-19] (reviewed in [20]). A small fraction of the total cellular iron (<5%) is maintained in a pool of redox-active iron complexes, the Labile Iron Pool (LIP), for immediate metabolic needs [21]. Excess iron that is not used for metabolic processes is stored in ferritin, an ubiquitous multimeric protein composed by 24 subunits of heavy and light chains that can accommodate up to 4500 iron atoms [22]. Ferritin allows cells to store iron in a redox inactive form, preventing iron-mediated oxidative stress. Even though most cell types can store small amounts of iron intracellularly in ferritin, hepatocytes in the liver and splenic macrophages are the major reservoirs for iron in the organism (reviewed in [4]). When needed, these cells can rapidly export iron to the bloodstream via the iron exporter ferroportin (a process coupled with the reoxidation of Fe^{2+} to Fe^{3+} by the multicopper oxidase ceruloplasmin) (Figure 1.1) [23].

Since TfR1 is ubiquitously expressed, it is believed that transferrin mediated iron uptake occurs in most cell types. Nevertheless, this cycle is particularly important to deliver a very large amount of iron to erythroid progenitors in the bone marrow for hemoglobin synthesis.

Iron recycling

The daily demand of iron for hemoglobin synthesis is 20-25 mg. However, under normal circumstances only 1-2 mg of iron per day is absorbed by enterocytes from dietary sources, which compensates for small iron losses mainly due to desquamation of epithelial surfaces or minor bleeding (reviewed in [4]). Most of the iron needed for erythropoiesis is provided by a very efficient recycling system (reviewed in [24]) (Figure 1.1). Aged or damaged erythrocytes are phagocytosed by reticuloendothelial macrophages, degraded within the phagolysosome and hemoglobin-derived heme is exported across the phagolysosomal membrane to the cytosol by the transmembrane heme permease HRG-1 (mammalian homologue heme responsive gene 1) [25]. In the cytosol, heme is catabolized by HO1 and iron is released [26, 27]. The export of cytosolic iron from macrophages back to the bloodstream occurs via ferroportin and is coupled to the activity of the multicopper oxidase ceruloplasmin, a homologue of hephaestin (Figure 1.1) [23]. Ferric iron binds to transferrin and can be reutilized for a new cycle of erythropoiesis.

It is worth to mention that the contributions of dietary iron absorption and recycling to the daily turnover differ between different species, depending on the daily iron losses and the lifetime of erythrocytes (reviewed in [28]).

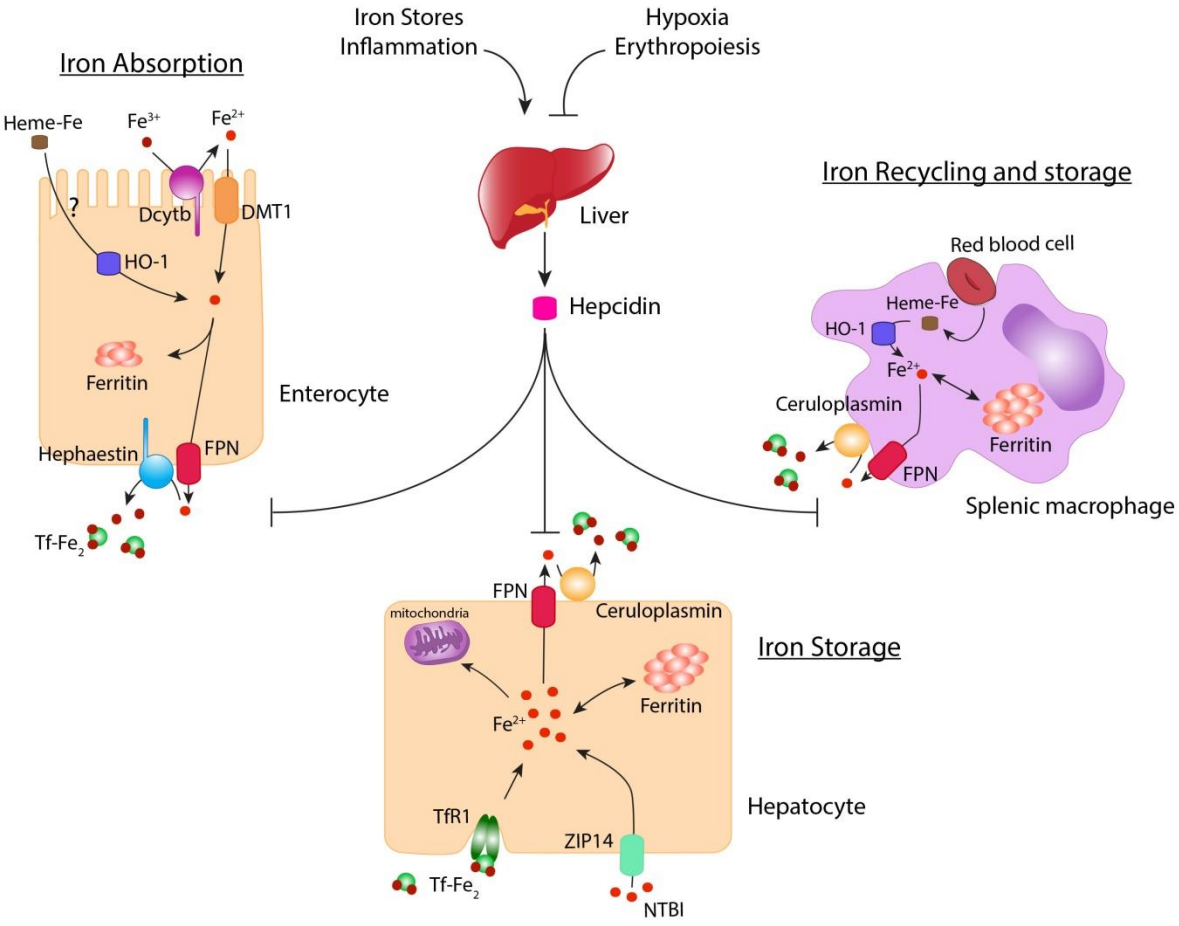

Figure 1.1 – Systemic iron homeostasis. Left panel: Dietary iron absorption occurs at the brush-border membrane of duodenal enterocytes. Ferric iron is reduced to ferrous iron by Duodenal cytochrome B (DcytB) and is transported across the membrane via Divalent metal transporter 1 (DMT1). Heme iron is taken up by an unknown mechanism and iron is released from heme intracellularly by heme oxygenase 1 (HO1). The export of iron across the basolateral membrane of enterocytes occurs via ferroportin (FPN) and is coupled with the reoxidation of ferrous to ferric iron – a process that is catalyzed by hephaestin. In the blood, ferric iron circulates bound to transferrin ($Tf\text{-}Fe_2$). Center lower panel: Transferrin-bound iron can be taken up via Transferrin receptor 1 (TfR1) by every cell type in the organism, including hepatocytes which store high amounts of iron in ferritin. Hepatocytes can also take up high amounts of non-transferrin-bound iron (NTBI) via ZIP14. When required, iron can be exported from hepatocytes via FPN back to circulation (a process coupled with the reoxidation of Fe^{2+} to Fe^{3+} by ceruloplasmin). Right panel: Senescent erythrocytes are engulfed by reticuloendothelial macrophages. Iron is released from heme by HO1 and it can be either stored in ferritin or released to circulation, depending on the body iron needs. Iron export from macrophages via FPN is also coupled with the activity of ceruloplasmin. Center upper panel: Hepcidin produced by hepatocytes has the ability to decrease cellular iron export by binding to FPN and promoting its internalization and degradation. Hepcidin expression is controlled by several factors: body iron stores, inflammation, erythropoietic signals and hypoxia. Image created based on image from Darshan et al., 2010 [29].

1.4 Cellular Iron Homeostasis

The coordination between cellular iron uptake, utilization, storage, and export is crucial to maintain cellular iron homeostasis: cells must have sufficient iron to meet their metabolic needs while avoiding toxic iron overload. The post-transcriptional regulatory system IRE/IRP plays a critical role in this process by controlling the expression of iron-related proteins according to intracellular levels of iron (Figure 1.2) (reviewed in [30] and [31]). It relies on the cytosolic iron regulatory protein 1 and 2 (IRP1 and IRP2) and their interaction with conserved hairpin structures known as iron-responsive elements (IREs) present in the 5' or 3' untranslated regions (UTRs) of mRNAs of several iron-regulated genes. Transcripts containing IREs in the 3' UTR are stabilized after the binding of IRPs whereas the translation of transcripts containing an IRE in the 5' UTR is blocked upon IRP binding.

In iron-depleted cells, IRPs bind to the IRE in the 5' UTR of ferritin light chain (*FtL*), ferritin heavy chain (*FtH*), and *Fpn* mRNA, inhibiting their translation [9, 10, 32, 33]. IRPs bind also to IREs in the 3' UTR of *TfR1* mRNA and to a single IRE in the 3' UTR of *Dmt1* mRNA, blocking their degradation [34-36]. This leads to increased iron uptake and decreased iron storage and export, resulting in higher intracellular iron availability. In iron-replete cells, IRP1 is converted from its RNA-binding form to the cytoplasmatic aconitase form containing a [4Fe–4S] cluster and IRP2 is targeted to proteasomal degradation [37-39]. Consequently, IRPs cannot bind to IREs. This leads to increased iron storage and export by increasing ferritin and *Fpn* mRNA translation and decreased iron uptake due to increased degradation of *TfR1* and *Dmt1* mRNAs.

The vital role of the IRE/IRP regulatory system is highlighted by the observation that genetic ablation of IRP1 and IRP2 in the mouse results in early embryonic lethality [40]. Interestingly, animals lacking only one of the IRPs are viable but present different phenotypes [41, 42], indicating that the two IRPs have only partially redundant functions (reviewed in [43]).

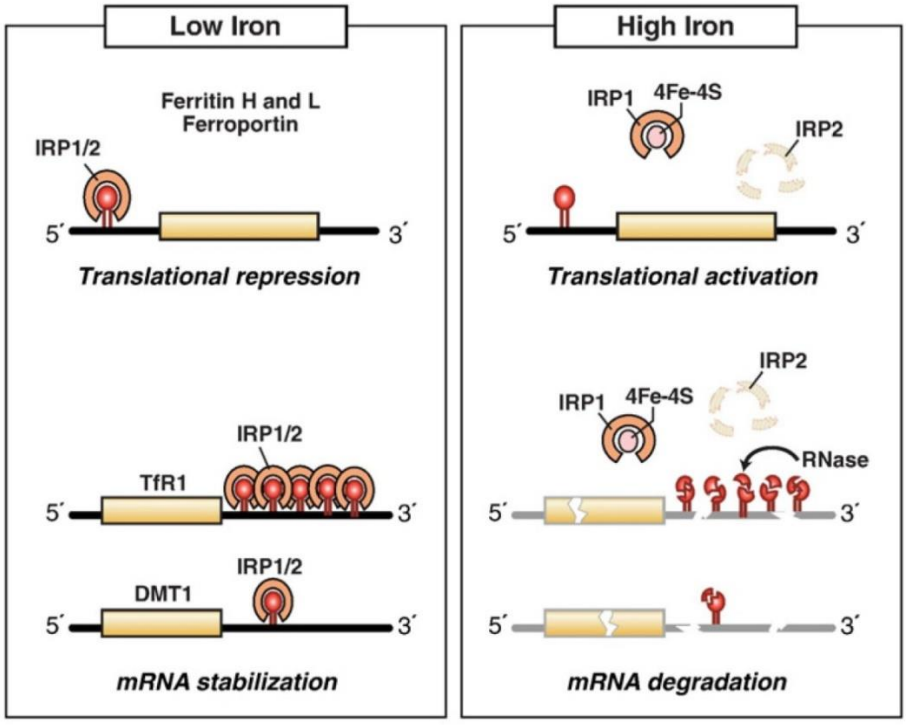

Figure 1.2 – Cellular iron homeostasis: IRE/IRP system. IRPs bind to IREs located in either the 5' UTR or 3' UTR of mRNAs and regulate their translation and stability, respectively. In iron-depleted cells, IRPs bind to an IRE localized in the 5' UTR of mRNAs and repress their translation whereas the binding to IREs in the 3' UTR stabilizes the mRNAs. In high iron conditions, IRPs do not bind to IREs leading to the translation of mRNAs containing an IRE in the 5' UTR and to the degradation of mRNAs containing IREs in the 3'UTR. This mechanism counterbalances both cellular iron deficiency and iron overload. Adapted from Anderson et al., 2012 [30].

1.5 Systemic Iron Homeostasis

Adequate plasma iron levels are crucial for the correct iron supply and homeostasis of different tissues and cells. In humans, approximately 30% of plasma transferrin is saturated with iron. A transferrin saturation below 16% reflects an iron deficient condition whereas a saturation above 45% indicates iron overload. If the transferrin saturation exceeds 60%, non-transferrin-bound iron (NTBI) accumulates in circulation and can easily lead to cell and tissue damage [44]. NTBI can be rapidly taken up by the liver (and to a lesser extent by other organs, as the heart), probably via Zrt/IRT-like protein (ZIP) 14 (Figure 1.1) [45]. Another member of the ZIP proteins, ZIP8, has also been reported to transport NTBI and is mainly expressed in the lung and placenta [46].

The coordination of iron fluxes from tissues to circulation is essential to maintain transferrin saturation at physiological levels and is mainly controlled by the hepcidin/ferroportin regulatory system (Figure 1.1) (reviewed in [5]).

1.5.1 Hepcidin/Ferroportin Axis

Hepcidin is a 25 amino acid peptide hormone synthesized and secreted to the plasma by hepatocytes [47]. It emerged as a key molecule in systemic iron homeostasis due to its ability to regulate cellular iron efflux: hepcidin acts by post-translationally controlling the plasma membrane concentration of ferroportin (reviewed in [5] and [28]). Ferroportin (FPN), a protein containing 12-transmembrane domains, is the only known cellular iron exporter [9, 10, 48]. It is highly conserved and has been identified in several vertebrates as well as in species as distant as *Caenorhabditis elegans* (reviewed in [28]). Ferroportin expression is abundant in cells that handle major iron fluxes such as duodenal enterocytes, kupffer cells and splenic macrophages, and to a lesser extent in hepatocytes.
Hepcidin binding to ferroportin induces its ubiquitination, internalization, and subsequent lysosomal degradation [49, 50]. This leads to a decrease in iron export from ferroportin-expressing cells and therefore lowers systemic iron levels.

1.5.2 Regulation of hepcidin expression

The expression of hepcidin in hepatocytes rapidly responds to different stimuli, such as systemic iron levels, inflammation, erythropoietic activity, and hypoxia (Figure 1.1). A dysregulation of hepcidin production leads to iron-related disorders.

The production of hepcidin by other cell types has been described in the literature but at a much lower level [51-54] and its role in systemic iron homeostasis is not clear yet.

<u>Hepcidin regulation by systemic iron availability</u>

Hepcidin plays a central role in the regulation of systemic iron levels. Conversely, its expression is regulated by plasma iron levels and iron stores. Mice maintained on a high iron diet increase hepatic hepcidin expression in order to decrease the levels of circulating iron whereas a low iron diet induces the opposite response [55].
The bone morphogenic protein (BMP)/mothers against decapentaplegic homologue (SMAD) pathway has been described as the key signaling system for the regulation of hepcidin. Through a yet to be identified mechanism, BMP6 levels are increased in conditions of iron overload [56].

BMP6 binds and activates the BMP serine/threonine kinase receptors expressed at the cell membrane of hepatocytes, which leads to the phosphorylation of the SMAD1/5/8 complex [56-58]. This complex recruits SMAD4 and translocates to the nucleus, inducing hepcidin transcription (reviewed in [59]). Consistently, BMP6 knock out mice show hepcidin deficiency and iron overload [60, 61]. A recent study showed that BMP6 is mainly produced by liver endothelial cells and that loss of BMP6 specifically in these cells recapitulates the hemochromatosis phenotype observed in the global BMP6 knock out mice [62]. BMP2 and BMP4 were shown to also up-regulate hepcidin expression *in vitro* [63]. The *in vivo* role of BMP2 in controlling hepcidin expression has recently been confirmed by Koch and colleagues [64].

The activation of the BMP signaling is enhanced by the BMP co-receptor hemojuvelin (HJV) [65]. Under iron deficient conditions, the transmembrane protease serine 6 (TMPRSS6, also known as matriptase 2) and the protease furin cleave HJV, abrogating its function as a BMP co-receptor and negatively regulating hepcidin expression [66, 67]. Attenuation of hepcidin activation can also be achieved through a negative feedback regulatory system mediate by SMAD proteins, such as SMAD7 [68].

The sensing of extracellular iron occurs by the interaction of transferrin-bound iron (holotransferrin) with a complex composed of TfR1, TfR2 (homologous to TfR1 but with lower affinity to holotransferrin), and human hemochromatosis protein (HFE), which is also expressed at the cell surface of hepatocytes and interacts with both TfR1 and TfR2 (reviewed in [5]). The interaction of HFE with TfR1 and TfR2 depends on the holotransferrin concentration. Under conditions of high iron levels, holotransferrin binds to TfR1 and HFE is released, since the binding site of holotransferrin overlaps the HFE binding site [69, 70]. As a consequence, HFE binds to TfR2 and this complex enhances hepcidin expression [69, 70]. The signaling pathway downstream of the HFE/TfR2 complex is still not completely understood but it might involve a cross-talk between BMP and mitogen-activated protein kinases (MAPK) signaling pathways [71].

Hepcidin regulation by inflammation

Iron is an essential element for pathogens. As a host defense strategy, hepcidin expression increases during inflammation in an attempt to decrease plasma iron availability for extracellular pathogens (reviewed in [72]). The inflammatory cytokine interleukin (IL) 6 seems to be a key factor that activates hepcidin expression in hepatocytes by triggering the activation of a signaling pathway mediated by Janus kinase (JAK) and signal transduction and activator of transcription (STAT) 3 [73-75]. Upon the binding of IL6 to its receptor, JAK kinase is activated and phosphorylates STAT3, which is then translocated to the nucleus and directly activates hepcidin expression by binding to its promoter. Interestingly, the integrity of the BMP signaling pathway is

necessary to increase hepcidin expression during inflammation since liver specific SMAD4 knock out mice fail to increase hepcidin levels upon IL-6 injection [76]. Moreover, a mutation in the BMP-responsive element in the hepcidin promoter impairs hepcidin expression in response to IL-6 [77].

Hepcidin regulation by erythropoietic signals

Erythropoiesis depends on iron availability since iron is needed for heme and hemoglobin synthesis: 20-25 mg of iron are recycled every day for the synthesis of new red blood cells. In conditions of high erythropoietic activity, hepcidin expression is downregulated in order to increase iron availability. In 2014, erythroferrone (ERFE), a hormone produced by erythroblasts, was identified as the erythroid factor responsible for hepcidin repression [78]. ERFE-deficient mice do not suppress hepcidin expression after hemorrhage. However, the ERFE receptor and ERFE signaling pathway are still not known [78]. Two other factors, growth differentiation factor 15 (GDF-15) and twisted gastrulation homolog 1 (TWSG1), might also be involved in reducing hepcidin expression in conditions of high erythropoietic demand [79, 80].

Hepcidin regulation by hypoxia

Hepcidin expression is inhibited by hypoxia and different mechanisms have been proposed to explain this observation.

The kidney senses systemic hypoxia and responds by producing an erythroid growth factor known as erythropoietin (EPO) [81]. The secretion of EPO stimulates erythropoiesis in the bone marrow in order to restore a proper delivery of oxygen to every cell type in the organism. EPO is likely to suppress hepcidin expression indirectly by stimulating erythropoiesis and therefore increasing ERFE [82] (section: “Hepcidin regulation by erythropoietic signals”).

The heterodimeric hypoxia-inducible factors (HIF-1α/HIF-β and HIF-2α/HIF-β) are known to regulate the transcription of several iron-related genes, such as *Fpn* and *Dmt1* in enterocytes [83, 84], and it was reported that HIFs might directly repress hepcidin promoter activity under hypoxic conditions [85]. Under normoxia, the oxygen- and iron-dependent prolyl hydroxylases (PHDs) hydroxylate the HIF-1α and HIF-2α subunits, which then associate with the von Hippel-Lindau tumor suppressor (pVHL). This complex is polyubiquitinated by an E3 ligase and HIFs subunits are rapidly degraded. Under hypoxic conditions, the activity of PHDs is reduced due to the lack of oxygen and HIF-1α and HIF-2α subunits are no longer hydroxylated and targeted for proteasomal degradation (reviewed by [86]). As a consequence, HIF-1α and HIF-2α are stable and recruit HIF-β (which is constitutively expressed), forming heterodimers that can directly regulate gene expression.

However, later studies suggested that hepcidin regulation during hypoxia does not occur via direct effects of the pVHL/PHD/HIF axis on the hepcidin promoter but probably through EPO-mediated erythropoiesis [87, 88].

Nevertheless, HIF-1α may indirectly regulate hepcidin expression. A functional hypoxia-responsive element was identified in the TMPRSS6 promoter region and mutations in this element impair HIF1α-dependent induction of TMPRSS6 expression [89]. Similarly, hypoxia also increases the expression of furin via HIF-1α [66, 90]. These observations suggest that increased expression of TMPRSS6 and furin under hypoxic conditions may be an additional mechanism to repress hepcidin expression.

1.5.3 Regulation of ferroportin expression

As previously mentioned, ferroportin (also known as SLC40A1, Ireg1 and MTP1) is the only known cellular iron exporter [9, 10]. The systemic inactivation of the *Fpn* gene in mice results in embryonic lethality [48]. Interestingly, mice in which the *Fpn* gene was inactivated in all tissues except placenta and the extraembryonic visceral endoderm were viable, likely reflecting a correct iron transfer from the mother to the embryo [48]. Nevertheless, these animals accumulate iron in enterocytes, splenic and liver macrophages, and hepatocytes shortly after birth – highlighting the major role of FPN in iron export in these cell types [48].

Contrary to hepcidin, FPN expression is regulated at several levels and not only at the transcription level.

<u>Transcriptional regulation of ferroportin</u>

Heme, a product of hemoglobin degradation, increases *Fpn* transcription in macrophages. The presence of heme induces the degradation of the transcriptional repressor Btb And Cnc Homology 1 (Bach1) and allows the transcriptional activator Nuclear Factor Erythroid 2-like (Nrf2) to bind to Small Maf proteins (sMAFs) and enhance *Fpn* transcription [91]. Additionally, *Fpn* transcription is also increased by iron in macrophages [92] but the molecular mechanism behind this observation is not known yet.

It has been reported that *Fpn* transcription is decreased under inflammatory conditions. Upon lipopolysaccharide (LPS) stimulation, *Fpn* mRNA levels decrease in macrophages from the spleen and the liver, probably in an attempt to reduce iron availability for extracellular pathogens [93-95]. The molecular mechanism behind *Fpn* transcriptional repression during inflammation is still not completely understood. The stimulation of toll-like receptors (TLR) 2/6 dependent signaling pathways by the *Mycoplasma*–derived molecule FSL1 was shown to repress *Fpn*

transcription [96]. Upon *Pseudomonas aeruginosa* infection or LPS stimulation, *Fpn* mRNA levels were shown to be reduced in a TLR 4 dependent manner [93, 97]. The direct effect of increased inflammatory cytokines such as TNFα still remains controversial [93, 98].

Hypoxia and iron deficiency were shown to induce *Fpn* transcription in duodenal enterocytes. In these conditions, HIF2-α is stabilized, forms a heterodimer with HIF-β, and binds directly to HIF response elements present in the promoter of *Fpn* [83, 84]. Upon binding, the HIF2 heterodimer stimulates *Fpn* expression and therefore increases the export of iron from enterocytes to the bloodstream; this ensures an increase in dietary iron absorption in order to counteract the iron deficiency or the hypoxia (by increasing the levels of iron available for erythropoiesis).

Post-transcriptional regulation of ferroportin

At the post-transcriptional level, FPN is regulated by the IRE/IRP system. As described in section 1.4, when intracellular levels of iron are low, IRP1 or 2 bind to the IRE present in the 5' UTR of *Fpn* mRNA, blocking its translation and therefore decreasing cellular iron export [9, 10]. When intracellular iron levels are high, *Fpn* mRNA is translated and iron export increases. This mechanism prevents both toxic intracellular iron overload as well as detrimental intracellular iron depletion (reviewed in [31]).

Interestingly, duodenal enterocytes and erythroid precursors additionally use an alternative upstream promoter to express a *Fpn* transcript with an identical open reading frame but that lacks the IRE in the 5' UTR [99]. These cells can evade translational repression of FPN in conditions of low iron levels. As a result, enterocytes can export iron into the plasma under iron deficient conditions in order to restore systemic iron levels. This alternative transcript accounts for most of the FPN expression in erythroid precursors and allows these cells to export iron in conditions of iron deficiency, in order to increase its availability to other tissues in need.

Post-translational regulation of ferroportin

As described in section 1.5.1, FPN is regulated post-translationally by hepcidin [49]. The binding of hepcidin to FPN, and the subsequent internalization and degradation of the latter, is dependent on the fourth extracellular loop of FPN, which contains the amino acid cysteine (C) at position 326. A point mutation in this amino acid (Cysteine ⟶ Serine) was identified in a family presenting an autosomal dominant form of hereditary hemochromatosis, with elevated transferrin saturation and iron deposition in hepatocytes, but not in kupffer cells [100]. Additional studies, both *in vitro* and *in vivo*, showed that this point mutation (C326S) prevents the binding of

hepcidin to FPN [101, 102], revealing the critical role of the thiol form of C326 for hepcidin binding.

The exact mechanism underling FPN internalization and degradation has been investigated thoroughly in the past years and it is believed that ubiquitination is the key signal for hepcidin-induced ferroportin endocytosis [50].

1.6 Iron related disorders

The study of the molecular mechanisms underlying iron-related disorders in humans has been very useful in the understanding of mechanisms regulating systemic and cellular iron homeostasis. Most of the iron-related diseases, both from iron overload and from iron deficiency, result from disruptions in the hepcidin/FPN regulatory system.

1.6.1 Iron overload diseases

Hereditary hemochromatosis (HH) is an iron overload disease characterized by excessive dietary iron absorption that results in elevated plasma iron levels, high transferrin saturation, and formation of NTBI. The excess of iron accumulates in several organs, e.g. the liver, leading to increased oxidative stress, cell damage, and tissue injury. Different forms of HH exist that present with different disease severities and result from different mutations. HH type 1, 2A and 3 are characterized by mutations in the iron-sensing machinery (HFE, HJV or TfR2, respectively) that result in inappropriate low or absent levels of hepcidin [103-106]. HH type 2B results from a mutation in the hepcidin gene itself [107]. Deficient hepcidin production observed in these patients leads to high levels of FPN at the cell membrane, causing an increase in dietary iron absorption by duodenal enterocytes and increased iron release from recycling macrophages. These four subtypes of HH are recessive forms of the disease. HH type 4 is an autosomal dominant form of hemochromatosis that results from “gain of function” mutations in FPN that confer resistance to hepcidin binding [100, 108]. As a consequence, ferroportin remains stable at the cell membrane independently of hepcidin levels, leading to elevated iron export into the circulation. Hepatic cells become iron overloaded whereas splenic macrophages and kupffer cells are iron depleted. This rare disorder is also known as non-classical ferroportin disease and is the only HH subtype that is associated with high hepcidin levels, since the iron sensing machinery still responds to increased systemic iron levels.

Loss of function mutations in FPN that lead to incorrect targeting of the protein to the plasma membrane or the production of an inactive iron exporter result in a disorder known as classical

ferroportin disease (reviewed in [109]). Due to the inability to export iron, specialized iron-exporting cells such as Kupffer cells and splenic macrophages are iron overloaded. As a consequence of iron restriction in these cells, patients present normal to low plasma transferrin saturation.

Other iron overload disorders, known as iron-loading anemias, can develop as a consequence of an impaired erythropoiesis system. For example, in β-thalassemia, the defective production of the β-globin chain in erythroid precursors leads to the precipitation of excess α-chains and results in the apoptosis of these cells. The lack of mature red blood cells and diminished oxygen transport capacity stimulate EPO production, which in turn stimulates erythropoiesis but fails to correct anemia because the precursors undergo apoptosis. High erythropoietic activity suppresses hepcidin expression, leading to hyperabsorption of dietary iron and, consequently, to systemic iron overload [110, 111].

1.6.2 Iron deficiency diseases

Insufficient dietary iron intake or blood losses can cause iron deficiency that commonly manifests as anemia; since erythropoiesis requires large amounts of iron, a depletion of body iron levels impairs this process and leads to low hemoglobin levels.
However, several other iron deficiency disorders result from elevated hepcidin expression. By limiting iron availability for erythropoiesis, these diseases are also often associated with anemia. Mutations in TMPRSS6 that inactivate its function as a negative regulator of hepcidin production result in an autosomal recessive disorder known as familial iron-refractory iron deficiency anemia (IRIDA) [112]. Although patients present with severe iron deficiency that should suppress hepcidin expression, serum hepcidin levels are abnormally increased, causing uncontrolled FPN degradation and preventing iron from being absorbed from diet and released from stores.
Very high levels of hepcidin are also responsible for another iron-deficiency disorder named anemia of inflammation or anemia of chronic diseases [113, 114]. The underlying cause of elevated hepcidin expression in these diseases is attributed to an excess of inflammatory cytokines, such as IL6 (reviewed in [115]). Despite the hypoferremia observed in these patients, overproduction of hepcidin inhibits intestinal iron absorption and macrophage iron release.

2. Mammalian Respiratory System

The oxidative metabolism of cells requires high amounts of oxygen (O_2). Oxygen is transported in the bloodstream bound to hemoglobin in erythrocytes and is delivered to every cell type in the body. During aerobic cellular respiration, oxygen is consumed and carbon dioxide (CO_2) is produced and released into the circulation.

In order to fulfill the cellular oxygen requirements and to excrete the waste CO_2, the respiratory system has evolved to allow an efficient gas exchange between the atmosphere and the bloodstream. Inhaled air travels through a highly branched conducting tract (nose, pharynx, larynx, trachea, bronchi, bronchioles) until it reaches the distal lung where most of the gas exchange occurs (reviewed in [116] and [117]). In this region, the surface for gas exchange is maximized by the septation into innumerous microscopic thin-walled air sacs called alveoli [118] (reviewed in [119]). These structures are in close contact to a dense capillary network.
The alveolar epithelium is composed by two cell types – alveolar epithelial cells type 1 and type 2 (also known as pneumocytes type 1 and 2) – whereas the conducting airways are lined by an epithelium composed of a variety of multi-ciliated and non-ciliated epithelial cells (Figure 1.3) (reviewed in [120]). In healthy conditions, alveolar macrophages are the most common cell type present within the alveolar space.

Millions of liters of air inhaled every day do not only provide the necessary oxygen to support life but also expose the respiratory system to pathogens and toxic particles. For this reason, multiple physical and chemical innate host-defense mechanisms exist within the respiratory tract. Tight adhesions between epithelial cells and the presence of mucus and antimicrobial molecules that enhance mucociliary clearance are among the most important features of the pulmonary innate immunity (reviewed in [121] and [122]). In addition, pulmonary epithelial cells and alveolar macrophages can recognize the presence of pathogens and trigger an inflammatory response, if necessary. These cells produce cytokines and chemokines and recruit and activate other cells of the immune system (reviewed in [121] and [123]).

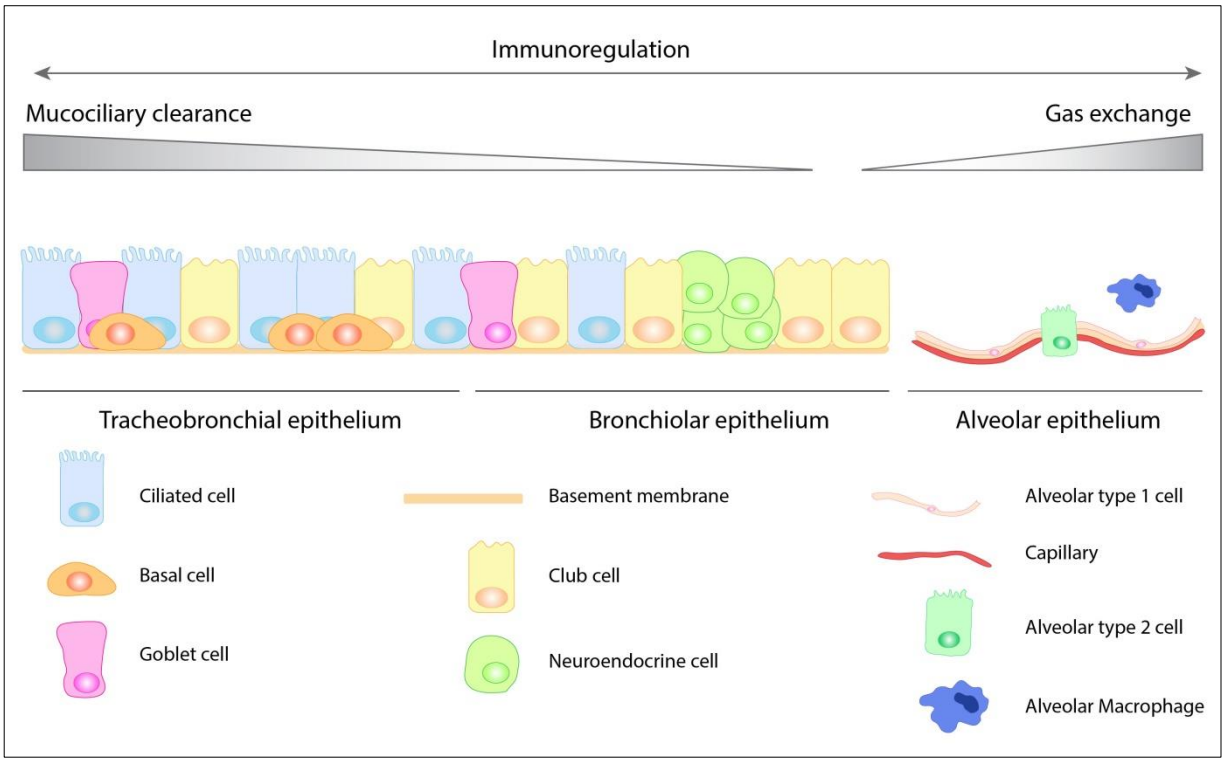

Figure 1.3 – Structure of the mouse airway epithelium. The larger airways (trachea and bronchi) are lining by a pseudostratified columnar epithelium mainly composed of ciliated airway epithelial cells, basal cells, few goblet cells and Club cells. As the conducting airway branches into smaller airways (bronchioles and bronchio-alveolar duct), the epithelium becomes a simple epithelium mainly composed of Club cells, with interspersed ciliated cells. Neuroendocrine cells are present in low numbers in the airway epithelium and are commonly found in small clusters called neuroepithelial bodies. Alveoli are lined by an uninterrupted epithelium consisting of alveolar epithelial type 1 and type 2 cells, surrounded by a dense capillary network. Alveolar macrophages are the primary immune cells present in the airway lumen of a healthy lung. Image created based on image from Wong et al., 2009 [124].

2.1 Pulmonary vasculature

After oxygenation of cells throughout the body, deoxygenated blood is pumped from the right ventricle of the heart to the lungs via the main pulmonary artery. This artery divides into the right and the left main branches, which transport blood to the four right lobes and the left lobe of the mouse lung (reviewed in [125]). Within each lobe, the arteries rapidly subdivide into branches that follow the bronchial tree: arteries break into small arteries, followed by arterioles and then innumerous capillaries that completely envelop the alveoli (reviewed in [125]).

Large pulmonary arteries are classified as elastic since their wall is mainly composed by elastic fibers and some smooth muscle cells. As they divide and their vascular diameter decreases, the composition of their wall changes leading to an increase in the smooth muscle cell layer and a

decrease in the elastic fibers – these arteries are classified as muscular arteries [126]. The wall thickness of the vessels gradually decreases when they further subdivide: small arterioles are surrounded by a non-uniform layer of smooth muscle cells and are followed by smaller non-muscular arterioles located proximal to the terminal bronchi [127]. At the alveoli region, these arterioles give rise to capillaries whose walls consist of a single layer of endothelial cells [128].
The thin pulmonary endothelium is ideal for gas exchange to occur: carbon dioxide is released and oxygen is taken up. Oxygenated blood travels through the capillaries into venules, which are in gross structure similar to arterioles (reviewed in [129]). Venules are distributed irregularly within the lung and do not follow the bronchial tree. These vessels come together to form the pulmonary veins and transport oxygenated blood to the left atrium of the heart. Oxygen can then be delivered to cells throughout the body through the systemic circulation.

2.2 Trachea, bronchi and bronchioles

The trachea, bronchi and bronchioles form a tree-like system of branched tubes that carries air to and from the alveoli. In the mouse lung, the trachea and main bronchi are lined by a pseudostratified columnar epithelium whereas the smaller airways are lined by a simple columnar epithelium (Figure 1.3) (reviewed in [120]). The epithelium is covered by the airway lining fluid, which protects the underlying cells against desiccation and damage, and plays an important role in the delivery of almost completely sterile gases to the alveoli.

Studies throughout the years have revealed a big diversity of cells that form the airway epithelium. These cells can be broadly divided into the following groups:

Ciliated airway epithelial cells: Ciliated epithelial cells are considered terminally differentiated cells [130]. They are present in large numbers in the mouse upper airways and each cell possesses up to 300 cilia on its apical surface. The coordinated movement of cilia is essential to move the mucus along the respiratory tract (see Goblet cells section). Cilia dysfunction impairs this process and leads to recurrent respiratory infections [131].

Goblet cells: Goblet cells are non-ciliated secretory cells that produce and secret mucin, i.e. highly glycosylated proteins that, together with water, form the mucus lining the airway epithelium [132] (reviewed in [133]). Inhaled materials/pathogens get trapped in this mucus and are subsequently removed from the respiratory system through the highly synchronized beat of cilia from ciliated airway epithelial cells, in a process called mucociliary clearance (reviewed in

[134]). The importance of the mucus in the healthy lung is highlighted by the observation that mice lacking the constitutively produced mucin MUC5b present chronic inflammation [135].

Basal cells: In the mouse lung, basal cells are mainly localized between ciliated and secretory cells in the larger airways. The abundant cytoskeleton and the presence of desmosomes and hemidesmosomes highlight the role of basal cells as major structural components of the epithelium, attaching it to the underlying basement membrane [136, 137]. Moreover, basal cells have also an important role in the homeostasis of the epithelium since they have the ability to self-renew and give rise to secretory and ciliated airway epithelial cells [138, 139].

Club cells: Club cells are the main cell type present in mouse small airways. These non-ciliated secretory cells produce and secrete several components of the airway lining fluid, such as the club cell secretory protein (CCSP) (reviewed in [140]). The study of $CCSP^{-/-}$ mice revealed the important role of club cells and their secretions in lung homeostasis: CCSP deficiency is associated with atypical airway lining fluid composition, increased susceptibility to lung injury and oxidative stress, as well as altered lung inflammatory responses [141-144] (reviewed in [124]). Despite being differentiated cells, club cells have the potential to reenter the cell cycle and contribute to the renewal of the bronchiolar airway epithelium [145, 146].

Pulmonary neuroendocrine cells: Pulmonary neuroendocrine cells (PNEC) are localized within the epithelium lining the trachea, bronchi, and bronchioles, and they can be grouped in small clusters called neuroepithelial bodies (reviewed in [147]). Even though these are the first specialized cells to differentiate in the airway epithelium during development, they are present in low numbers in the adult lung. During lung development, PNECs act as modulators of lung growth and differentiation (reviewed in [147]); their function in the adult lung is not well known yet but they might be involved in airway oxygen sensing [148]. Also, a recent study shows that PNECs control lung immune responses by producing neuropeptides [149].

2.3 Alveoli structure

Alveoli are lined by an uninterrupted epithelium consisting of alveolar epithelial type 1 and type 2 cells (AT1 and AT2), which are in close contact with underlying capillaries and fibroblasts (Figure 1.3) [118] (reviewed in [150]). The alveolar surface is covered by the alveolar lining fluid, which protects the underlying epithelial cells against desiccation and pathogens, and facilitates the diffusion of gases.

AT1 cells are flat and cover >90% of the surface of alveoli [151]. Their high membrane to cytoplasm ratio and close apposition to alveolar capillaries create a very thin air-blood barrier, essential for a proper gas exchange. These cells are generally regarded as non-proliferative, fully differentiated cells [152].

AT2 cells are cuboidal-shaped and are often localized in the “corners” of alveoli. Contrary to AT1, AT2 cells have the ability to self-renew and differentiate into AT1 cells [153]. AT2 cells synthetize, secrete, and recycle the pulmonary surfactant – a mix of extracellular proteins and lipids present within the alveolar lining fluid that decreases alveolar surface tension and contributes to host defense [154-156]. These cells contain large and abundant secretory vesicles called lamellar bodies, which reflect their important secretory function [157].

The lung volume does not remain constant during respiration: it increases during inspiration and decreases during expiration. By reducing the surface tension at the gaseous-aqueous interphase of the alveoli, the surfactant plays an essential role in preventing the collapse of alveoli at the end of expiration and reducing the effort needed to expand the lungs during inspiration (reviewed in [158]). This way, the surfactant increases lung compliance, i.e. the change in lung volume per unit of pressure change, meaning the ease with which the lungs can be extended. Inversely, the surfactant decreases lung elastance which is a measure of lung stiffness and is defined as the change in the pressure per unit of volume change.

Even though the exact composition of the surfactant is not completely known yet, it is believed to be composed of four surfactant proteins (SP) that account for 10% of the surfactant and by several different lipids that comprise 90% of the surfactant layer (reviewed in [158]). The hydrophobic SP-B and SP-C have a major role in surfactant structure and function while the other two surfactant proteins, SP-A and SP-D, are hydrophilic proteins and contribute to lung immunity [159] (reviewed in [156]). They interact with various microorganisms and pathogen-derived components and act as opsonins by binding and agglutinating pathogens, thus enhancing phagocytosis. Moreover, these proteins also directly modulate the activity of alveolar macrophages and other immune cells [160, 161] (reviewed in [156]). Consistently, mice deficient in SP-D or SP-A are more susceptible to lung inflammation and infection than wild-type mice [162-164].

AT2 cells play an important role in host defense not only by producing surfactant proteins but also by producing cytokines and expressing ligands that regulate the activity of immune cells [165-167] (reviewed in [168]).

Finally, both AT1 and AT2 cells express ion channels and might be involved in alveolar fluid homeostasis [169, 170].

The thin air-blood barrier is exposed to two main physical stresses: the pressure within the capillaries and the increased longitudinal tension of the alveolar wall when the lung is inflated to high volumes (reviewed in [171]). Interstitial fibroblasts play an essential role in supporting the alveolar structure by secreting extracellular matrix (ECM). In a healthy lung, fibroblasts synthetize small amounts of ECM, enough to preserve the integrity of the alveolar barrier while maintaining it as thin as possible. Different pathological conditions that lead to the recruitment and activation of fibroblasts, differentiation into myofibroblasts, and increased production of ECM contribute for increased lung stiffness and pathology of fibrotic lung diseases [172-174].

2.4 Alveolar Macrophages

Alveolar macrophages (AMs) are the primary immune cells present in the airway lumen of a healthy lung. Due to the techniques used to investigate the biology of these cells, most studies do not distinguish between macrophages present within the alveolar space and those present within larger airspaces. For this reason, in this thesis, the term “alveolar macrophage” is used to describe a mixed population of macrophages that reside in the lumen of the airways.

Being the first immune cells to contact with inhaled pathogens, AMs are extremely important in lung immunological responses. However, they also play an equally important role in clearing apoptotic cells, excessive surfactant and cellular debris in health and disease situations (reviewed in [123]).

The unique environment in which AMs exist has a strong influence on their phenotype and function, which is illustrated by the observation that peritoneal macrophages acquire expression markers of AMs when transferred into the lung [175]. In mice, AMs are phenotypically very different from other macrophage populations (reviewed in [123]). They express high levels of cluster of differentiation (CD)-11c (also known as integrin α_x), a molecule that is not typically expressed in macrophages but is a typical marker of dendritic cells [175-177]. Similarly, AMs express CD205 (also known as DEC-205), which is also expressed by dendritic cells and has not been reported to be expressed by macrophages [175, 178]. In contrast, AMs express low levels of CD11b, which is typically expressed by other macrophage populations [175, 177]. Moreover, mouse AMs express intermediate/low levels of CD14 [176] and high levels of sialic acid-binding immunoglobulin-like lectin F (SiglecF), which is mainly expressed by eosinophils [176, 179].

Origin and differentiation of alveolar macrophages

The initial colonization of the airways with AMs is dependent on embryonically derived fetal monocytes, which fully differentiate into AMs in the first days after birth [180] (reviewed in [181]). Throughout life, AMs have the ability to self-renew and maintain the population with minor contribution from circulating monocytes [182]. Even though conflicting studies exist, it is believed that circulating monocytes only contribute to AM repopulation when these cells have a limited capacity for proliferation, as in the case of radiation-induced depletion of AMs [182].

Both differentiation and survival of AMs is highly dependent on the granulocyte-macrophage colony-stimulating factor (GM-CSF, also known as CSF2) and possibly also on surfactant proteins [175, 180, 182]. The essential role of GM-CSF is highlighted by the observation that GM-CSF$^{-/-}$ mice fail to generate mature and fully functional AMs [180].

GM-CSF has long been described as a key factor in the proliferation and maturation of myeloid lineages (reviewed in [183]) but it has also been reported to act in other biological contexts such as proliferation of endothelial progenitor cells and during embryo implantation and development [184] (reviewed in [185]). The effects of GM-CSF are mediated through a heterodimeric receptor composed of a ligand-specific α-subunit (GM-Rα) and a common β-subunit that is also a component of IL-3 and IL-5 receptors [186-188]. The GM-Rα subunit binds to GM-CSF with low affinity as a monomer but with high affinity when associated with the β subunit [187]. Even though the GM-Rβ subunit is incapable of binding to GM-CSF as a monomer, it plays an important role in GM-CSF-induced signal transduction. The high-affinity complex (GM-Rα/GM-Rβ) transduces signals through JAK-STAT-, MAPK-, and phosphatidylinositol 3-Kinase (PI3K)-dependent pathways to alter the expression of target genes [184, 189-191].

Regulatory effects of the lung microenvironment

Due to their unique position in the airspace, AMs are exposed to air pollutants, pathogens, and dust. AMs have to accurately discriminate between situations that require an inflammatory response (pathogens) and those that require a tolerogenic response (lung microbiome [192] and innocuous stimuli). For this reason, and in order to prevent unwanted inflammatory responses, AM activation is negatively regulated via cell-cell interactions with airway epithelial cells (reviewed in [123]). For example, the airway epithelium expresses CD200 which interacts with its receptor expressed in AMs and inhibits their activation [166]. Additionally, the non-inflammatory status of AMs is also maintained by the presence of secreted factors such as surfactant proteins (SP-A and SP-D), transforming growth factor β (TGF-β), and IL-10 produced by the lung epithelium [161, 193, 194] (reviewed in [123]). Hence, a combination of events that overcome

the inhibitory stimuli must occur for an inflammatory response to initiate. The presence of pathogens in the airways activates TLR-dependent signaling pathways in AMs, releasing them from the suppression mediated by epithelial cells and triggering their activation [193]. Furthermore, the destruction of the airway epithelium during inflammation leads to the loss of negative regulators, such as CD200, enhancing the inflammatory status.

Once activated, AMs have a high phagocytic capacity and produce high levels of inflammatory cytokines and chemotactic factors, which leads to the recruitment of other immune cells, such as neutrophils, to the bronchoalveolar space [195-197] (reviewed in [198]).

3. Lung iron homeostasis

Like every other cell type in the body, lung cells take up iron from the bloodstream and use it to fulfill their metabolic needs. However, they must also prevent toxic iron overload. In the particular case of the lung, the risk of oxidative stress is very high since this organ is exposed to the atmosphere and therefore to high levels of oxygen. Moreover, lung cells are not only exposed to iron circulating in the blood but also to iron present in inhaled particles - the atmosphere is a vehicle for the movement and redistribution of metals, such as iron (reviewed in [199]). Human activities have contributed to increased levels of atmospheric iron via the production of air pollution particles [200]. Iron is also present in cigarette smoke (a factor with a strong causative link to pulmonary pathology) and accumulates in the lung: pulmonary iron levels are higher in cigarette smokers when compared with nonsmokers [201].
Even though high levels of antioxidants, such as glutathione and ascorbic acid, are present in the respiratory tract lining fluid, an imbalance in iron levels in the lung can lead to oxidative stress [202] (reviewed in [203]).

3.1 Iron metabolism in the lung

Contrary to duodenal enterocytes, the lung did not evolve to absorb iron to meet the body nutritional requirements. Instead, by being exposed to iron from blood and from inhaled particles, the lung has an essential role in iron detoxification (review in [204]). In a healthy lung, iron homeostasis is tightly controlled and the availability of free iron is limited. It has been suggested that lung cells sequester iron intracellularly bound to ferritin and therefore in a less reactive form (review in [204]). In fact, pulmonary ferritin levels increase upon iron exposure [204, 205].
Several studies showed that lung cells express the same iron-related proteins that are expressed in enterocytes and hepatocytes (reviewed in [204]) (Figure 1.4). However, how iron homeostasis is maintained in the lung is not completely understood and conflicting data exist between different studies.

Iron uptake by lung epithelial cells: Similar to duodenal enterocytes, lung epithelial cells express DMT1 in their apical membrane and take up non-transferrin bound iron from the airway lumen (Figure 1.4) [206, 207]. However, it is still not clear how the expression of DMT1 responds to increased iron concentrations. Wang *et al.* observed that the mRNA and protein levels of the DMT1 isoform without IRE increase in the airway epithelium *in vitro* and *in vivo* upon exposure to

iron whereas Giorgi *et al.* observed that the protein levels of DMT1 in the lung are unchanged in mice injected intraperitoneally with iron-saccharate [206, 208]. The uptake of iron via DMT1 needs to be coupled with the reduction of ferric iron to ferrous iron (described in section 1.3.). Turi *et al.* reported that DcytB is expressed in airway epithelial cells (similar to enterocytes) and probably reduces iron before its uptake [209].
Giorgi *et al.* showed that ZIP14 is expressed in airway epithelial cells and that its expression increases in conditions of iron overload [208]. Wang *et al.* reported that *Zip14* levels in the lung are very low but demonstrated that *Zip8* is highly expressed in the lung [46]. For this reason, ZIP8 is another candidate for the uptake of non-transferrin bound iron by lung cells.

Iron export by lung epithelial cells: In the model which proposes that iron is detoxified in the lung, airway epithelial cells not only take up and store iron, but are also able to export it in a less reactive form via ferroportin or bound to ferritin or transferrin (reviewed in [204]). The authors suggested that iron could then be transported out of the lung via the mucociliary pathway or via blood to the reticuloendothelial system for long term storage. However, conflicting data exist regarding this model. Yang *et al.* reported that FPN is expressed at the apical membrane of airway epithelial cells while Giorgi *et al.* showed that FPN is expressed in the cytoplasm of these cells [208, 210]. On the other hand, the idea that FPN expression increases in lung cells upon exposure to iron seems to be consistent in different studies [208, 211]. Taken together, more studies are needed to fully understand if lung epithelial cells are able to export iron or not.

Alveolar macrophages: AMs play a key role in lung iron homeostasis. These cells have the capacity to sequester large quantities of iron intracellularly bound to ferritin and therefore in a less reactive form. AMs from smokers show very high levels of iron and it was suggested that this storage prevents oxidative stress by decreasing the generation of extracellular hydroxyl radicals [212]. Moreover, AMs from mice injected intraperitoneally with iron-saccharate (which present increased pulmonary iron content) show increased iron levels, suggesting that AMs take up the excess of iron in conditions of iron overload [208].
It was reported that AMs may take up both transferrin and non-transferrin bound iron as they express TfR1 and DMT1 [207, 213, 214]. Via phagocytosis, alveolar macrophages can also retain iron derived from senescent cells and from inorganic iron-rich dust (reviewed in [215]).
Whether AMs are able to export iron is currently not clear. It has been suggested that they might export it via ferritin or FPN [204], but there is a lack of strong evidence to support this idea. Further studies are necessary to confirm or exclude this hypothesis.

Hepcidin expression in the lung: Giorgi *et al.* showed that unlike hepatic hepcidin expression, total lung hepcidin levels do not increase in response to iron [208]. Moreover, they suggested that hepcidin expression in the lung does not alter iron homeostasis in this organ [208]. Frazier *et al.* studied the expression of hepcidin in human airway epithelial cells *in vitro* and have come to the same conclusion [216]. Contrasting these findings, Chen *et al.* showed that the silencing of hepcidin expression in airway epithelial cells leads to a reduced degradation of FPN in the lung in a mouse model of sepsis-induced acute lung injury [217]. They also observed a decrease in intracellular iron content of AMs, probably as a consequence of increase FPN protein levels [217]. Nguyen *et al.* reported that AMs also produce hepcidin and that its expression increases upon treatment with LPS [214]. However, its role in lung iron homeostasis was not elucidated in this study.

3.2 Lung diseases associated with iron overload

A dysregulation of lung iron homeostasis caused by either endogenous or exogenous factors is likely to increase the availability of free iron. Increased iron levels in the lung caused by the injection of intravenous iron result in increased oxidative stress [202], which can lead to tissue injury and contribute to the pathogenesis of several diseases. In fact, increasing evidence shows that several chronic and acute lung diseases are associated with a dysregulation of pulmonary iron homeostasis (reviewed in [204]). Patients with idiopathic pulmonary alveolar proteinosis, acute respiratory distress syndrome, cystic fibrosis, and chronic obstructive pulmonary disease (COPD) show higher levels of iron and iron-related proteins (e.g. ferritin and TfR1) in the lung when compared to healthy individuals [218-221]. In most of these studies, iron was detected both extracellularly in the bronchoalveolar space and intracellularly. AMs were described as the predominant iron loaded cell type and the percentage of iron loaded AMs in patients with COPD was correlated with increased disease severity [218]. However, these studies mostly remain on the observational level. Whether increased pulmonary iron levels contribute to the development of these lung diseases is still poorly understood.

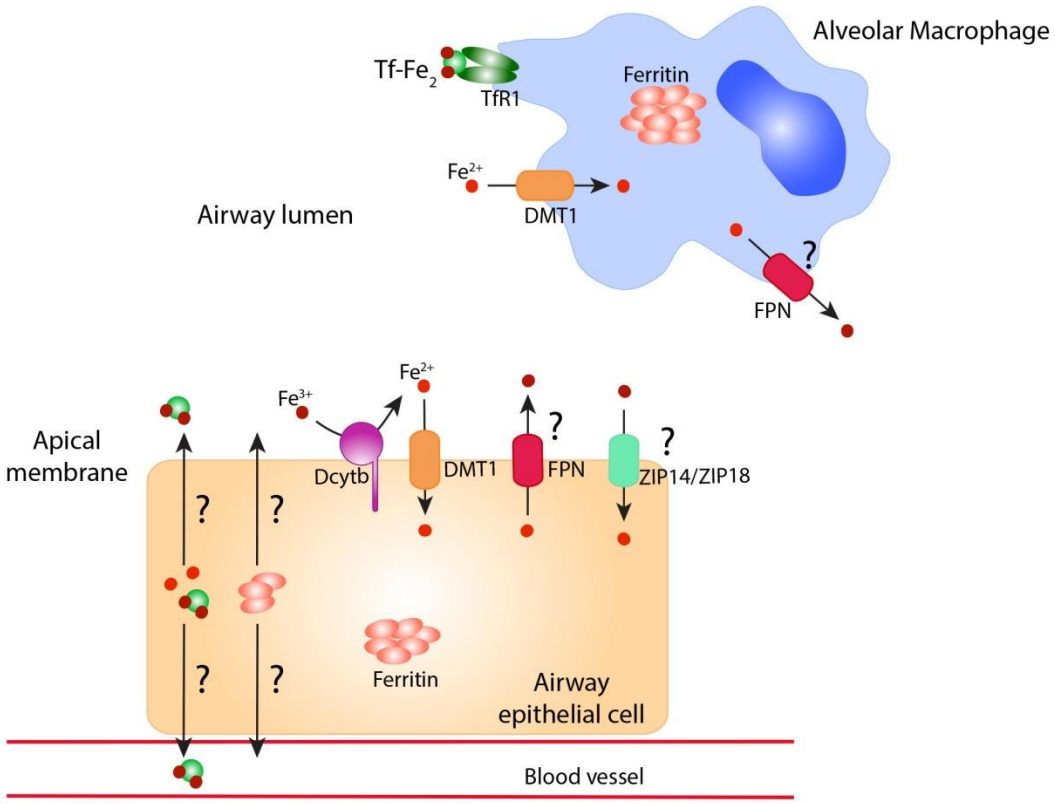

Figure 1.4 – Lung iron homeostasis. A model was proposed in which iron is detoxified in the lung. This involves the uptake of iron by airway epithelial cells and alveolar macrophages. These cells store iron intracellularly bound to ferritin. Airway epithelial cells can take up iron from the airway space via DMT1 (a process coupled with the activity of DcytB) and possibly via ZIP14 or ZIP8. It is still not clear if these cells can export iron but several mechanisms have been proposed: export of iron via ferroportin (FPN) or bound to transferrin or ferritin. Alveolar macrophages take up transferrin and non-transferrin bound iron via TfR1 and DMT1, respectively. It is also not clear if these cells can export iron via FPN.

4. Research Aims

The pathogenesis of lung diseases associated with iron overload is poorly understood. It is not clear whether the observed increase in lung iron levels contributes to disease onset and progression or if it represents a secondary effect resulting from lung injury.
Some studies have addressed the impact of increased lung iron content by the inhalation of particles containing iron [222-224]. However, limited data exist regarding the impact of increased circulating iron levels on pulmonary iron content and function.

The major aim of this work was to understand whether a disruption of the hepcidin/FPN regulatory system and the subsequent increase in systemic iron levels affect lung iron homeostasis and function. We analyzed a mouse model of hereditary hemochromatosis type 4 ($Slc40a1^{C326S}$) which is characterized by a disrupted hepcidin/FPN regulatory circuitry [102]. The disruption of the hepcidin/FPN interaction is caused by a missense mutation (C326S) introduced into the murine ferroportin gene. This mutation was previously identified in patients [100] and was shown to impair the binding of hepcidin to FPN in cellular assays [101]. As a consequence of FPN stabilization and uncontrolled iron export, these mice show elevated plasma iron levels, hepatic iron overload, and iron depletion in duodenal enterocytes and reticuloendothelial macrophages [102].

The specific goals of this study were to:

- understand how the lung iron content and distribution is affected by a disruption of the hepcidin/FPN regulatory system and increased systemic iron levels;
- characterize the expression of iron-related genes in order to dissect the molecular mechanisms controlling lung iron homeostasis;
- identify the (patho)physiological consequences of increased pulmonary iron content in terms of lung inflammation and lung function.

Chapter II

Materials and Methods

Mice

Slc40a1^{C326S} mice analyzed were maintained on a pure C57BL/6N genetic background (>99.9% congenic). As controls, age- and gender-matched wild-type C57BL/6N mice born and maintained in the same breeding facility were used. Mice were housed in the Heidelberg University animal facility under a constant light-dark cycle and maintained on a standard mouse diet (LASQCdiet Rod18-A - LASvendi) containing 200 ppm iron with *ad libitum* access to food and water.

All mouse breeding and animal experiments were approved by the Regierungspräsidium Karlsruhe (Projects Nr T-81/14, T-66/13, G-41/16, G-39/16).

Since *Hamp*$^{-/-}$ mice have a different genetic background (C57BL/6J), wild-type and Slc40a1^{C326S} mice with the same genetic background were used for the comparison of lung non-heme iron content between these three mouse models. These mice were housed in the EMBL animal facility. Mouse breeding and the experiment were approved by and conducted in compliance with the guidelines of the EMBL Institutional Animal Care and Use Committee.

Bronchoalveolar lavage and differential cell count

Mice were anesthetized via intraperitoneal injection of a combination of ketamine (Pfizer) and xylazine (Bayer) (120 and 16 mg/kg respectively) and sacrificed by exsanguination. A median sternotomy was performed, the trachea cannulated and the left mainstem bronchus ligated and the right lung was lavaged with Phosphate Buffered Saline (PBS, Sigma). Bronchoalveolar lavage (BAL) samples were centrifuged (5 minutes, 600g, 4°C) and BAL fluid supernatant was harvested and stored at -80ºC. Total cell counts were determined using a haemocytometer and differential cell counts were determined in cytospin preparations stained with May–Grünwald–Giemsa (Merck). Alveolar macrophage size was determined in cytospin preparations by measuring their surface area using the Analysis B imagine analysis software (Olympus).

Isolation and differentiation of bone marrow-derived macrophages (BMDM)

Bone marrow cells were flushed from tibia and femur using ice-cold Hank's balanced salt solution (HBSS, Sigma) and filtered through a 70 µm cell strainer (BD biosciences). Cells were seeded at a density of 350000 cells/cm^2 in RPMI1640-Glutamax medium (Life Technologies) supplemented with 10% of heat-inactivated fetal bovine serum (Thermo scientific), 1% Penicillin/streptomycin (Gibco) and 10 ng/mL M-CSF (Petrotech) and/or GM-CSF (Petrotech).

After 4 days, non-adherent cells were removed by HBSS washing and the medium was replaced daily until cell harvesting (6 days after seeding).
To test the presence of ROS upon acute iron treatment, BMDM differentiated in the presence of M-CSF were treated overnight with 75 µM of iron-nitrilotriacetate (FeNTA) before harvesting.

Isolation of splenic macrophages

Mouse splenic macrophages were magnetically separated from splenic cell suspensions in PBS-EDTA 2mM using anti-F4/80 biotin antibody and anti-biotin MicroBeads (MACS, Miltenyi Biotec), according to manufacturer's instructions. Briefly, spleens were smashed using a 100 µm cell strainer and splenic cell suspensions were subject to ACK lysing buffer (Gibco) to lyse red blood cells. The suspensions were then incubated for 30 minutes with anti-F4/80 biotin antibody (MACS, Miltenyi Biotec) at 4ºC, washed and incubated for 30 minutes with anti-biotin MicroBeads (MACS, Miltenyi Biotec) at 4ºC. After washing, splenic macrophages were isolated by magnetic cell sorting using MACS separation columns (Miltenyi Biotec).

RNA Extraction, Reverse transcription and qRT-PCR

RNA from tissues was isolated using Trizol (Life technologies). RNA from BMDM or splenic macrophages was isolated using the RNeasy Plus Mini Kit (Qiagen). Alveolar macrophages isolated through bronchoalveolar lavage from 6 mice were pooled and RNA extracted using the Arcturus PicoPure RNA Isolation kit (Life technologies). The concentration and purity of the RNA was determined by Nanodrop2000 (Thermo Scientific).
The isolated RNA was reverse transcribed in a 25 µl reaction mixture containing 1 µg (or 0,5 µg) of RNA, 0,4 mM dNTPs (Carl Roth GMBH), 100 units of RevertAid H Minus Reverse Transcriptase (Thermo Scientific), reaction buffer for RT (Thermo Scientific) and 8 ng/µl random oligomers as primers (invitrogen). After denaturating the RNA and primers for 10 minutes at 70°C, the mix was incubated at 42°C for 90 minutes and then at 70°C for 10 minutes to stop the reaction. The cDNA was diluted for subsequent quantitative reverse transcription-PCR (qRT-PCR) analysis by adding 475 µl of H_20 to cDNA obtained from tissues or 175 µl of H_20 to cDNA from cells.
SYBR green qRT-PCR was performed using the StepONE Plus real-time PCR system (Applied Biosystems), under the following amplification conditions: 95°C 10 minutes, (95°C 15 seconds, 60°C 1 minute) × 40 cycles. The primers used are listed in Table 1.1. Relative mRNA expression of the gene of interest was normalized to *Rpl19* (Ribosomal Protein L19) or *Ppia* (Peptidylprolyl isomerase A) mRNA expression. Results were calculated using the ΔΔCt method [225].

Table 1.1 - SYBR green qRT-PCR primers

	Primer Forward	Primer Reverse
TfR1	CCCATGACGTTGAATTGAACCT	GTAGTCTCCACGAGCGGAATA
Dmt1 IRE	AGCTAGGGCATGTGGCACTCT	ATGTTGCCACCGCTGGTATC
Fpn	TGTCAGCCTGCTGTTTGCAGGA	TCTTGCAGCAACTGTGTCACCG
HO-1	AGGCTAAGACCGCCTTCCT	TGTGTTCCTCTGTCAGCATCA
Rpl19	AGGCATATGGGCATAGGGAAGAG	TTGACCTTCAGGTACAGGCTGTG
Gm-csf	GCATGTAGAGGCCATCAAAGA	CGGGTCTGCACACATGTTA
M-csf	GGTGGACTGCCAGTATAGAAAG	TCCCATATGTCTCCTTCCATAAA
Tnfα	TGCCTATGTCTCAGCCTCTTC	GAGGCCATTTGGGAACTTCT
IL6	GCTACCAAACTGGATATAATCAGGA	CCAGGTAGCTATGGTACTCCAGAA
IL1β	GCAACTGTTCCTGAACTCAACT	ATCTTTTGGGGTCCGTCAACT
Cd11b	TGTCCCTGGCTGTTTCTACTG	ATTCTCCTTGCAGTTTTGGTG
Cd11c	TCGTATTTGGCTTCCCAGA	CCATCATTAGACACCGTCACAT
SiglecF	GAACTTACCTGGCACTGGTGTT	GCTCCACTCTGCAGGACTTT
Spi-C	TCCGCAACCCAAGACTCTTCAA	GGGTTCTCTGTGGGTGACATTCC
Hepcidin	ATACCAATGCAGAAGAGAAGG	AACAGATACCACACTGGGAA
Zip8	GCAACAATTTTGCTCCCAAT	TCCCTATGGAGATGTTTCTGTG
Zip14	TGGAACCCTCTACTCCAACG	CTGAGGGTTGAAGCCAAAAG
Ppia	ACGGCCGATGACGAGCCCTT	TCTCCAGTGCTCAGAGCTCGAAA
Cd205	CTGAAGGCTGGCACACTTT	CGATTCTTTCTATATGGAACACCTT
Cd14	AAAGAAACTGAAGCCTTTCTCG	AGCAACAAGCCAAGCACAC
Cxcl1	AGACCATGGCTGGGATTCAC	CGCGACCATTCTTGAGTGTG
Cxcl2	CCTGGTTCAGAAAATCATCCA	CTTCCGTTGAGGGACAGC
Ccl2	CATCCACGTGTTGGCTCA	GATCATCTTGCTGGTGAATGAGT
Ccl3	AGATTCCACGCCAATTCATC	GCCGGTTTCTCTTAGTCAGGA
Ccl4	CTCAGCCCTGATGCTTCTCAC	AGAGGGGCAGGAAATCTGAAC
Ccl20	AACTGGGTGAAAAGGGCTGT	GTCCAATTCCATCCCAAAAA

Tissue iron quantification

Tissue non-heme iron content was measured using the bathophenanthroline method and calculated against dry weight tissue [226]. Briefly, lung tissue was dried for 3 days at 45°C. Dried tissue was weighted and a solution of 10% TCA (Carl Roth), 10% HCl (Merck) was added in the proportion of 2µl of solution per 100µg of dried tissue, followed by incubation for 2 days at 65°C with mild shaking. After centrifugation at 2500g for 5 minutes to remove cell debris, the supernatant was used for iron quantification. A chromogenic solution of 3 M Na-acetate, 0,01% bathophenanthrolone-disulfonic acid, 0,1% thioglycolic acid was used and a non-chromogenic solution of 3 M Na-acetate, 0,1% thioglycolic acid was used as blank. Absorbance was measured in a spectrophotometer at 535 nm. Non-heme iron levels are given as µg of iron per gram of dried tissue.

Western blot

Protein lysates were obtained by homogenizing snap-frozen tissues or bone marrow-derived macrophages in RIPA buffer (10 mM Tris-HCl pH8, 150 mM NaCl, 1 mM EDTA, 1% NP-40, 0,1% SDS) supplemented with protease inhibitors (Roche Diagnostics), as previously described [227]. Lysates were incubated for 30 minutes on ice and debris was removed by centrifugation at 14500g at 4°C for 10 minutes. Protein concentration was determined using the DC protein assay following manufacturer's instructions (BioRad). 50 µg of protein were subjected to western-blot analysis with the antibodies listed in Table 1.2. Briefly, samples were mixed with 4x Laemmli buffer (250 mM Tris-HCl pH 6,8, 8% SDS, 40% glycerol, 10% β-mercaptoethanol, 0,08% bromophenol blue) and denaturated by heating at 95°C for 5 min. Samples were not denatured for FPN protein analysis. After running the samples on a 12% SDS-PAGE, the proteins were transferred to a PVDF membrane using wet transfer method. The membrane was blocked with 5% nonfat dry milk in TBS-T buffer (20 mM Tris-HCl pH 7,6, 150mM NaCl, 0,1% Tween-20) for 1 hour at room temperature. Primary antibodies were incubated for 1 hour at room temperature or overnight at 4°C. After washing the membrane with TBS-T, the membranes were incubated with secondary antibodies for 1 hour at room temperature (anti-rabbit IgG, anti-goat IgG or anti-mouse IgG from Sigma-Aldrich). After washing the membrane with TBS-T, ECL-Plus substrate (Amersham Biosciences) was used to visualize the immune complexes formed on the blot. Western blot images were quantitatively acquired with the Vilber Lourmat Fusion-FX Chemiluminescence system (Eberhardzell). β-actin was used as loading control.

Table 1.2 - Antibodies used for Western Blot (WB), immunohistochemistry (IHC) and immunocytochemistry (ICC)

Antigen	Host	WB dilution	IHC dilution	ICC dilution	Reference/Supplier
FPN	rabbit	1:500	/	1:200	MTP11-A / Alphadiagnostics
DMT1	rabbit	/	1:100	/	Gently provided by Dr. Bruno Galy [228]
FtL	goat	1:500	/	/	sc-14420 / SCBT
TfR1	mouse	1:1000	/	/	136800 / Invitrogen
β-actin	mouse	1:5000	/	/	A1978 / Sigma-Aldrich
β-tubulin IV	mouse	/	1:500	/	MU178-UC / Biogenex
proSP-C	rabbit	/	1:5000	/	ab28744-50 / Abcam
α-SMA	rabbit	/	1:300	/	ab5694 / Abcam
ZIP8	rabbit	2 µg/ml	/	/	Gently provided by Dr. Mitchell Knutson
Desmin	rabbit	/	1:100	/	Abcam

Lipid peroxidation - TBARS measurements

Thiobarbituric acid reactive substances (TBARS) levels were measured in samples of mouse total lung using the QuantiChrom TBARS Assay Kit (BioAssay Systems) following manufacturer's instructions.

Iron quantification in the bronchoalveolar lavage fluid supernatant

BAL fluid supernatant was concentrated through Speed-Vacuum. Iron measurements were performed using the SFBC kit (Biolabo) following manufacturer's instructions.

Measurement of cytokine protein levels in bronchoalveolar lavage fluid supernatant

Cytokine protein levels were determined in BAL fluid supernatant (50 µl) by applying Multiplex bead-array based technology. Measurements were performed on a BioPlex200 System using the Bio-Plex Pro Cytokine Reagent Kit and Bio-Plex Pro Mouse Cytokine sets (Bio-Rad) according to manufacturer's instructions. Cytokine protein levels are given as picograms (pg) in total BAL fluid supernantant.

Flow cytometry analysis

Cells obtained from BAL were stained with CD45.2, CD11c and SiglecF antibodies for 30 minutes on ice (antibody dilutions and catalog numbers are reported in Table 1.3). To measure oxidative stress, BAL cells and BMDM were incubated for 30 minutes at room temperature with 5 µM CellROX Green reagent (ThermoFisher). After washing, cells were analyzed by flow cytometry using the BD LSRFortessa Cell Analyzer.

Table 1.3 - Antibodies used for Flow cytometry

Antigen	Dilution	Reference/Supplier
CD45.2	1/200	109820 / Biolegend
CD11c	1/200	550261 / BD Pharmingen
SiglecF	1/200	552126 / BD Pharmingen

Lung Function

Mice were anesthetized via intraperitoneal injection of Na^+-pentobarbital (80 mg/kg), tracheostomized and placed on the FlexiVent system (SCIREQ, Montreal, QC, Canada) for measurements of pulmonary function. Mice were then paralyzed with pancuronium bromide injected intraperitoneally (0,8 mg/kg) to avoid breathing artefacts during the measurement. Mice were mechanically ventilated at a frequency of 150 breaths/minute, with a tidal volume of 11 mL/kg and a positive end expiratory pressure of 3 cm H_2O to prevent alveolar collapse. A maximum pressure of 30 cm H_2O and a maximum volume of 1-2 mL were used to prevent hyperinflation of the lung. Pressure-volume curves, total lung capacity, pulmonary compliance and elastance were measured as previously described [172, 229]. All perturbations were performed until at least three acceptable measurements were reached. Mice were then sacrificed by exsanguination.

Blood Oxygen Saturation

Blood oxygen saturation was determined using a noninvasive pulse oximeter for laboratory animals (MouseOx® Plus, Starr life science) following manufacturer's instructions. Arterial blood oxygen saturation was analyzed in conscious mice exposed to room air with a thigh clip sensor. The oxygen saturation was measured when pulse waves were stable and regular in order to obtain valid values.

Immunohistochemistry

Lungs were inflated with 4% neutral buffered formalin (Fischar) to 25 cm of fixative pressure, fixed overnight by immersion in the same solution, dehydrated and paraffin embedded. Lungs were sectioned at 1,5 or 5 µm and mounted on Superfrost Plus slides (Thermo scientific). Lung sections were rehydrated and treated for 10 minutes with 3% H_2O_2 (Sigma Aldrich) to block endogenous peroxidases. After washing in distilled water, tissue slides were subjected to microwave-mediated antigen retrieval using the Citraplus reagent (Biogenex). After 30 minutes of cooling, slides were washed 3 times in PBS and subjected to immunorecognition using the Vectastain ABC mouse and rabbit kits (Vector Lab, Burlingame, CA, USA) following manufacturer's instructions. Antibody dilutions and catalog numbers are reported in Table 1.2. Isotype antibodies were used at the same concentration as the primary antibodies to control for antibody specificity. Tissue slides were developed using the Vector AEC substrate (Vector lab), rinsed with distilled water, counterstained with Hematoxylin, washed in PBS and mounted using the VectaMount AQ mounting medium (Vector lab). Images were digitally acquired with a Nikon Ni-E microscope, using the Nikon NIS-Elements software.

Immunocytochemistry

BAL cells in cytospin preparations were fixed in cold acetone (-20ºC) for 10 minutes, washed in PBS and treated for 10 minute with 3% H_2O_2 (Sigma Aldrich) to block endogenous peroxidases. After washing in PBS, slides were subjected to immunorecognition using the Vectastain ABC rabbit kit (Vector Lab, Burlingame, CA, USA) following manufacturer's instructions. FPN antibody dilution and catalog number are reported in Table 1.2. An isotype antibody was used at the same concentration as the primary antibody to control for antibody specificity. Cytospin preparations were developed using the Vector AEC substrate (Vector lab), rinsed with distilled water, counterstained with Hematoxylin, washed in PBS and mounted using the VectaMount AQ mounting medium (Vector lab). Images were digitally acquired with a Nikon Ni-E microscope, using the Nikon NIS-Elements software. Splenic cells in cytospin preparations were subjected to the same protocol and used as a positive control for FPN immunocytochemistry.

DAB-enhanced Perls' stain

Lungs were inflated with 4% neutral buffered formalin (Fischar) to 25 cm of fixative pressure, fixed overnight by immersion in the same solution, dehydrated and paraffin embedded. Lungs were sectioned at 1,5 or 5 µm and mounted on Superfrost Plus slides (Thermo scientific). Lung sections were rehydrated and stained for 10 minutes with potassium ferrocyanide/HCl solution

(Sigma Aldrich). After washing in distilled water, slides were treated with 3,3-diaminobenzidinetetrahydrochloride (DAB) (Sigma Aldrich). Slides were washed again in distilled water, counterstained with Hematoxylin, washed in PBS, dehydrated and mounted using the Eukitt quick-hardening mounting medium (Sigma Aldrich). Images were digitally acquired with a Nikon Ni-E microscope, using the Nikon NIS-Elements software.

Perls' stain

BAL cells in cytospin preparations were stained with potassium ferrocyanide solution/HCl (Sigma Aldrich), washed in distilled water and counterstained with Fast Red (Sigma Aldrich). Images were digitally acquired with a Nikon Ni-E microscope, using the Nikon NIS-Elements software.

Hematoxylin and eosin stain

Paraffin lung sections were rehydrated and stained for 6 minutes with Mayer's Hematoxylin (Sigma Aldrich). Slides were washed in water, rinsed in HCl/EtOH, washed again in water and stained for 1 minute with Eosin Y (Sigma Aldrich). Slides were dehydrated and mounted using the Entellan new mounting medium (Merck).

Masson Goldner Trichrome Stain

Paraffin lung sections were rehydrated and stained with Masson Goldner Trichrome Staining Kit (Carl Roth) following manufacturer's instructions.

Analysis of lung collagen content

Paraffin lung sections (3 µm) were stained with 0,1% Sirius red solution as previously described [230]. The degree of fibrosis was calculated by the analysis of the total amount of collagen in the left lung using a Leica QWin V3 computer assisted image analysis software (Leica Microsystem, Wetzlar, Germany). For evaluation of the percentage of collagen, the collagen positive areas (red fibers) were determined in a minimum of 300 images per animal.

Stereology of lung tissue

Lungs from 36 week old mice were instilled via the trachea with 1,5% paraformaldehyde, 1,5% glutaraldehyde in 0,15 M Hepes buffer at hydrostatic pressure of 25 cm and stored in the same solution at 4°C until further processing. The lungs were embedded in glycol methacrylate according to standard protocol [231] and 1,5 µm thick sections were cut. Light microscopy was

performed using a Leica DM6000B microscope (Leica, Wetzlar, Germany) attached to a computer with the newCAST stereology software (Visiopharm, Horsholm, Denmark). Design-based stereology was used to quantify the volume of the lung parenchyma and non-parenchyma as previously described [231].

Erythropoietin (EPO) ELISA

Blood was centrifuged at 2000g for 10 minutes and plasma EPO levels were determined using a mouse EPO ELISA kit (R&D systems) following manufacturer's instructions.

CCL2 ELISA

Blood was centrifuged at 2000g for 10 minutes and plasma CCL2 levels were determined using a mouse CCL2 ELISA kit (R&D systems) following manufacturer's instructions.

Statistical analyses

Data are shown as mean ± standard error of the mean (SEM) and the number of mice (n) is indicated. Statistical analyses were performed using Prism v6 (GraphPad Software, La Jolla, CA). For comparisons between 2 groups, the two-tailed, Student's t-test was used. For comparisons between 3 or 4 groups, a one-way or two-way ANOVA with the Bonferroni post-test was used. p-values <0.05 (*), <0.01 (**), <0.001 (***) and <0.0001 (****) are indicated.

Chapter III

Results

Increased pulmonary iron content in Slc40a1^{C326S} mice

The Slc40a1^{C326S} mouse model exhibits a phenotype that resembles human hereditary hemochromatosis type 4, presenting elevated plasma iron levels, high transferrin saturation, parenchymal iron overload, and iron depletion in iron-exporting tissues such as duodenal enterocytes and reticuloendothelial macrophages [102].

To assess whether a disruption in the hepcidin/FPN regulatory circuitry affects pulmonary iron content, lungs from wild-type (Slc40a1$^{wt/wt}$), heterozygous (Slc40a1$^{wt/C326S}$) and homozygous (Slc40a1$^{C326S/C326S}$) mutant male and female mice were analyzed at different ages. Measurements of non-heme iron levels revealed a genotype-specific and age-dependent increase in pulmonary iron content in Slc40a1^{C326S} mice, regardless of the gender (Fig. 2.1A).

To confirm that the increase in pulmonary iron content observed in Slc40a1$^{C326S/C326S}$ is caused by the disruption of the hepcidin/FPN regulatory circuitry and is not a direct consequence of the C326S point mutation *per se*, we compared the lung non-heme iron content of Slc40a1$^{C326S/C326S}$ mice and hepcidin knock out (*Hamp*$^{-/-}$) mice – both mouse models present a disrupted hepcidin/FPN system but result from different genetic mutations. As observed in Fig. 2.1B, pulmonary iron levels are similar between Slc40a1$^{C326S/C326S}$ and *Hamp*$^{-/-}$ mice and increased when compared to wild-type mice, indicating that the increased lung iron content of Slc40a1$^{C326S/C326S}$ mice results from a non-functional hepcidin/FPN system.

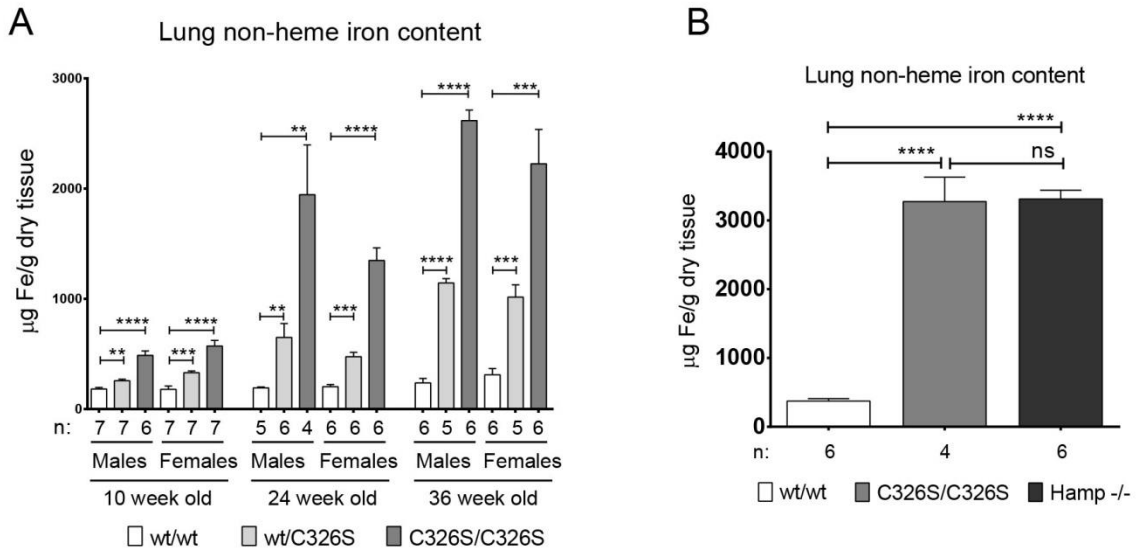

Figure 2.1 – Lung iron content of Slc40a1^{C326S} mice

(A) Total lung non-heme iron levels measured in 10-, 24- and 36-week old male and female mice.

(B) Total lung non-heme iron levels measured in 50-week old male mice.

ns – non-significant

A molecular analysis of iron-related genes in the lung was performed to evaluate whether their expression responds to increased pulmonary iron content. At mRNA level, the expression of *TfR1* and *Dmt1* isoform containing an IRE are decreased in Slc40a1$^{wt/C326S}$ and Slc40a1$^{C326S/C326S}$ mice (Fig. 2.2A, B). TfR1 is decreased also at the protein level and correlates with an increase in FtL protein levels (Fig. 2.2C). FPN shows a genotype-specific upregulation both at mRNA and protein levels (Fig. 2.2C, D).

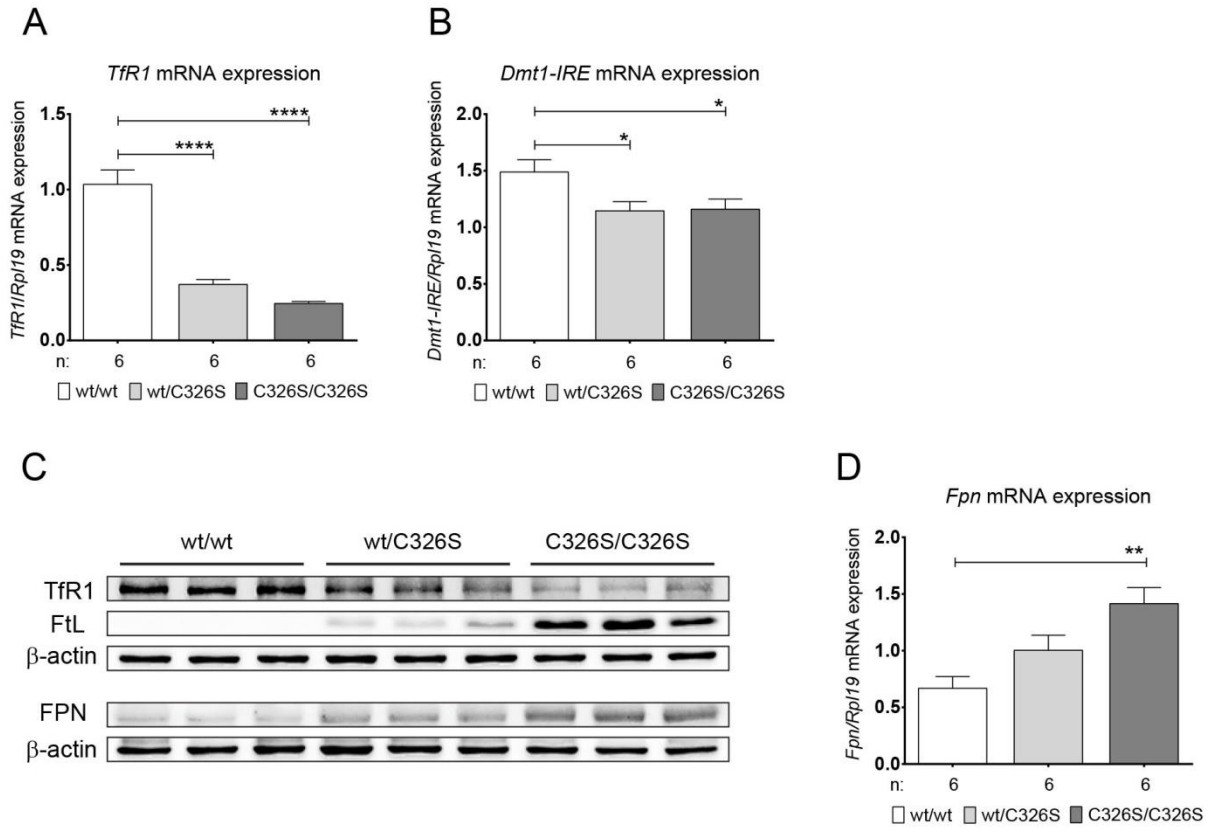

Figure 2.2 – Expression of iron-related genes in the lung of Slc40a1^{C326S} mice

(A) qRT-PCR analysis of *TfR1* mRNA expression in total lung of 36-week old female mice.

(B) qRT-PCR analysis of *Dmt1 IRE* mRNA expression in total lung of 36-week old female mice.

(C) Western blot analysis of TfR1 (~100 kDa), FtL (~20 kDa), and FPN (~65 kDa) protein expression in total lung of 36-week old female mice. β-actin (42 kDa) was used as loading control.

(D) qRT-PCR analysis of *Fpn* mRNA expression in total lung of 36-week old female mice.

We have also analyzed the expression of two recently identified iron transporters: ZIP8 and ZIP14, which were reported to mediate the uptake of NTBI [232]. We observed that *Zip8* is highly expressed in the lung compared to the liver (Fig. 2.3A), an observation that supports a study by Wang and colleagues [46]. The same group has shown that ZIP8 protein levels increase in response to iron loading due to a post-transcriptional mechanism, without alterations

at the mRNA level [46]. Consistently, we did not detect differences in pulmonary *Zip8* mRNA levels between wild-type and Slc40a1^{C326S} mice (Fig. 2.3A, B). However, we also did not observe an increase in ZIP8 protein levels in the lung of Slc40a1^{C326S} mice (Fig. 2.3C). Like ZIP8, ZIP14 expression is up-regulated by iron in a post-transcriptional manner [45]. In agreement, we did not detect differences in *Zip14* mRNA levels in the lung of Slc40a1$^{C326S/C326S}$ mice when compared with wild-type controls (Fig. 2.3D). Unfortunately, we failed to detect ZIP14 protein in lung lysates by Western blot analysis (data not shown).

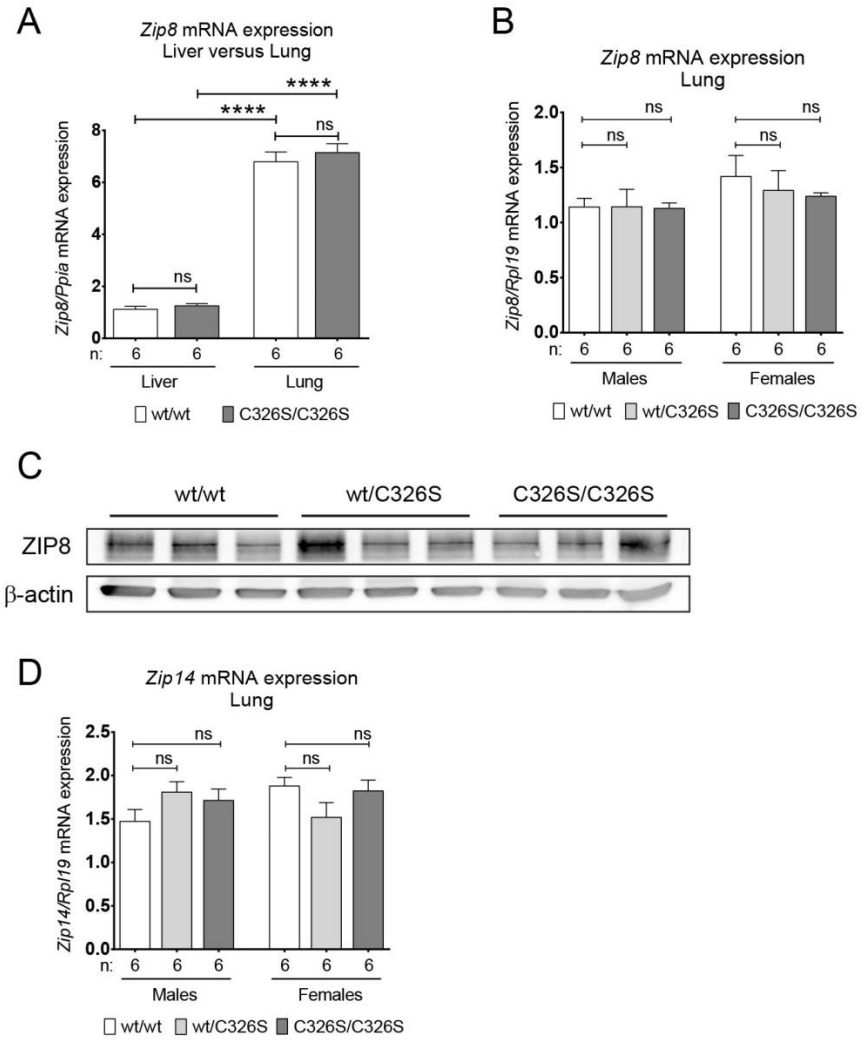

Figure 2.3 – Expression of Zip8 and Zip14 in wild-type and Slc40a1^{C326S} mice.

(A) qRT-PCR analysis of *Zip8* mRNA expression in total lung and liver of 36-week old female mice.

(B) qRT-PCR analysis of *Zip8* mRNA expression in total lung of 36-week old male and female mice.

(C) Western blot analysis of ZIP8 (~150 kDa) protein expression in total lung of 36-week old female mice. β-actin (42 kDa) was used as loading control.

(D) qRT-PCR analysis of *Zip14* mRNA expression in total lung of 36-week old male and female mice.

ns – non-significant

Hepcidin expression in the liver of Slc40a1$^{C326S/C326S}$ mice increases in response to increased iron levels [102] (Fig. 2.4). We have analyzed its expression in the lung and have detected extremely low hepcidin mRNA levels in this organ compared to the liver (Fig. 2.4). Moreover, lung hepcidin levels do not respond to increased pulmonary iron content as no differences were observed between wild-type and Slc40a1$^{C326S/C326S}$ mice (Fig. 2.4).

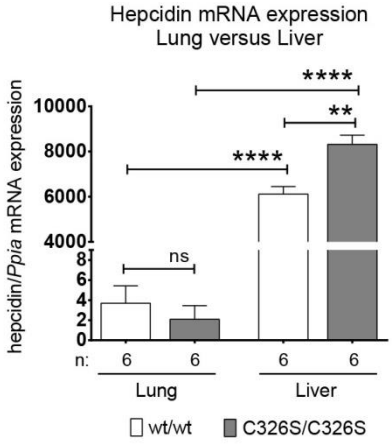

Figure 2.4 – Hepcidin expression in the lung and liver of wild-type and Slc40a1$^{C326S/C326S}$ mice

qRT-PCR analysis of hepcidin mRNA expression in total lung and total liver of 36-week old female mice.

ns – non-significant

Excess of iron can lead to the generation of reactive oxygen species (ROS), which cause deleterious effects by damaging proteins, lipids, and DNA [102, 233]. Increased iron levels in the lung of Slc40a1$^{C326S/C326S}$ mice are associated with increased HO-1 expression, a marker of oxidative stress, and with increased lipid peroxidation, as shown by an increase in thiobarbituric acid reactive substances (TBARS) (Fig. 2.5).

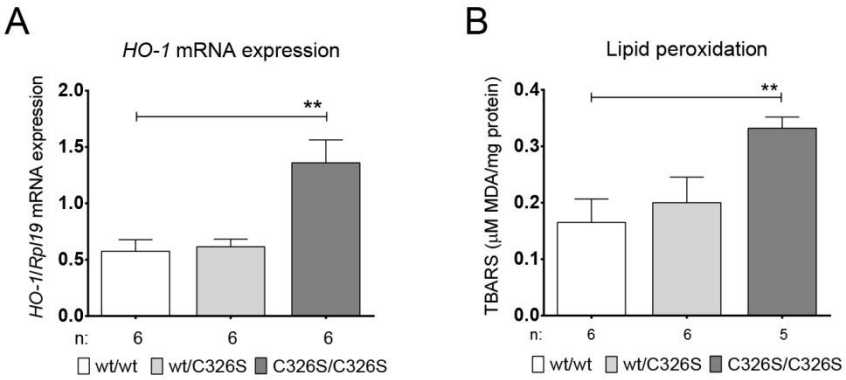

Figure 2.5 – Markers of oxidative stress in the lung of Slc40a1^{C326S} mice.

(A) qRT-PCR analysis of HO-1 mRNA expression in total lung of 36-week old female mice.

(B) Lipid peroxidation measured through the TBARS assay in total lung of 36-week old female mice.

Iron accumulation in the lung of Slc40a1^{C326S} mice is restricted to specific cell types

Histological analysis of the lung of Slc40a1^{C326S} mice confirmed the iron overload phenotype (Fig. 2.6). Furthermore, it revealed that iron does not accumulate uniformly in all lung cell types but it is instead restricted to specific sub-sets of the lung cell population (Fig. 2.6).

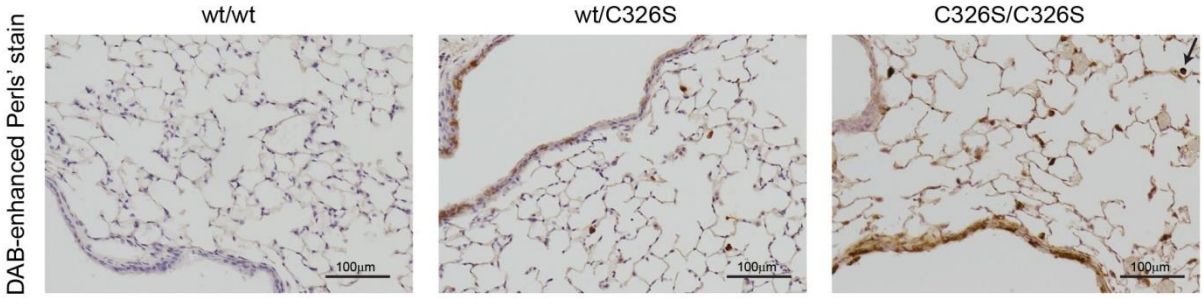

Figure 2.6 – Iron accumulation in the lung of Slc40a1^{C326S} mice is restricted to specific cell types

DAB-enhanced Perls' stain of lung sections of 36-week old female mice. The arrow shows an alveolar macrophage with strong iron accumulation.

It has been previously proposed that airway epithelial cells can take up iron from the airway lumen via DMT1 [204]. Using β-tubulin IV as a marker of cilia, we detected DMT1 mainly at the apical membrane of ciliated airway epithelial cells in wild-type mice (Fig. 2.7A). In line with this observation, iron was frequently detected in ciliated epithelial cells lining the conducting airways of Slc40a1$^{C326S/C326S}$ mice (Fig. 2.7B, C).

Iron deposition was occasionally detected in another epithelial cell type – alveolar type 2 cells (Fig. 2.8). These secretory cells are present in the alveolar epithelium and can be identified by the expression of the prosurfactant protein C.

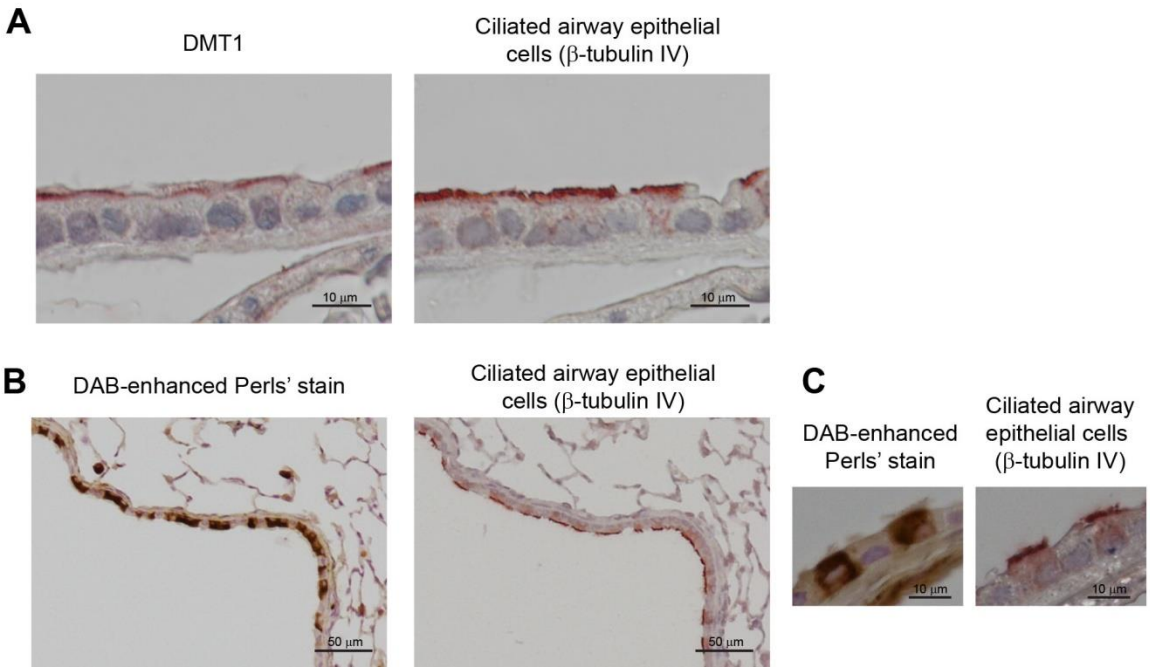

Figure 2.7 – Iron accumulation in ciliated airway epithelial cells of Slc40a1$^{C326S/C326S}$ mice.

(A) Immunohistochemistry for DMT1 (left) and β-tubulin IV (right) of consecutive lung sections from 36-week old female wild-type mice.

(B) DAB-enhanced Perls' stain (left) and immunohistochemistry for β-tubulin IV (right) of consecutive lung sections from 26-week old female Slc40a1$^{C326S/C326S}$ mice.

(C) Higher magnification of DAB-enhanced Perls' stain (left) and immunohistochemistry for β-tubulin IV (right) of consecutive lung sections from 26-week old female Slc40a1$^{C326S/C326S}$ mice.

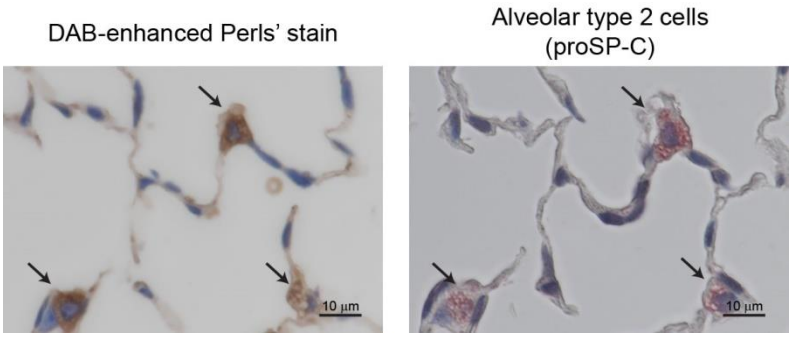

Figure 2.8 – Iron accumulation in alveolar type 2 cells of Slc40a1$^{C326S/C326S}$ mice.

DAB-enhanced Perls' stain (left) and immunohistochemistry for prosurfactant protein C (proSP-C, right) of consecutive lung sections from 36-week old female Slc40a1$^{C326S/C326S}$ mice.

In addition, we detected iron accumulation in vascular smooth muscle cells (SMC) in the lung of Slc40a1$^{C326S/C326S}$ mice, which were identified by the expression of alpha smooth muscle actin (αSMA) (Fig. 2.9A). However, we have also detected iron-spared vascular SMCs (Fig. 2.9B), suggesting that the lung contains different populations of vascular SMCs in regard to iron trafficking. Interestingly, iron accumulates in vascular SMCs that express low levels of desmin whereas vascular SMCs expressing high levels of desmin are iron-spared (Fig. 2.10A). The disparity in desmin expression between different vascular SMCs is not a consequence of the C326S point mutation and/or alterations in iron levels since a differential expression of desmin between different vascular SMCs was also observed in wild-type mice (Fig. 2.10B).

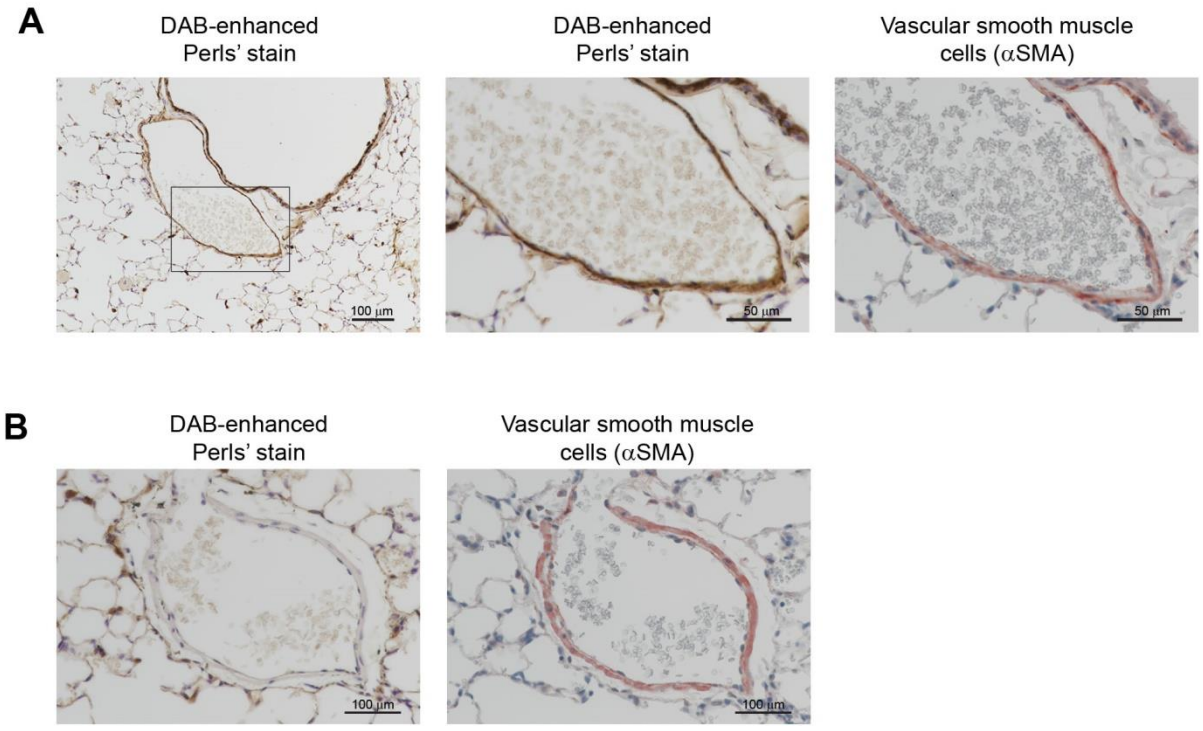

Figure 2.9 – Iron accumulation in lung vascular smooth muscle cells of Slc40a1$^{C326S/C326S}$ mice.

(A) DAB-enhanced Perls' stain (left and center) and immunohistochemistry for alpha smooth muscle actin (αSMA) (right) of consecutive lung sections from 36-week old female Slc40a1$^{C326S/C326S}$ mice.

(B) DAB-enhanced Perls' stain (left) and immunohistochemistry for alpha smooth muscle actin (αSMA; right) of consecutive lung sections from 36-week old female Slc40a1$^{C326S/C326S}$ mice.

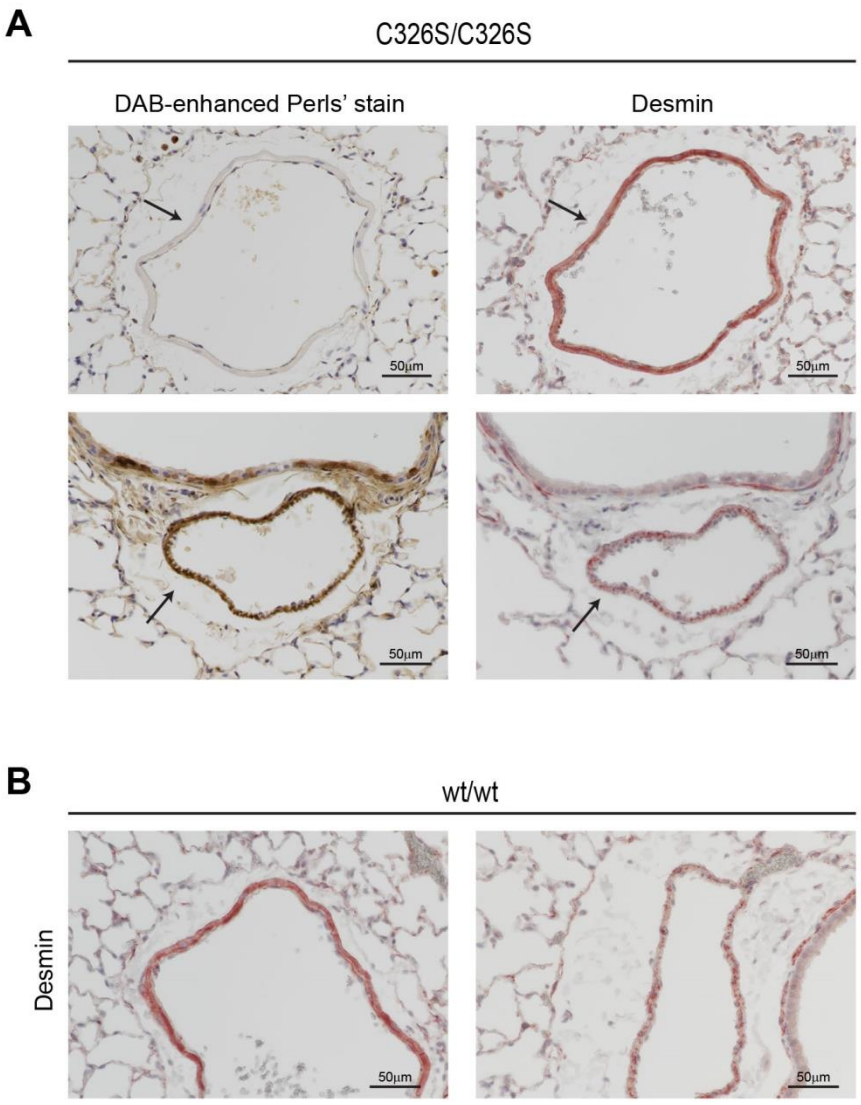

Figure 2.10 – Iron accumulates differently in functionally distinct vascular smooth muscle cells.

(A) DAB-enhanced Perls' stain (left) and immunohistochemistry for desmin (right) of consecutive lung sections from 36-week old female Slc40a1$^{C326S/C326S}$ mice. Arrows indicate vascular SMCs.

(B) Immunohistochemistry for desmin of lung sections from 36-week old female wild-type mice.

It is important to mention that increased iron levels were also detected extracellularly in the bronchoalveolar lavage (BAL) fluid of Slc40a1^{C326S} mice (Fig. 2.11).

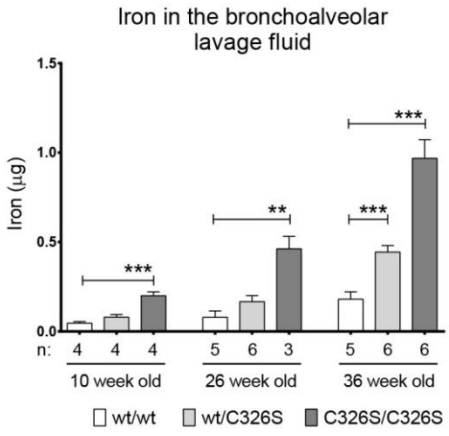

Figure 2.11 – Iron accumulates extracellularly in the bronchoalveolar space of Slc40a1$^{C326S/C326S}$ mice.
Iron levels measured in the bronchoalveolar lavage (BAL) fluid supernatant of 10-, 26- and 36-week old mice.

Iron loaded alveolar macrophages in Slc40a1^{C326S} mice

Iron deposition in alveolar macrophages (AM) has been observed in different lung diseases [218, 219]. Interestingly, histological analysis of lung sections from Slc40a1$^{C326S/C326S}$ mice revealed the presence of strongly iron loaded AMs (Fig. 2.6 arrow). To further confirm this observation, we analyzed the cellular fraction of the BAL. Differential May-Grünwald-Giemsa stain of cytospin preparations showed that AMs were the predominant cell type in the BAL fluid of wild-type and Slc40a1$^{C326S/C326S}$ mice (Fig. 2.12A, B). This analysis further revealed that the total number of cells in the BAL fluid of Slc40a1$^{C326S/C326S}$ mice was increased when compared to wild-type animals, mainly due to an increase in the number of AMs (Fig. 2.12B). The identity of AMs was additionally confirmed by flow cytometry (gating strategy Fig. 2.12C) – more than 90% of the immune cells in the BAL fluid of both wild-type and Slc40a1$^{C326S/C326S}$ mice corresponded to AMs (CD45.2^{+} CD11c^{+} SiglecF^{+}) (Fig. 2.12D) [176].

The increase in the number of AMs can result either from proliferation of a progenitor population within the lung or from recruitment of circulating monocytes (reviewed in [123]). Interestingly, the plasma levels of CCL2 in Slc40a1$^{C326S/C326S}$ mice have a strong tendency to be increased (p-value = 0,06), which may directly contribute to the recruitment of monocytes and, as a consequence, to an increase in the number of macrophages (Fig. 2.13A). We further analyzed the mRNA levels of different chemokines in the lung of Slc40a1$^{C326S/C326S}$ mice. The mRNA levels of C-C motif chemokine ligand (Ccl) 2, *Ccl3*, *Ccl4, Ccl20* and C-X-C motif chemokine ligand (Cxcl) 2 were not significantly up-regulated in the lung of Slc40a1$^{C326S/C326S}$ mice but we observed a small increase in the expression levels of *Cxcl1* (Fig. 2.13B-G). We have also analyzed the expression levels of two cytokines involved in macrophage differentiation: macrophage colony-stimulating factor (*M-csf*), which was decreased in the lung of Slc40a1$^{C326S/C326S}$ mice, and granulocyte macrophage colony-stimulating factor (*Gm-csf*), which showed a robust increase (Fig. 2.13H, I). The increase in *Gm-csf* mRNA levels is of particular interest as this cytokine is a key player in the differentiation of AMs. Additional studies will be necessary to understand the underlying mechanism causing the increase in the number of AMs in Slc40a1$^{C326S/C326S}$ mice.

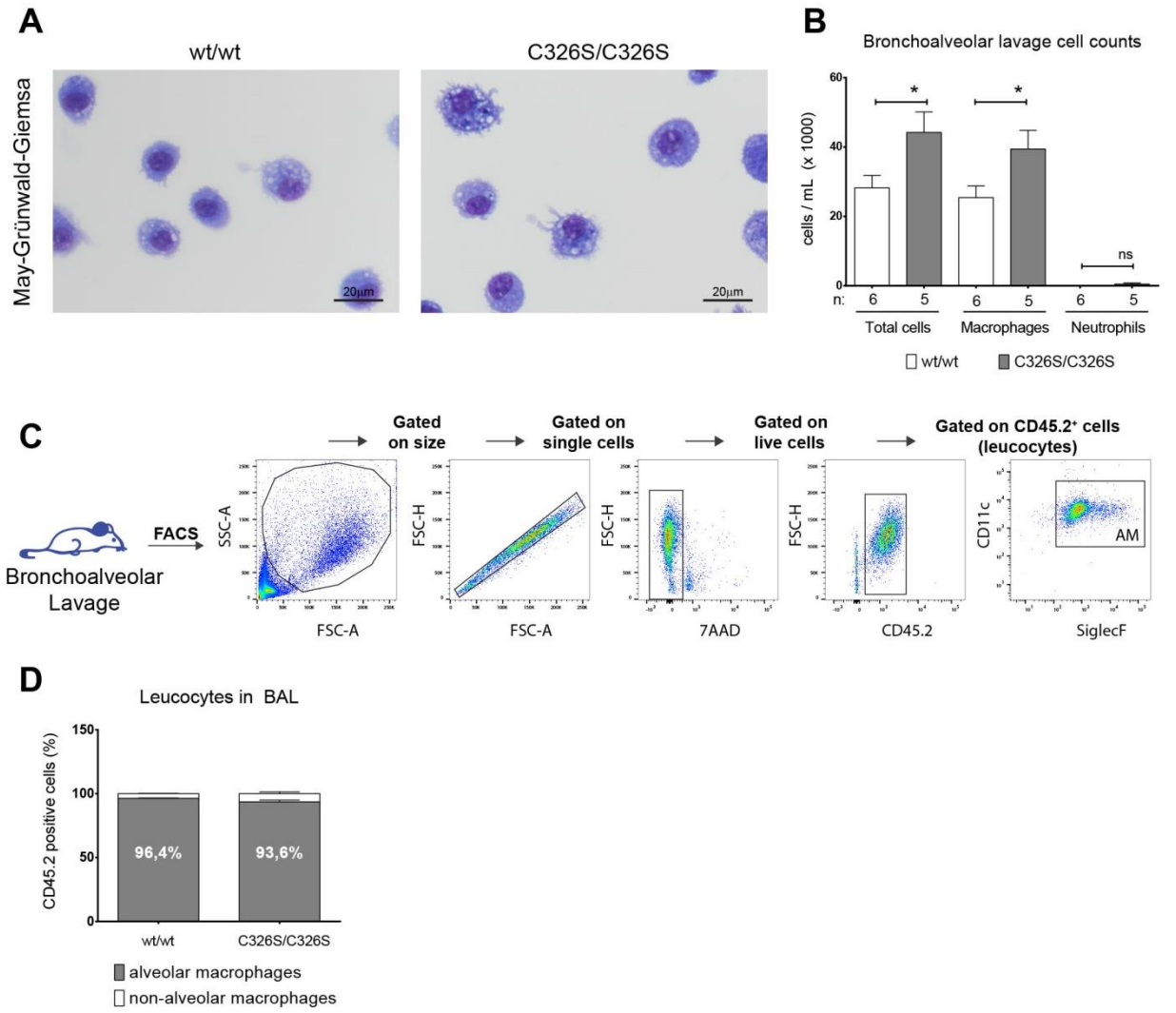

Figure 2.12 – Alveolar macrophages in the bronchoalveolar space of Slc40a1$^{C326S/C326S}$ mice

(A) May-Grünwald-Giemsa stain of cytospin preparations obtained from the bronchoalveolar lavage of 26-week old male mice.

(B) Total cell count and differential cell count of the cell fractions of the bronchoalveolar lavage of 26-week old male mice.

(C) Gating strategy used to identify the cells present in the bronchoalveolar lavage fluid of wild-type and Slc40a1$^{C326S/C326S}$ mice.

(D) Percentage of AM (CD11c^{+} Siglec^{+}) present in the leukocyte fraction (CD45.2^{+}) in the bronchoalveolar lavage fluid of 24-week old male mice (n=3).

ns – non-significant

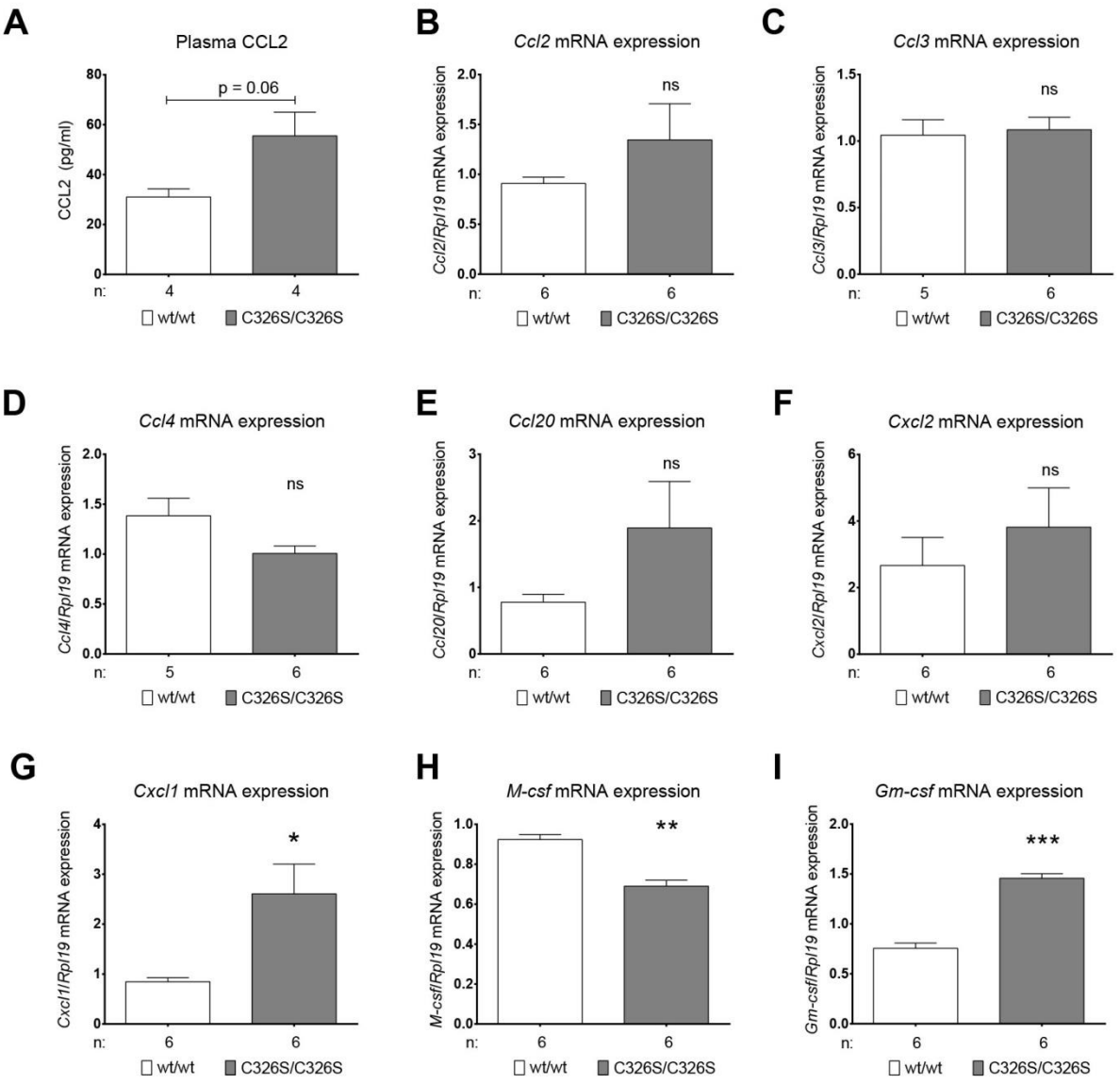

Figure 2.13 – Expression of cytokines in Slc40a1$^{C326S/C326S}$ mice

(A) CCL2 protein levels measured in the plasma of 13-week old mice.

(B-I) qRT-PCR analysis of *Ccl2* (B), *Ccl3* (C), *Ccl4* (D), *Ccl20* (E), *Cxcl2* (F), *Cxcl1* (G), *M-csf* (H) *and Gm-csf* (I) mRNA expression in total lung of female mice.

ns – non-significant

The presence of iron-loaded AMs in Slc40a1$^{C326S/C326S}$ mice was confirmed by Perls' stain on cytospin preparations of BAL cells (Fig. 2.14A). Intracellular iron accumulation in AMs distinguishes them from hepatic Kupffer cells and splenic macrophages in Slc40a1$^{C326S/C326S}$ mice: these cells are iron depleted due to uncontrolled iron export caused by the resistance of FPN to hepcidin binding [102]. Curiously, we also detected iron spared AMs in BAL cytospin preparations from Slc40a1$^{C326S/C326S}$ mice (Fig. 2.14A arrow). This finding indicates that the population of AMs in Slc40a1$^{C326S/C326S}$ mice is heterogeneous regarding iron handling. This heterogeneity in iron accumulation correlates with a heterogeneous expression of FPN in AMs from Slc40a1$^{C326S/C326S}$ mice, probably explaining the phenotype (Fig. 2.14B). Interestingly, we could not detect FPN in AMs from wild-type mice (Fig. 2.14B).

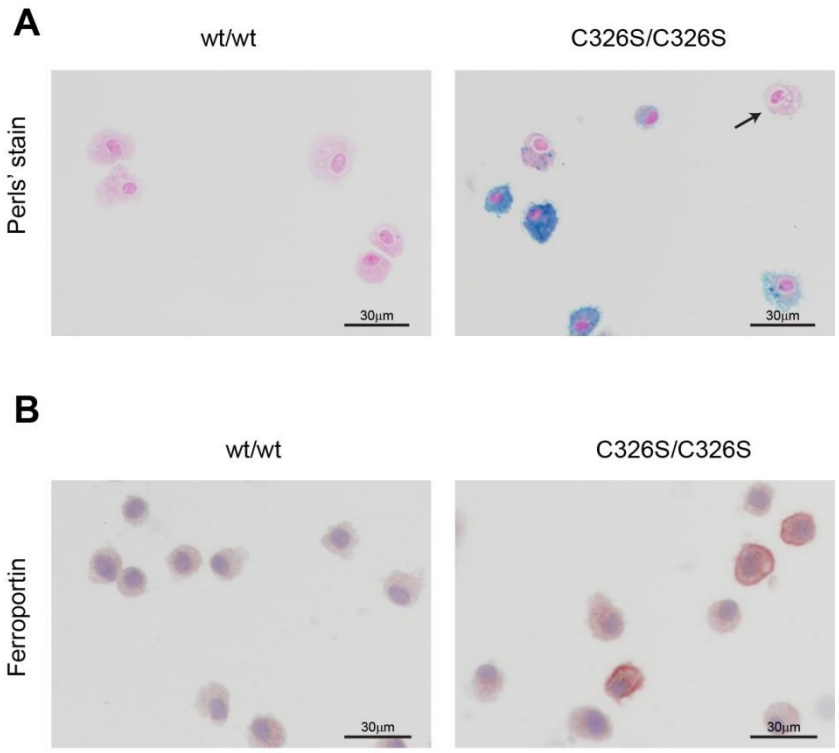

Figure 2.14 – Iron loaded alveolar macrophages in Slc40a1$^{C326S/C326S}$ mice

(A) Perls' stain of cytospin preparations of cells isolated from the bronchoalveolar lavage fluid of 24-week old male mice. Arrow shows an iron spared alveolar macrophage.

(B) Immunocytochemistry for FPN in cytospin preparations of cells isolated from the bronchoalveolar lavage fluid of 24-week old male mice.

To further confirm the absence of FPN expression in AMs isolated from wild-type mice, we analyzed the mRNA levels of *Fpn* in these cells. To this end, we compared AMs, which were isolated from the bronchoalveolar lavage and identified by the expression of high levels of the AM markers *Cd11c* and *SiglecF*, to splenic macrophages, which were isolated through magnetic cell sorting and identified by the expression of high levels of the markers *Cd11b* and *Spi-C* (Fig. 2.15A-D). We observed that AMs express very low levels of *Fpn* mRNA in comparison to splenic macrophages (Fig. 2.15E).

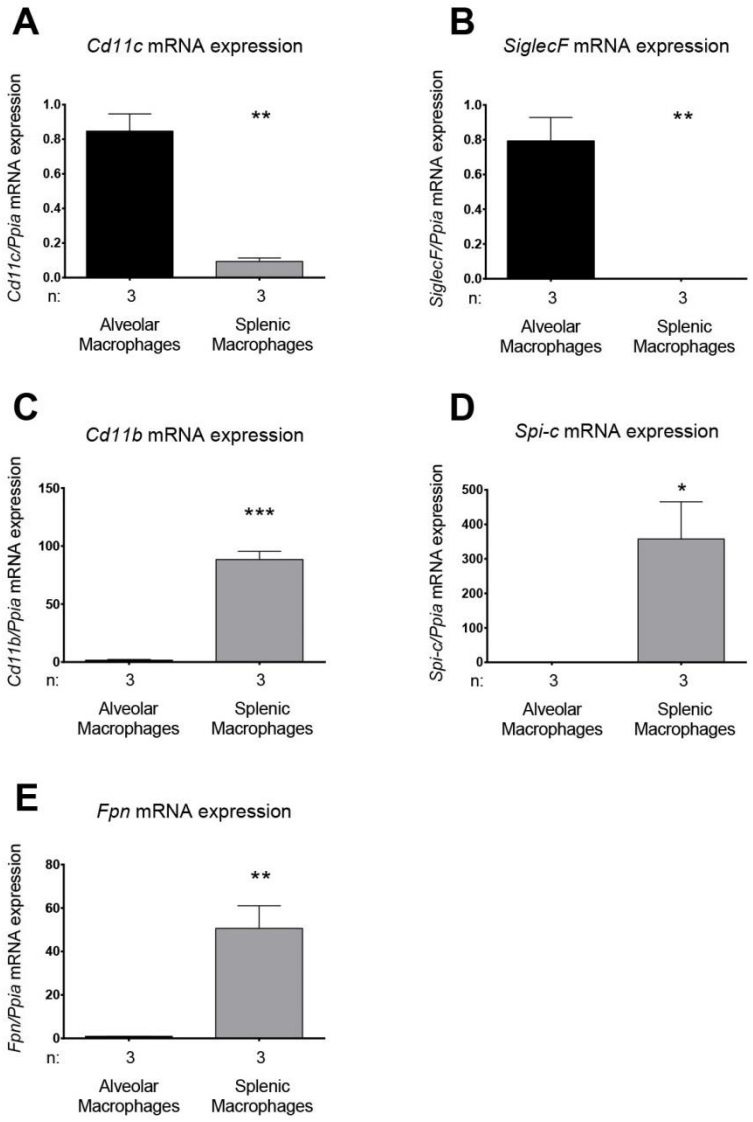

Figure 2.15 – Comparison between alveolar macrophages and splenic macrophages isolated from wild-type mice

qRT-PCR analysis of *Cd11c* (A), *SiglecF* (B), *Cd11b* (C), *Spi-C* (D), and *Fpn* (E) mRNA expression in alveolar macrophages and splenic macrophages isolated from 12-week old wild-type mice.

Ferroportin transcription is regulated by different mechanisms, which mostly depend on the cell type. For example, ferroportin transcription in duodenal enterocytes is mainly regulated by hypoxia [84] while reticuloendothelial macrophages control ferroportin expression via a heme-dependent pathway [91]. How ferroportin expression is regulated in AMs is still unknown.

GM-CSF is a key regulator of the differentiation of AMs: GM-CSF$^{-/-}$ mice fail to generate mature and functional AMs [180]. Interestingly, GM-CSF was reported to repress FPN expression in monocyte-derived macrophages after stressed erythrocyte challenge [234]. Since GM-CSF is highly expressed in the lung compared to the spleen (Fig. 2.16A), where macrophages express FPN, it is possible that GM-CSF represses ferroportin expression in AMs.

To test this hypothesis, we differentiated bone marrow hematopoietic progenitors *in vitro* in the presence of GM-CSF and compared them to bone marrow hematopoietic progenitors differentiated in the presence of M-CSF – cytokine that is commonly used to differentiate bone marrow-derived macrophages (BMDM) *in vitro*. We observed that BMDM differentiated in the presence of GM-CSF upregulate the expression of AMs markers *SiglecF*, *Cd11c*, and *Cd205* (Fig. 2.16B-D) [123, 175, 176]. Moreover, the presence of GM-CSF leads to a downregulation of *Cd14*, which is also expressed at intermediate/low levels in AMs (Fig. 2.16E) [123, 176]. These observations indicate that BMDM differentiated in the presence of GM-CSF present an AM-like phenotype, supporting the major role of GM-CSF in the differentiation of AMs in the lung. However, AMs express low levels of *Cd11b* [176] (Fig. 2.15C), but its expression is not reduced in BMDM differentiated in the presence of GM-CSF (Fig. 2.16F), suggesting that other factors present within the alveolar microenvironment might be necessary to fully differentiate AMs.

We observed that in the presence of GM-CSF, the expression of FPN is downregulated both at mRNA and protein level when compared to BMDMs differentiated in the presence of M-CSF (Fig. 2.16G, H). The effect of GM-CSF is dominant, since it is able to downregulate *Fpn* expression also in the presence of M-CSF (Fig. 2.16I). These observations support our hypothesis that GM-CSF may mediate the suppression of ferroportin expression in AMs.

However, we observed AMs expressing FPN in Slc40a1$^{C326S/C326S}$ mice. These FPN^{+} AMs might correspond to recruited macrophages that do not respond to the pulmonary GM-CSF or AMs that are still undergoing the differentiation process.

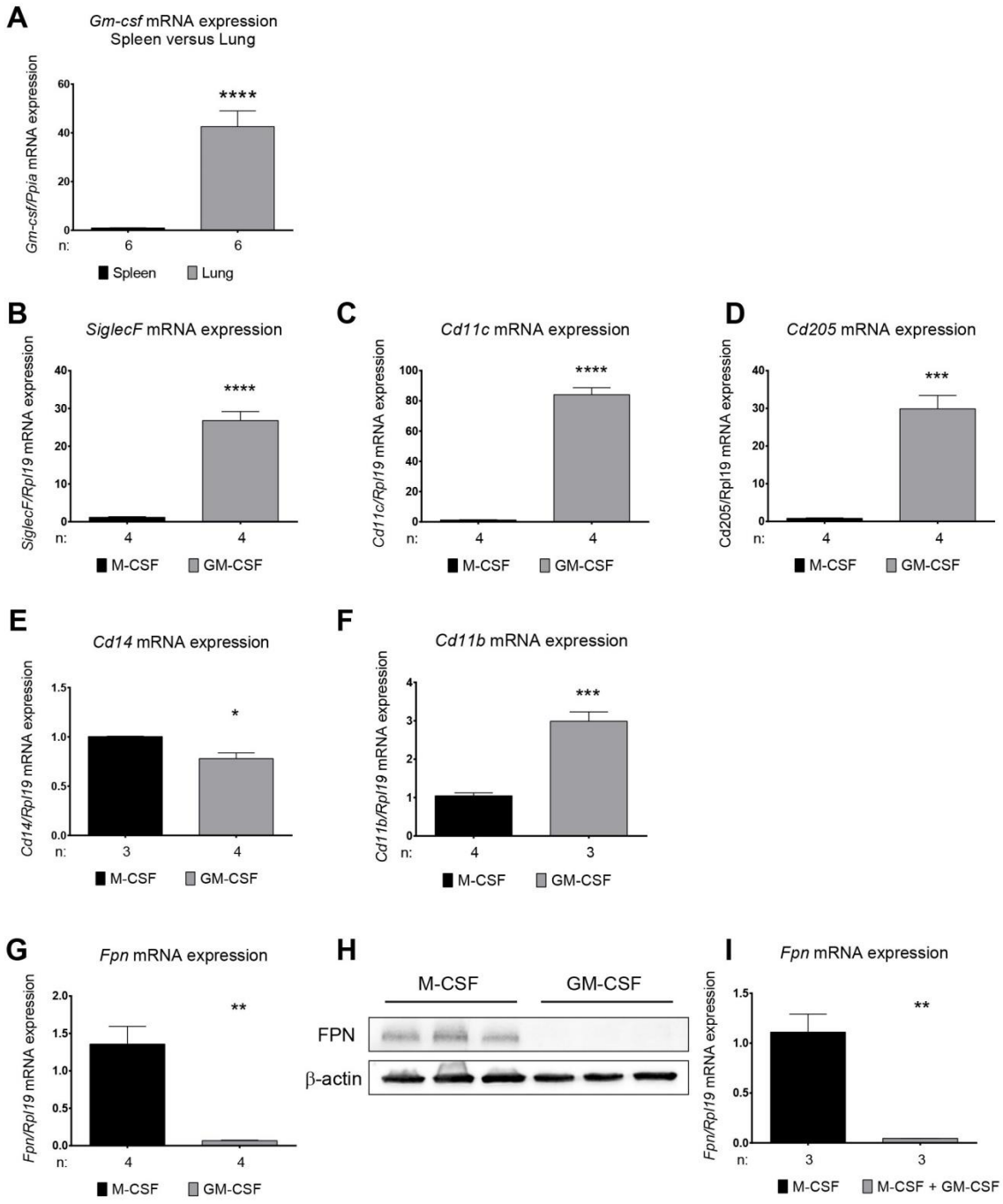

Figure 2.16 – GM-CSF represses FPN expression in BMDM

(A) qRT-PCR analysis of *Gm-csf* mRNA expression in total lung and total spleen of adult wild-type mice.

(B-G) qRT-PCR analysis of *SiglecF* (B), *Cd11c* (C), *Cd205* (D), *Cd14* (E) , *Cd11b* (F) and *Fpn* (G) mRNA expression in wild-type BMDMs differentiated during 6 days in the presence of M-CSF or GM-CSF.

(H) Western Blot analysis of FPN (~65 kDa) protein expression in wild-type BMDM differentiated during 6 days in the presence of M-CSF or GM-CSF. β-actin (42 kDa) was used as loading control.

(I) qRT-PCR analysis of *Fpn* mRNA expression in wild-type BMDM differentiated during 6 days in the presence of M-CSF or M-CSF + GM-CSF.

Both phenotype and function of macrophages are shaped by the environment to which these cells are exposed (reviewed in [235]). Several studies have described that iron overload in macrophages results in oxidative stress, which triggers a switch towards a pro-inflammatory state [236-238]. Since we detected iron overloaded AMs in Slc40a1$^{C326S/C326S}$ mice (Fig. 2.14A), we analyzed the degree of oxidative stress in these cells as well as the pulmonary inflammatory status of Slc40a1$^{C326S/C326S}$ mice. Lung inflammation is hallmarked by an increased expression of pro-inflammatory cytokines and a recruitment of immune cells into the bronchoalveolar compartment.

Using the CellRox green as ROS reporter (a fluorogenic probe, which exhibits a strong fluorescence upon oxidation by ROS), we did not detect differences in oxidative stress in AMs between wild-type and Slc40a1$^{C326S/C326S}$ mice (Fig. 2.17A). In contrast, acute iron treatment of BMDM causes the formation of ROS (Fig. 2.17B).

Despite the increase in the number of AMs (Fig. 2.12B), but consistent with the absence of oxidative stress in these cells (Fig. 2.17A), AMs in Slc40a1$^{C326S/C326S}$ mice do not seem to be morphologically activated as no significant difference in cell size was observed when compared with wild-type AMs (Fig. 2.17C). In agreement, we did not detect an increase in mRNA and protein levels of pro-inflammatory cytokines IL1β, IL6, and TNFα in total lung or in the BAL fluid supernatant, respectively (Fig. 2.17D, E). Since inflammatory responses are regulated by complex networks involving different cell types and the production of different cytokines, we further analyzed the expression levels of the anti-inflammatory cytokines IL10 and IL13. We failed to detect differences in the protein levels of these cytokines between wild-type and Slc40a1$^{C326S/C326S}$ mice (Fig. 2.18).

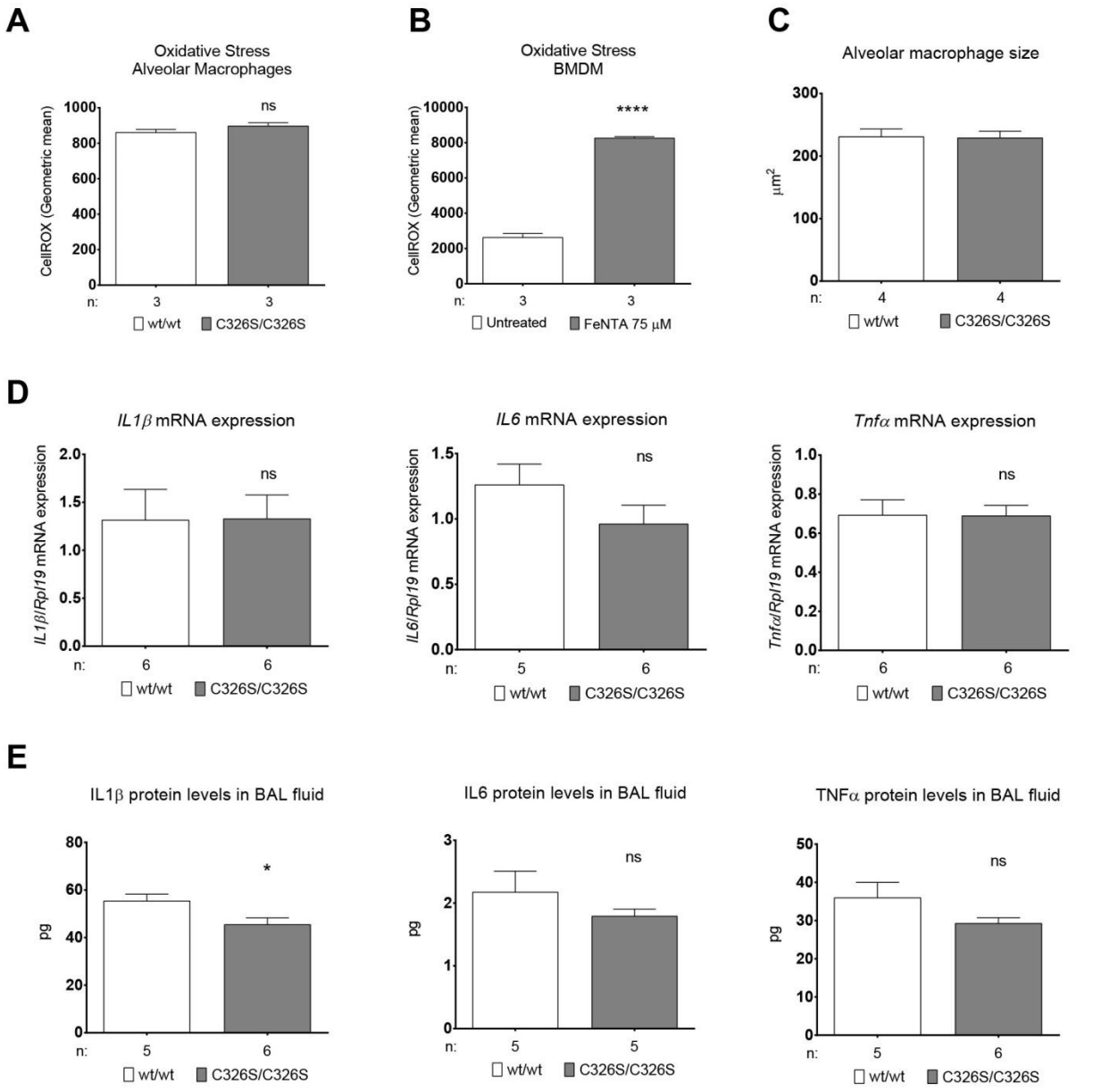

Figure 2.17 – Slc40a1$^{C326S/C326S}$ mice do not show signs of pulmonary inflammation

(A) FACS analysis of the CellROX oxidative stress tracer of AMs isolated from the BAL of 24-week old male mice.

(B) FACS analysis of the CellROX oxidative stress tracer of iron-treated BMDM.

(C) Area of alveolar macrophages isolated from the bronchoalveolar lavage of 36-week old female mice.

(D) qRT-PCR analysis of *IL1β*, *IL6* and *Tnfα* mRNA expression in total lung from 36-week old female mice.

(E) Luminex analysis of IL1β, IL6 and TNFα protein levels in the bronchoalveolar lavage fluid supernatant of 36-week old female mice.

ns – non-significant , pg – picograms

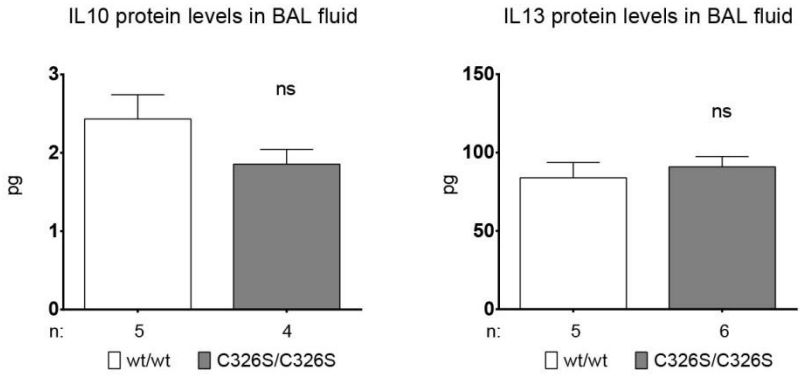

Figure 2.18 – Expression of anti-inflammatory cytokines in the lung of Slc40a1$^{C326S/C326S}$ mice

Luminex analysis of IL10 and IL13 protein levels in the bronchoalveolar lavage fluid supernatant of 36-week old female mice.

ns – non-significant , pg – picograms

Slc40a1$^{C326S/C326S}$ mice present classical signs of restrictive lung disease

Increased iron levels and consequent increase in oxidative stress are known to cause cellular damage and tissue injury [2, 102, 233]. We next investigated whether aged Slc40a1$^{C326S/C326S}$ mice present alterations in lung function.

Measurements of lung function were performed in tracheostomised anaesthetized mice using a lung function measurement device for small animals (FlexiVent of Scireq, Canada). This analysis revealed classical signs of restrictive lung disease in Slc40a1$^{C326S/C326S}$ mice, such as a decrease in total lung capacity and a decrease in pulmonary compliance, which reflects a decrease in lung elasticity (Fig. 2.19A, B). Consistently, Slc40a1$^{C326S/C326S}$ mice showed an increase in pulmonary elastance, a measurement of lung rigidity (Fig. 2.19C). This finding was further confirmed by exposing the mice to fixed air pressures. As shown in the pressure-volume curve, an increase in the applied pressure correlated with an increase in lung volume but to a lesser extent in Slc40a1$^{C326S/C326S}$ mice when compared to wild-type mice (Fig. 2.19D).

We excluded the possibility that the observed differences between wild-type and Slc40a1$^{C326S/C326S}$ mice were due to differences in body size. Despite the fact that aged Slc40a1$^{C326S/C326S}$ mice present a lower body weight, most likely due to exocrine pancreatic failure [102], the tibia length (a marker of body size) was comparable to age-matched wild-type animals, indicating that both groups of mice have a similar size (Fig. 2.19E, F).

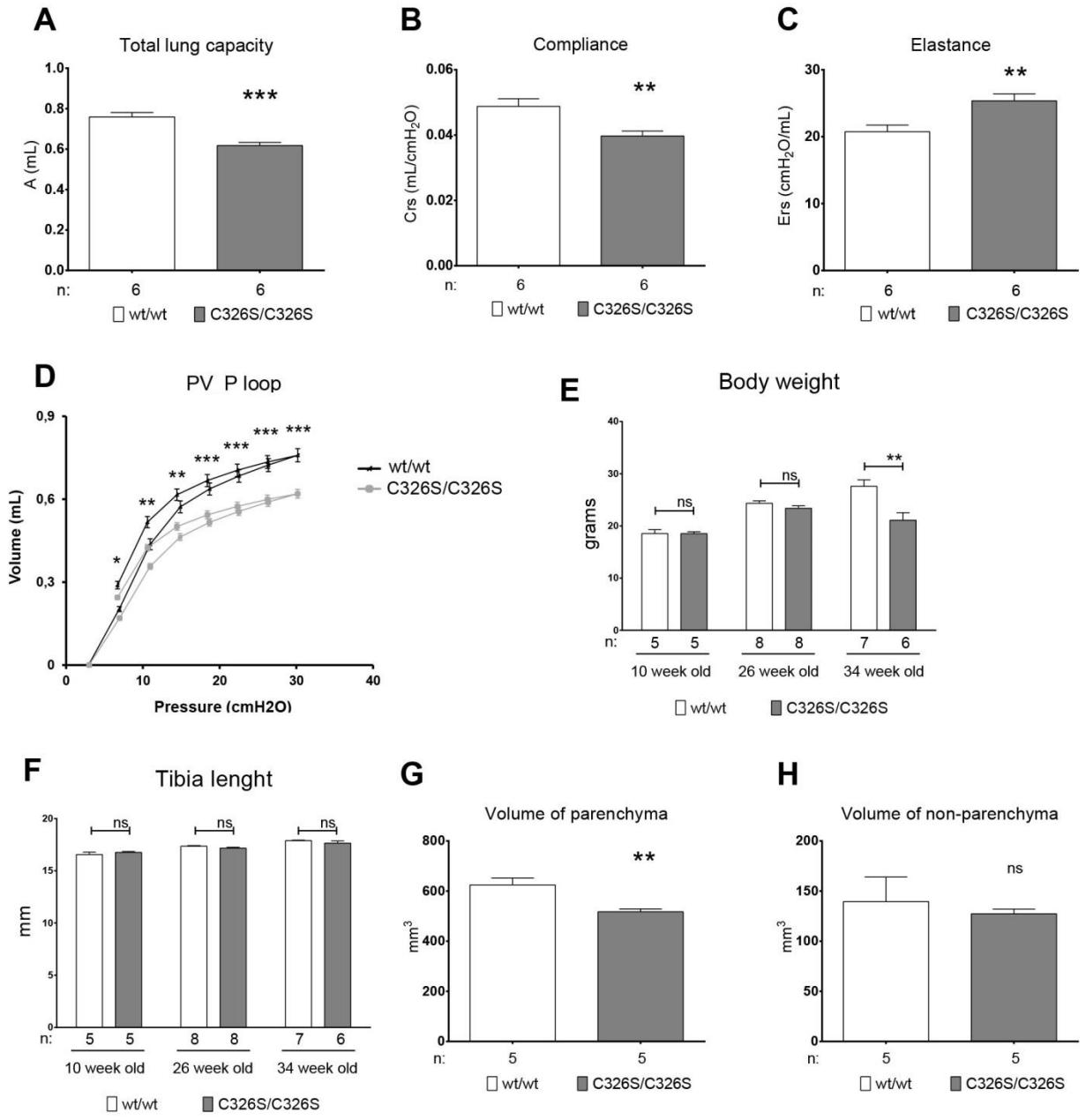

Figure 2.19 – Lung function measurements and stereological analysis of the lung of Slc40a1$^{C326S/C326S}$ mice

(A-D) Lung function measurements performed in 36-week old female mice. A) Total Lung Capacity; (B) Pulmonary Dynamic Compliance; C) Pulmonary Elastance; D) Pressure-Volume (PV) curve with controlled pressure applied.

(E) Body weight of 10-, 26- and 34-week old female mice.

(F) Tibia size of 10-, 26- and 34-week old female mice.

(G) Volume of lung parenchyma measured in 36-week old female mice.

(H) Volume of lung non-parenchyma measured in 36-week old female mice.

ns – non-significant

Together with Prof. Christian Mühlfeld and Dr. Christina Brandenberger (Hannover Medical School), we performed a stereological analysis of the lung of Slc40a1$^{C326S/C326S}$ mice, as previously described [231]. We applied a grid on images of lung sections obtained by light microscopy and counted the number of points overlapping with the alveolar septa (P(alvsept)), alveolar airspace (P(alvair)) and alveolar duct airspace (P(ductair)), which together correspond to points overlapping the lung parenchyma. We have also counted the points overlapping with the lung non-parenchyma (P(non parenchyma)), e.g. conducting airways and blood vessels. We estimated the volume fraction (Vv) of the lung parenchyma and lung non-parenchyma as following:

$$Vv\left(\frac{parenchyma}{lung}\right) = \frac{[P(ductair) + P(alvsept) + P(alvair)]}{P(lung)}$$

$$Vv\left(\frac{non\ parenchyma}{lung}\right) = \frac{P(non\ parenchyma)}{P(lung)}$$

$P(lung) -$ sum of points overlapping the lung parenchyma and the lung non-parenchyma.

By multiplying the volume fraction of these compartments by the total volume of the lung (assessed by the fluid displacement method), we calculated the total volume of the lung parenchyma and the total volume of the lung non-parenchyma [231]. This analysis revealed a reduction in the volume of the lung parenchyma in Slc40a1$^{C326S/C326S}$ mice, without alterations in the volume of the lung non-parenchyma (Fig. 2.19G, H). These observations support the restrictive pattern observed by measurements of lung function and indicate that the decrease in total lung capacity results from a reduction in the volume of the lung parenchyma.

A pulmonary restrictive pattern is commonly associated with conditions that increase lung stiffness, such as an increase in collagen deposition [172]. However, a marked replacement of normal lung parenchyma by fibrotic tissue was not observed (Fig. 2.20).

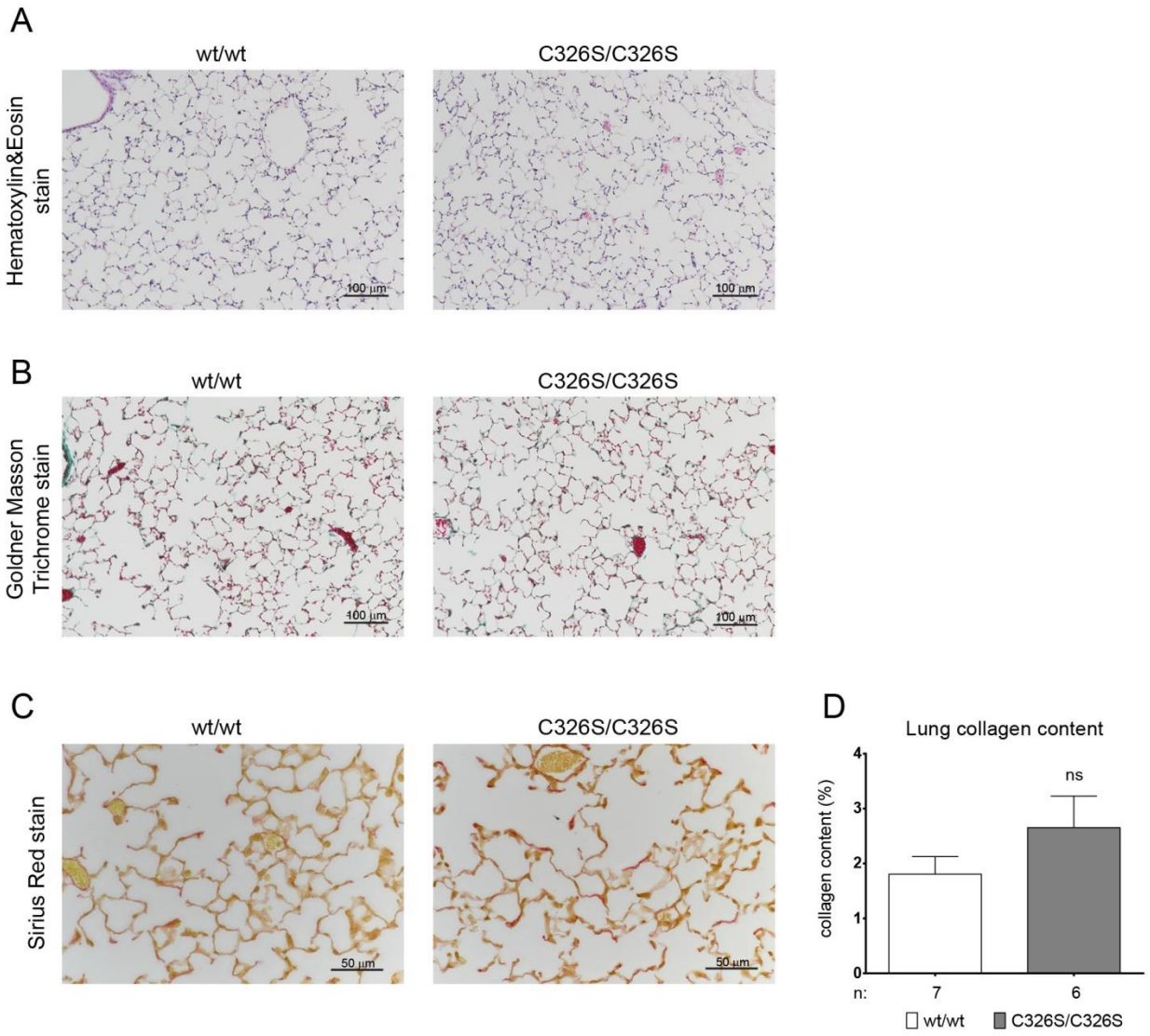

Figure 2.20 – The lung structure in Slc40a1$^{C326S/C326S}$ mice is unaltered compared to wild-type mice.

(A) Hematoxylin & Eosin stain of lung sections from 36-week old female mice.

(B) Goldner Masson Trichrome stain of lung sections from 36-week old mice.

(C) Sirius red stain of lung sections from 36-week old mice.

(D) Collagen content calculated on Sirius Red stained lung sections from 34-week old mice.

Quantification of lung collagen deposition was performed by our collaborators Dr. Simone Kraut and Prof. Dr. Norbert Weissmann.

ns – non-significant

Slc40a1$^{C326S/C326S}$ mice show decreased blood oxygen saturation

The respiratory system has evolved to maximize the gas exchange between the bloodstream and the atmosphere. We observed a strong reduction in blood oxygen saturation in aged Slc40a1$^{C326S/C326S}$ mice when compared to wild-type mice (Fig. 2.21A) suggesting that the gas exchange in the lung might be compromised. In adult mammals, the kidney is responsible for sensing systemic hypoxia and producing the erythroid growth factor erythropoietin (EPO). In agreement with the observed decrease in blood oxygen saturation, plasma EPO levels were increased in Slc40a1$^{C326S/C326S}$ mice (Fig. 2.21B). Increased levels of circulating EPO stimulate erythropoiesis in the bone marrow in order to increase the number of circulating red blood cells and improve the delivery of oxygen to every cell in the organism. Consistently, we observed higher levels of red blood cells, hemoglobin and hematocrit in Slc40a1$^{C326S/C326S}$ mice (Table 2.1) [102].

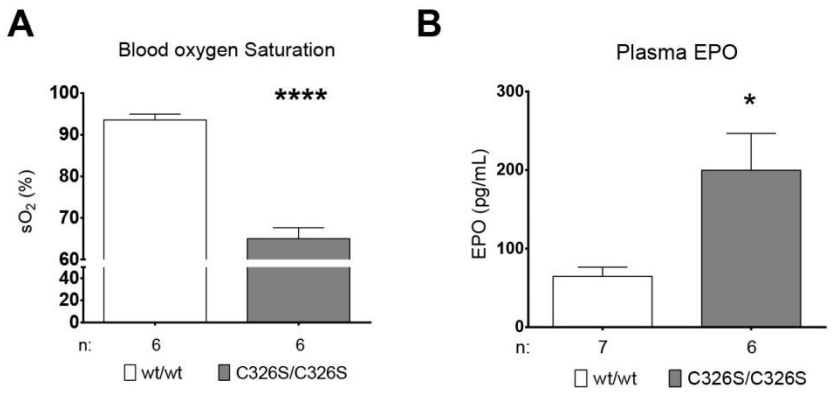

Figure 2.21 – Blood oxygen saturation measurement in Slc40a1$^{C326S/C326S}$ mice

(A) Blood oxygen measurements performed in 36-week old female mice.

(B) EPO levels measured in the plasma of 36-week old female mice.

Table 2.1 – Hematological parameters in 36-week old mice (n=4)

Parameter	wt/wt	C326S/C326S	p-value
Hemoglobin (g/dl)	16,36 ± 0,06	17,66 ± 0,41	* 0,0199
Hematocrit (%)	53,22 ± 0,53	56,73 ± 1,12	* 0,0296
Red blood cells (10^6/µL)	10,60 ± 0,09	11,47 ± 0,05	*** 0,0002

Chapter IV

Discussion

Imbalances in iron homeostasis have been reported in a spectrum of lung diseases [204, 219]. However, the role of iron in lung pathology is poorly understood. In this work, we aim at understanding whether a disruption in the hepcidin/ferroportin regulatory circuitry and the subsequent increase in systemic iron levels affect lung iron homeostasis and function.

Here we show that resistance of ferroportin to hepcidin binding causes an age-dependent pulmonary iron deposition in defined lung cell types (Fig. 3.1). Increased iron levels in this organ correlated with increased lipid peroxidation, suggesting that iron-mediated oxidative stress may contribute to the pathogenesis of lung diseases. Homozygous Slc40a1$^{C326S/C326S}$ mice show classical signs of restrictive lung disease and a significant decrease in blood oxygen saturation. These findings implicate iron overload in lung pathology, which has to date not been considered a classical iron-related disorder.

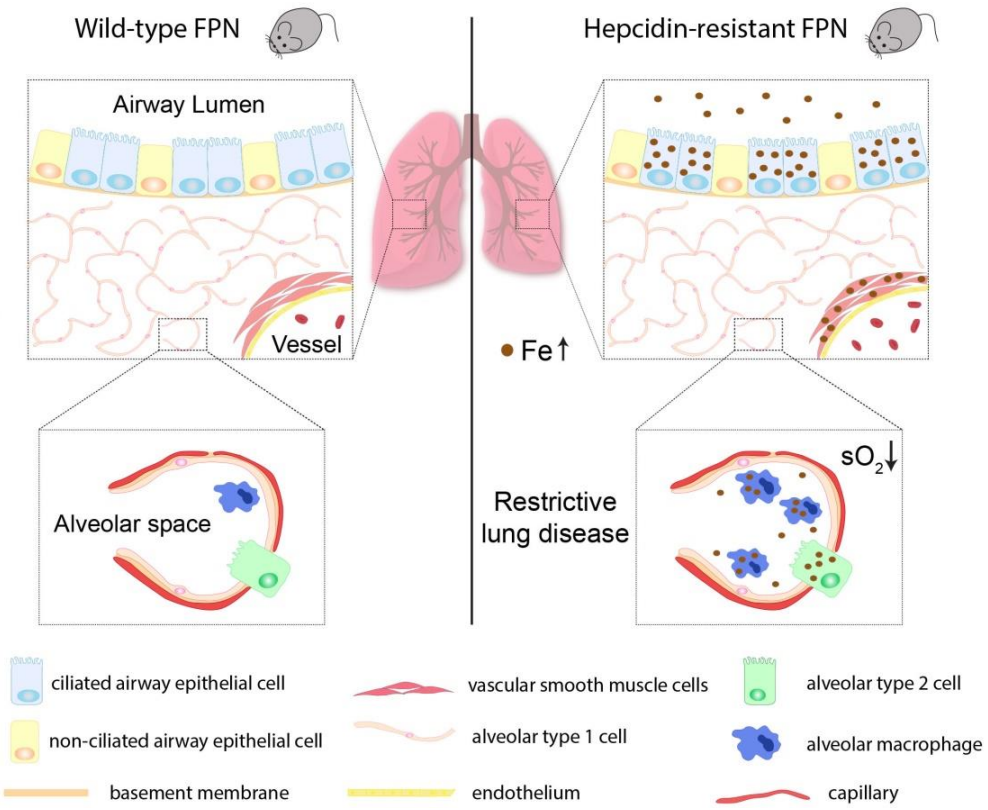

Figure 3.1 – Lung iron accumulation and pathophysiological consequences of pulmonary iron overload in Slc40a1$^{C326S/C326S}$ mice

Iron accumulates in specific cell types of the lung of Slc40a1$^{C326S/C326S}$ mice: ciliated airway epithelial cells, vascular smooth muscle cells, alveolar type 2 cells and alveolar macrophages. Iron was also detected extracellularly in the bronchoalveolar space. Although there is an increase in the number of alveolar macrophages, Slc40a1$^{C326S/C326S}$ mice do not show strong signs of pulmonary inflammation. Slc40a1$^{C326S/C326S}$ mice show a pulmonary restrictive pattern and decreased blood oxygen saturation.

FPN – Ferroportin; Fe – iron; sO_2 – blood oxygen saturation.

Slc40a1^{C326S} mice show increased iron levels in the lung

There are limited reports regarding how lung iron homeostasis is affected by imbalanced systemic iron levels. Here, we report that a disruption in the hepcidin/FPN regulatory circuitry and the subsequent increase in systemic iron levels cause pulmonary iron accumulation in a mouse model of HH type 4 (Slc40a1^{C326S}). The observed increase in lung iron levels is not a result of the point mutation in FPN *per se*, since hepcidin knock out mice showed similar levels of pulmonary iron accumulation when compared to Slc40a1$^{C326S/C326S}$ mice. Increased systemic and pulmonary iron levels in Slc40a1^{C326S} mice result from an increase in dietary iron uptake caused by the resistance of FPN to hepcidin binding.

To date, no data is available regarding the pulmonary iron content of patients with HH type 4. However, the idea that increased pulmonary iron levels in humans can be caused by increased dietary iron uptake is supported by the report of a patient that presented signs of intracellular and extracellular lung iron accumulation after receiving therapeutic oral iron supplementation [239]. Moreover, patients with thalassemia major, a disease characterized by transfusional iron overload, were reported to accumulate iron in alveolar macrophages, further supporting the idea that increased systemic iron levels in humans can affect pulmonary iron content [240, 241].

The IRE/IRP system is inactivated by increased intracellular iron levels (see introduction, section 1.4). This causes the degradation of the IRE-containing transcripts encoding for DMT1 and TfR1 and allows the translation of FtL and FPN. Consistent with the increase in pulmonary iron content in Slc40a1^{C326S} mice, we observed a decrease in mRNA and protein levels of TfR1 and mRNA levels of the IRE-containing transcript of *Dmt1*, as well as an increase in the protein levels of FtL. These results show that the expected molecular signature is preserved in the lung of Slc40a1^{C326S} mice. Furthermore, FPN protein levels showed a genotype-specific increase, which may result from a combined effect of increased expression at transcriptional level (Fig. 2.2D), derepression of FPN translation by the inhibition of the IRE/IRP system [30] and the hepcidin-resistant phenotype that post-translationally stabilizes the protein [102].

Giorgi *et al.* reported that intraperitoneal injection of iron-saccharate in mice leads to increased systemic and pulmonary iron levels [208], supporting our finding that altered systemic iron homeostasis affects lung iron content. However, in their study the expression of TfR1 and DMT1 in the lung did not change in response to increased pulmonary iron content [208]. The differences in our observations might be explained by different sources of iron (dietary iron versus iron-saccharate) and/or may reflect the fact that lung cells in Slc40a1^{C326S} mice are chronically exposed to high levels of iron in contrast to the acute iron treatment in iron-

saccharate injected mice. Regarding FPN expression, they observed an increase in lung FPN protein levels, consistent with our findings in Slc40a1^{C326S} mice [208]. In their work, Giorgi and colleagues further observed an increase in ZIP14 protein levels. Unfortunately, we were unable to detect ZIP14 protein by western blot or immunohistochemistry in the lung of wild-type and Slc40a1^{C326S} mice.

The hormone hepcidin is mainly produced and secreted by hepatocytes and plays a major role in systemic iron regulation (reviewed in [28]). Hepcidin expression in cells other than hepatocytes has been reported, but at a much lower level [51-54]. We observed that in the lung, hepcidin mRNA levels are very low compared to those in the liver. Furthermore, we observed that contrary to hepatic hepcidin, pulmonary hepcidin expression does not respond to increased iron levels, as no differences were observed between wild-type and Slc40a1$^{C326S/C326S}$ mice. Giorgi and colleagues have also analyzed the expression of hepcidin in the lung of mice injected intraperitoneally with iron-saccharate. Consistent with our data, they observed that pulmonary hepcidin expression does not respond to an increased lung iron content [208].
Liver-specific hepcidin knock out mice completely recapitulate the hemochromatosis phenotype observed in the global knock out mice, highlighting the predominant role of hepatic hepcidin in the regulation of body iron homeostasis [242]. The role of extra-hepatic hepcidin in maintaining cellular or/and systemic iron homeostasis is not completely known yet. A recently published study has revealed a role for cardiac hepcidin in cardiac iron homeostasis through the analysis of mice with a cardiomyocyte-specific deletion of hepcidin [243]. Airway epithelial cells in the lung were shown to express hepcidin but its role in lung iron homeostasis is not clear yet [216, 217]. Frazier and colleagues reported that an increase in hepcidin expression in human airway epithelial cells *in vitro* does not cause a decrease in FPN protein levels in these cells [216]. In contrast, Chen and colleagues observed that, in a mouse model of sepsis-induced acute lung injury, there is an increase in lung FPN protein levels upon the knock down of hepcidin in airway epithelial cells [217]. The generation of mice with lung cell-type specific deletion of hepcidin would help to better understand a possible role of lung hepcidin in the context of pulmonary iron homeostasis.

The risk for oxidative stress in the respiratory tract is exceptionally high since it is continuously exposed to the atmosphere and consequently to high levels of oxygen and pollutants. Under healthy conditions, oxidative stress is prevented by the presence of antioxidants in the respiratory lining fluid and the presence of alveolar macrophages, which are capable of sequestering large amounts of iron intracellularly [203, 212]. Endogenous or exogenous

conditions that cause an increase in the availability of free iron in the lung can result in oxidative stress. For example, the pulmonary inhalation of iron oxide nanoparticles in rats leads to an increase of ROS in the lung [223]. We observed an increase in oxidative stress in the lung of Slc40a1$^{C326S/C326S}$ mice, which correlates with increased pulmonary iron content and the presence of extracellular iron in the BAL fluid, probably reflecting a saturated ability of AMs and other lung cells to store iron in a chemically inert form.

Iron accumulation in the lung of Slc40a1^{C326S} mice is restricted to specific cell types

We observed that iron does not accumulate uniformly in the lung of Slc40a1^{C326S} mice but in specific cells types: ciliated epithelial cells lining the conducting airways, alveolar type 2 cells, vascular smooth muscle cells and AMs. Giorgi *et al.* reported that in the lung of mice injected intraperitoneally with iron-saccharate, iron accumulates mainly in AMs [208]. Our observation that iron accumulates in cell types other than AMs might be explained by an acute versus chronic iron overload and/or differences in iron fluxes in wild-type mice intraperitoneally-injected with iron compared to a genetic model with a disrupted hepcidin/FPN regulatory circuitry.

Previous work suggested that airway epithelial cells take up free catalytically active iron from the airway lumen [204]. We observed that in wild-type mice DMT1 is mainly expressed at the apical membrane of ciliated airway epithelial cells. Consistently, we frequently detected iron loaded ciliated cells in the conducting airways of Slc40a1$^{C326S/C326S}$ mice. These observations support the idea that these cells might be able to take up NTBI from the airway lumen.
However, contrary to what was suggested by Ghio and colleagues [211], we believe that ciliated airway epithelial cells do not export iron through FPN since we detected iron deposition in these cells in Slc40a1$^{C326S/C326S}$ mice – the resistance of FPN to hepcidin binding should otherwise cause uncontrolled iron export. Interestingly, Giorgi and colleagues have detected FPN in the cytoplasm and not in the plasma membrane of airway epithelial cells, a finding that would argue against an active iron export via FPN [208].
Occasionally, we detected iron in another epithelial cell type of the lung of Slc40a1^{C326S} mice – alveolar type 2 cells. How iron is imported into these cells still remains to be elucidated.

Finally, we observed iron accumulation in vascular SMCs of the lung of Slc40a1$^{C326S/C326S}$ mice. Notably, we could also detect iron-spared vascular SMCs in Slc40a1$^{C326S/C326S}$ mice indicating

that vascular SMCs are heterogeneous in regard to iron loading. Phenotypic diversity has been described in vascular SMCs and correlates with different functions, ranging from a contractile to a synthetic function [244]. The expression levels of different SMC markers are commonly used to define different phenotypes; for example, higher levels of desmin expression were associated with a contractile phenotype [244]. In Slc40a1$^{C326S/C326S}$ mice, iron accumulates in vascular SMCs that appear to be functionally different: iron-spared vascular SMCs express high levels of desmin whereas iron-loaded vascular SMCs show lower levels of desmin. Since vascular SMCs have a critical role in the normal regulation of the blood flow and pressure, we have an ongoing project in the laboratory to address how increased systemic iron levels and/or iron accumulation in a sub-population of vascular SMCs in Slc40a1$^{C326S/C326S}$ mice affects their role in maintaining appropriate blood pressure under physiological and/or pathophysiological conditions. It is worth to mention that altered iron homeostasis was reported in patients with idiopathic pulmonary arterial hypertension [245]. Iron deficiency in rats was shown to cause pulmonary vascular remodeling and was associated with increased pulmonary arterial hypertension, which can be reverted by iron treatment [246].

Iron loaded alveolar macrophages and inflammatory status of Slc40a1^{C326S} mice

Iron sequestration by AMs has been described in different lung diseases and has been recognized as a powerful protective mechanism against cytotoxic iron catalyzed oxidants [204, 212, 218]. We analyzed AMs from Slc40a1$^{C326S/C326S}$ mice and showed that their number is increased when compared to wild-type animals. Whether this increase is due to a recruitment of circulating monocytes or results from the proliferation of a progenitor population within the lung is still not known. Even though monocyte recruitment has been mainly connected with increased tissues levels of CCL2, we did not detect an increase in mRNA levels of *Ccl2* in the lung of Slc40a1$^{C326S/C326S}$ mice. Nevertheless, we observed a strong tendency for an increase in the levels of CCL2 in the plasma of Slc40a1$^{C326S/C326S}$ mice, which may contribute for the recruitment of monocytes into tissues. It is worth to mention that Slc40a1$^{C326S/C326S}$ mice also show an increase in the number of peritoneal macrophages (unpublished data from our laboratory), which might also be a consequence of increased systemic levels of CCL2. To further understand if there is a recruitment of circulating monocytes to the lung of Slc40a1$^{C326S/C326S}$ mice, it would be interesting to perform fate-mapping studies to trace monocyte progeny in Slc40a1$^{C326S/C326S}$ mice [182]. We have also detected a mild increase in the levels of *Cxcl1* in the lung of

Slc40a1$^{C326S/C326S}$ mice, which is commonly associated with neutrophil recruitment. However, the increase in the number of neutrophils in the bronchoalveolar space was not statistically significant (Fig. 2.12B).

We detected strong iron deposition in AMs from Slc40a1$^{C326S/C326S}$ mice. This was an unexpected result since, in the same mouse model, other resident macrophages such as Kupffer cells and splenic macrophages are iron depleted due to the presence of a hepcidin-resistant FPN on the cell surface of these cells [102]. Interestingly, we also observed iron spared AMs, indicating that the population of AMs in Slc40a1$^{C326S/C326S}$ mice is heterogeneous in regard to iron handling. This heterogeneity in iron accumulation most likely results from a heterogeneous expression of FPN in AMs isolated from Slc40a1$^{C326S/C326S}$ mice. Notably, we could not detect AMs expressing FPN in wild-type mice. This result contrasts with a previous study, in which FPN was detected in intracellular vesicles of murine AMs [210].
How FPN expression is regulated in AMs is still not known. GM-CSF, which is known for its key role in AM differentiation and which is highly expressed in the lung, has been described to repress FPN expression in monocyte-derived macrophages upon stressed erythrocyte challenge [234]. In line with this idea, we demonstrated the ability of GM-CSF to downregulate FPN expression in BMDM *in vitro*. Nevertheless, we observed AMs expressing FPN in Slc40a1$^{C326S/C326S}$ mice. The presence of GM-CSF in the lung would be expected to suppress FPN expression. We speculate that FPN-positive AMs correspond to recruited macrophages that do not respond to the presence of GM-CSF in the lung or to macrophages still undergoing the differentiation process.

Our laboratory has previously described that iron overload in reticuloendothelial macrophages results in oxidative stress and triggers a pro-inflammatory status [238]. Since we detected increased iron levels in AMs, we analyzed the degree of oxidative stress in these cells and the pulmonary inflammatory status of Slc40a1$^{C326S/C326S}$ mice. We did not detect differences in oxidative stress between AMs of wild-type and Slc40a1$^{C326S/C326S}$ mice. By contrast, BMDM show a strong increase in oxidative stress after an acute iron treatment. The absence of oxidative stress in AMs probably results from an adaptation of these cells to chronic iron accumulation. Consistent with the absence of oxidative stress, AMs from Slc40a1$^{C326S/C326S}$ mice do not appear to be morphologically activated since we did not detect an increase in cell size when compared to wild-type AMs.
Lung inflammation is hallmarked by an increased expression of pro-inflammatory cytokines and a strong recruitment of immune cells into the bronchoalveolar compartment [247]. Despite the

increase in the number of AMs, but in agreement with the lack of oxidative stress in these cells, we did not observe a strong and robust increase in the expression of inflammatory cytokines in the lung of Slc40a1$^{C326S/C326S}$ mice (Fig. 2.13; Fig. 2.17). Interestingly, the inhalation of iron-rich particles leads to increased oxidative stress and lung inflammation [222-224]. This difference in terms of pulmonary inflammation in response to increased iron levels is probably a consequence of the different sources of iron (dietary iron versus inhalation of iron-rich particles) and a difference in the exposure to iron (chronic versus acute). Despite the absence of pulmonary inflammation in Slc40a1$^{C326S/C326S}$ mice, increased iron levels in the lung, and in particular in the AMs, might affect the inflammatory response to pathogens. For example, low intracellular iron in macrophages impairs signaling via the TLR4 pathway leading to reduced production of LPS-induced cytokines [248]. An interesting follow up would be to perform LPS instillation in Slc40a1$^{C326S/C326S}$ mice and analyze the production of inflammatory cytokines and the recruitment of neutrophils to the bronchoalveolar space. Previous work from our group has described the acute pulmonary inflammatory response of *Hfe* knock out mice upon intratracheal instillation of LPS [247]. The study showed that the production of inflammatory cytokines was affected and that there was an impairment in the recruitment of neutrophils to the lung of *Hfe* knock out mice. However, in this study it was not possible to understand whether the observed effects were due to the increase in systemic iron levels or due to the absence of HFE itself. Furthermore, *Hfe* knock out mice do not present increased pulmonary iron content when compared to wild-type mice [247].

In healthy lungs, the availability of free iron must be limited not only to reduce the risk of oxidative stress but also to prevent pulmonary infections [249]. For example, increased iron levels in the airways were related to the persistence of *Pseudomonas aeruginosa* infection in cystic fibrosis patients [250]. Moreover, during *Pseudomonas aeruginosa* infection, the murine host up-regulates the expression of proteins involved in iron-sequestration, highlighting the concept that the competition for iron between the host and the pathogens is crucial to determine the outcome of an infection [251]. Due to the increase in pulmonary iron content in Slc40a1$^{C326S/C326S}$ mice, and particularly the presence of extracellular iron in the bronchoalveolar space, it would be interesting to infect these animals with *Pseudomonas aeruginosa* and determine whether they are more susceptible to infection.

Slc40a1$^{C326S/C326S}$ mice show classical signs of restrictive lung disease and decreased blood oxygen saturation

An increase in oxidative stress, resulting from increased iron levels, is known to cause cellular damage and tissue injury [2, 102, 233]. Increased pulmonary iron levels in Slc40a1$^{C326S/C326S}$ correlate with an increase in lipid peroxidation, suggesting that iron-mediated oxidative stress could contribute to the pathogenesis of lung diseases. To determine whether increased iron content affects pulmonary function, we performed measurements of lung function on aged mice. This analysis revealed that Slc40a1$^{C326S/C326S}$ mice present classical signs of restrictive lung disease, such as decreased total lung capacity, decreased pulmonary compliance and increased elastance. Furthermore, stereological analysis of the lung revealed that the decrease in total lung capacity in Slc40a1$^{C326S/C326S}$ mice results from a reduction in the volume of the lung parenchyma.

To date, there are no reports of impaired lung function in human patients with HH type 4. However, this may reflect the fact that patients identified with the FPN C326S mutation were heterozygous [100] and clinical iron overload has been controlled by phlebotomy.

Interestingly, restrictive lung disease is the major pulmonary dysfunction observed in patients with thalassemia major [252-257]. These patients are hallmarked by increased systemic iron levels and parenchymal iron overload. Furthermore, iron accumulation has been observed in AMs isolated from the BAL [240, 241]. Some studies reported that the restrictive pattern correlates with serum ferritin levels and/or with age (which may reflect a chronic effect of iron overload) [254, 256]. Our results strengthen the idea that the pulmonary restrictive pattern in thalassemia patients may be a consequence of chronic iron overload.

A restrictive pattern is commonly associated with pulmonary fibrosis. However, histological analysis of the lung of Slc40a1$^{C326S/C326S}$ mice did not reveal significant alterations in lung collagen deposition. Even though the mechanism(s) leading to restrictive lung disease in Slc40a1$^{C326S/C326S}$ mice is still not known, we can speculate about two possible causes: pulmonary edema or altered function of the surfactant.

Increased iron levels and iron-mediated oxidative stress have been reported to disrupt the blood-brain barrier permeability [258]. Consistently, unpublished data from our laboratory also indicate that blood vessel permeability is affected by increased iron levels and/or oxidative stress. We hypothesize that vessel permeability in the lung of Slc40a1$^{C326S/C326S}$ mice might be compromised due to increased systemic and pulmonary iron levels and the subsequent increase in oxidative stress. This would lead to fluid accumulation within the lung and contribute to the

decrease in total lung capacity measured by pulmonary function tests. In addition, the increase in blood vessel permeability in the lung would also offer a plausible explanation for the increase in iron levels in the bronchoalveolar space. We have tried to test this hypothesis by injecting Evans blue dye into the tail vein of Slc40a1$^{C326S/C326S}$ mice. Due to its high affinity to serum albumin, this dye should not accumulate in the tissues when vessel permeability is intact. Unfortunately, for reasons that are still not clear, vessels in the Slc40a1$^{C326S/C326S}$ mice are very fragile, making tail vein injection hard to perform in a consistent and reproducible way.

The pulmonary surfactant decreases surface tension at the gaseous-aqueous interphase of the lung, preventing it from collapsing and facilitating inflation [158]. We can speculate that the oxidation of surfactant proteins and lipids by the presence of extracellular iron in the bronchoalveolar space of Slc40a1$^{C326S/C326S}$ mice might alter the structure and function of the surfactant, increasing the surface tension and making it harder to inflate. This would explain the decrease in pulmonary compliance and increase in elastance observed in Slc40a1$^{C326S/C326S}$ mice. Supporting this hypothesis, Rodriguez-Capote and colleagues showed that surfactant oxidation caused by ROS interferes with its function through the oxidation of surfactant phospholipids and proteins [259].

The main function of the lung is to allow for an efficient gas exchange between the atmosphere and the bloodstream, in order to fulfill the oxygen requirements of all cells of the organism and to excrete the waste CO_2 produced during cellular respiration. Since lung function is impaired in Slc40a1$^{C326S/C326S}$ mice, we analyzed blood oxygen saturation. We observed a strong decrease in oxygen saturation in Slc40a1$^{C326S/C326S}$ compared to wild-type mice. The restrictive pattern observed in Slc40a1$^{C326S/C326S}$ mice probably contributes to the observed hypoxemia but most likely cannot fully explain such a strong phenotype. We can hypothesize that the reduction in blood oxygen saturation can be caused by 1) a substantial ventilation/perfusion mismatch, 2) a shunt flow of the blood, or 3) by a low cardiac output. Regarding the first hypothesis, it is possible that an impairment of surfactant production and/or activity might lead to a partial collapse of gas exchanging units within the lung resulting in ventilation/perfusion mismatch and hypoxemia. Second, alterations in the vasculature may cause a shunting of unoxygenated blood across the heart or the lungs. Finally, low cardiac output could also contribute to such a phenotype by causing low venous oxygenation and leading to low arterial O_2 saturation. Future studies will be necessary to address these possibilities.

In adult mammals, systemic hypoxia is mainly sensed by the kidney, in particular by peritubular fibroblasts of the renal cortex [81]. These cells produce and secrete EPO in response to

hypoxia: low oxygen levels lead to the stabilization of the transcription factor subunit HIF-2α which, together with HIF-β, activates *Epo* transcription [86]. Consistently, we detected increased levels of EPO in the plasma of Slc40a1$^{C326S/C326S}$ mice. Erythropoiesis in the bone marrow is stimulated by increased levels of circulating EPO, in an attempt to restore the proper delivery of oxygen to cells. In agreement with these findings, high levels of red blood cells, hemoglobin and hematocrit were detected in Slc40a1$^{C326S/C326S}$ mice. It is worth to mention that elevated intracellular iron levels in Slc40a1$^{C326S/C326S}$ mice can also directly activate EPO production via the IRP/IRE system – IRP1 is converted from its RNA-binding form to the cytoplasmatic aconitase form containing a [4Fe–4S] cluster and consequently cannot bind the IRE present in the 5' UTR of the HIF-2α mRNA, leading to an increase in its translation [260].

Hepatic hepcidin transcriptional expression is regulated by different stimuli (see introduction, section 1.5.2). Interestingly, Slc40a1$^{C326S/C326S}$ mice show increased systemic iron levels but decreased blood oxygen saturation. These two stimuli are expected to have opposite effects on hepcidin transcription: high levels of iron stimulate hepcidin expression whereas hypoxia represses hepcidin expression. As previously reported by us, liver hepcidin expression is increased in Slc40a1$^{C326S/C326S}$ mice [102], indicating that increased iron levels are dominant over hypoxic signals in controlling hepcidin expression. Nevertheless, since hypoxia represses hepcidin expression indirectly by inducing erythropoiesis and therefore increasing ERFE, it would be interesting to analyze ERFE levels in the plasma of Slc40a1$^{C326S/C326S}$ mice. Additionally, hypoxia can also indirectly repress hepcidin expression by the upregulation of TMPRSS6 and furin expression caused by HIF-1α stabilization [66, 89].

Slc40a1$^{C326S/C326S}$ mice present increased plasma iron levels, hepatic iron overload, body weight loss, and exocrine pancreatic failure [102]. For this reason, we cannot exclude that pathophysiological consequences of iron overload in Slc40a1$^{C326S/C326S}$ mice other than the lung may contribute to our observations. The restrictive pattern and decreased blood oxygen saturation may result from a combination of high iron levels in the lung and other impairments caused by increased systemic iron levels and tissue iron deposition. Finally, we can speculate that an impaired lung function may contribute to the premature death observed in Slc40a1$^{C326S/C326S}$ mice [102].

As a conclusion, our findings implicate iron overload in lung pathology, which is so far not considered a classical iron-related disorder. With the exception of some studies in thalassemia

patients, there is limited information regarding the pulmonary consequences of systemic and lung iron overload in humans. Future analysis of lung iron content and lung function in patients with iron-related diseases such as hereditary hemochromatosis will be essential to further understand the physiological consequences of iron overload in human lung disorders.

Chapter VI

References

1. Ilbert, M. and V. Bonnefoy, 2013, *Insight into the evolution of the iron oxidation pathways, Biochim Biophys Acta, 1827, 161-75*
2. Stohs, S.J. and D. Bagchi, 1995, *Oxidative mechanisms in the toxicity of metal ions, Free Radic Biol Med, 18, 321-36*
3. Papanikolaou, G. and K. Pantopoulos, 2005, *Iron metabolism and toxicity, Toxicol Appl Pharmacol, 202, 199-211*
4. Ganz, T., 2013, *Systemic iron homeostasis, Physiol Rev, 93, 1721-41*
5. Hentze, M.W., et al., 2010, *Two to tango: regulation of Mammalian iron metabolism, Cell, 142, 24-38*
6. McKie, A.T., et al., 2001, *An iron-regulated ferric reductase associated with the absorption of dietary iron, Science, 291, 1755-9*
7. Gunshin, H., et al., 1997, *Cloning and characterization of a mammalian proton-coupled metal-ion transporter, Nature, 388, 482-8*
8. Ferris, C.D., et al., 1999, *Haem oxygenase-1 prevents cell death by regulating cellular iron, Nat Cell Biol, 1, 152-7*
9. McKie, A.T., et al., 2000, *A novel duodenal iron-regulated transporter, IREG1, implicated in the basolateral transfer of iron to the circulation, Mol Cell, 5, 299-309*
10. Donovan, A., et al., 2000, *Positional cloning of zebrafish ferroportin1 identifies a conserved vertebrate iron exporter, Nature, 403, 776-81*
11. Vulpe, C.D., et al., 1999, *Hephaestin, a ceruloplasmin homologue implicated in intestinal iron transport, is defective in the sla mouse, Nat Genet, 21, 195-9*
12. Schade, A.L. and L. Caroline, 1946, *An Iron-binding Component in Human Blood Plasma, Science, 104, 340-1*
13. Harding, C., J. Heuser, and P. Stahl, 1983, *Receptor-mediated endocytosis of transferrin and recycling of the transferrin receptor in rat reticulocytes, J Cell Biol, 97, 329-39*
14. Dautry-Varsat, A., A. Ciechanover, and H.F. Lodish, 1983, *pH and the recycling of transferrin during receptor-mediated endocytosis, Proc Natl Acad Sci U S A, 80, 2258-62*
15. Ohgami, R.S., et al., 2005, *Identification of a ferrireductase required for efficient transferrin-dependent iron uptake in erythroid cells, Nat Genet, 37, 1264-9*
16. Fleming, M.D., et al., 1998, *Nramp2 is mutated in the anemic Belgrade (b) rat: evidence of a role for Nramp2 in endosomal iron transport, Proc Natl Acad Sci U S A, 95, 1148-53*
17. Taketani, S., et al., 2003, *Involvement of ABC7 in the biosynthesis of heme in erythroid cells: interaction of ABC7 with ferrochelatase, Blood, 101, 3274-80*
18. Shaw, G.C., et al., 2006, *Mitoferrin is essential for erythroid iron assimilation, Nature, 440, 96-100*
19. Paradkar, P.N., et al., 2009, *Regulation of mitochondrial iron import through differential turnover of mitoferrin 1 and mitoferrin 2, Mol Cell Biol, 29, 1007-16*
20. Hentze, M.W., M.U. Muckenthaler, and N.C. Andrews, 2004, *Balancing acts: molecular control of mammalian iron metabolism, Cell, 117, 285-97*
21. Kakhlon, O. and Z.I. Cabantchik, 2002, *The labile iron pool: characterization, measurement, and participation in cellular processes(1), Free Radic Biol Med, 33, 1037-46*
22. Arosio, P. and S. Levi, 2010, *Cytosolic and mitochondrial ferritins in the regulation of cellular iron homeostasis and oxidative damage, Biochim Biophys Acta, 1800, 783-92*
23. Harris, Z.L., et al., 1999, *Targeted gene disruption reveals an essential role for ceruloplasmin in cellular iron efflux, Proc Natl Acad Sci U S A, 96, 10812-7*
24. Ganz, T., 2012, *Macrophages and systemic iron homeostasis, J Innate Immun, 4, 446-53*
25. White, C., et al., 2013, *HRG1 is essential for heme transport from the phagolysosome of macrophages during erythrophagocytosis, Cell Metab, 17, 261-70*
26. Delaby, C., et al., 2012, *Subcellular localization of iron and heme metabolism related proteins at early stages of erythrophagocytosis, PLoS One, 7, e42199*

27. Poss, K.D. and S. Tonegawa, 1997, *Heme oxygenase 1 is required for mammalian iron reutilization, Proc Natl Acad Sci U S A, 94, 10919-24*
28. Ganz, T. and E. Nemeth, 2012, *Hepcidin and iron homeostasis, Biochim Biophys Acta, 1823, 1434-43*
29. Darshan, D., D.M. Frazer, and G.J. Anderson, 2010, *Molecular basis of iron-loading disorders, Expert Rev Mol Med, 12, e36*
30. Anderson, C.P., et al., 2012, *Mammalian iron metabolism and its control by iron regulatory proteins, Biochim Biophys Acta, 1823, 1468-83*
31. Muckenthaler, M.U., B. Galy, and M.W. Hentze, 2008, *Systemic iron homeostasis and the iron-responsive element/iron-regulatory protein (IRE/IRP) regulatory network, Annu Rev Nutr, 28, 197-213*
32. Hentze, M.W., et al., 1987, *Identification of the iron-responsive element for the translational regulation of human ferritin mRNA, Science, 238, 1570-3*
33. Muckenthaler, M., N.K. Gray, and M.W. Hentze, 1998, *IRP-1 binding to ferritin mRNA prevents the recruitment of the small ribosomal subunit by the cap-binding complex eIF4F, Mol Cell, 2, 383-8*
34. Gunshin, H., et al., 2001, *Iron-dependent regulation of the divalent metal ion transporter, FEBS Lett, 509, 309-16*
35. Mullner, E.W. and L.C. Kuhn, 1988, *A stem-loop in the 3' untranslated region mediates iron-dependent regulation of transferrin receptor mRNA stability in the cytoplasm, Cell, 53, 815-25*
36. Casey, J.L., et al., 1988, *Iron-responsive elements: regulatory RNA sequences that control mRNA levels and translation, Science, 240, 924-8*
37. Haile, D.J., et al., 1992, *Cellular regulation of the iron-responsive element binding protein: disassembly of the cubane iron-sulfur cluster results in high-affinity RNA binding, Proc Natl Acad Sci U S A, 89, 11735-9*
38. Haile, D.J., et al., 1992, *Reciprocal control of RNA-binding and aconitase activity in the regulation of the iron-responsive element binding protein: role of the iron-sulfur cluster, Proc Natl Acad Sci U S A, 89, 7536-40*
39. Iwai, K., R.D. Klausner, and T.A. Rouault, 1995, *Requirements for iron-regulated degradation of the RNA binding protein, iron regulatory protein 2, EMBO J, 14, 5350-7*
40. Smith, S.R., et al., 2006, *Complete loss of iron regulatory proteins 1 and 2 prevents viability of murine zygotes beyond the blastocyst stage of embryonic development, Blood Cells Mol Dis, 36, 283-7*
41. Ghosh, M.C., et al., 2013, *Deletion of iron regulatory protein 1 causes polycythemia and pulmonary hypertension in mice through translational derepression of HIF2alpha, Cell Metab, 17, 271-81*
42. Galy, B., et al., 2005, *Altered body iron distribution and microcytosis in mice deficient in iron regulatory protein 2 (IRP2), Blood, 106, 2580-9*
43. Wilkinson, N. and K. Pantopoulos, 2014, *The IRP/IRE system in vivo: insights from mouse models, Front Pharmacol, 5, 176*
44. Brissot, P., et al., 2012, *Non-transferrin bound iron: a key role in iron overload and iron toxicity, Biochim Biophys Acta, 1820, 403-10*
45. Nam, H., et al., 2013, *ZIP14 and DMT1 in the liver, pancreas, and heart are differentially regulated by iron deficiency and overload: implications for tissue iron uptake in iron-related disorders, Haematologica, 98, 1049-57*
46. Wang, C.Y., et al., 2012, *ZIP8 is an iron and zinc transporter whose cell-surface expression is up-regulated by cellular iron loading, J Biol Chem, 287, 34032-43*
47. Park, C.H., et al., 2001, *Hepcidin, a urinary antimicrobial peptide synthesized in the liver, J Biol Chem, 276, 7806-10*

48. Donovan, A., et al., 2005, *The iron exporter ferroportin/Slc40a1 is essential for iron homeostasis, Cell Metab, 1, 191-200*
49. Nemeth, E., et al., 2004, *Hepcidin regulates cellular iron efflux by binding to ferroportin and inducing its internalization, Science, 306, 2090-3*
50. Qiao, B., et al., 2012, *Hepcidin-induced endocytosis of ferroportin is dependent on ferroportin ubiquitination, Cell Metab, 15, 918-24*
51. Pinto, J.P., et al., 2010, *Hepcidin messenger RNA expression in human lymphocytes, Immunology, 130, 217-30*
52. Sow, F.B., et al., 2007, *Expression and localization of hepcidin in macrophages: a role in host defense against tuberculosis, J Leukoc Biol, 82, 934-45*
53. Kulaksiz, H., et al., 2005, *The iron-regulatory peptide hormone hepcidin: expression and cellular localization in the mammalian kidney, J Endocrinol, 184, 361-70*
54. Merle, U., et al., 2007, *The iron regulatory peptide hepcidin is expressed in the heart and regulated by hypoxia and inflammation, Endocrinology, 148, 2663-8*
55. Pigeon, C., et al., 2001, *A new mouse liver-specific gene, encoding a protein homologous to human antimicrobial peptide hepcidin, is overexpressed during iron overload, J Biol Chem, 276, 7811-9*
56. Kautz, L., et al., 2008, *Iron regulates phosphorylation of Smad1/5/8 and gene expression of Bmp6, Smad7, Id1, and Atoh8 in the mouse liver, Blood, 112, 1503-9*
57. Steinbicker, A.U., et al., 2011, *Perturbation of hepcidin expression by BMP type I receptor deletion induces iron overload in mice, Blood, 118, 4224-30*
58. Mayeur, C., et al., 2014, *BMP type II receptors have redundant roles in the regulation of hepatic hepcidin gene expression and iron metabolism, Blood, 124, 2116-23*
59. Parrow, N.L. and R.E. Fleming, 2014, *Bone morphogenetic proteins as regulators of iron metabolism, Annu Rev Nutr, 34, 77-94*
60. Andriopoulos, B., Jr., et al., 2009, *BMP6 is a key endogenous regulator of hepcidin expression and iron metabolism, Nat Genet, 41, 482-7*
61. Meynard, D., et al., 2009, *Lack of the bone morphogenetic protein BMP6 induces massive iron overload, Nat Genet, 41, 478-81*
62. Canali, S., et al., 2017, *Endothelial cells produce bone morphogenetic protein 6 required for iron homeostasis in mice, Blood, 129, 405-414*
63. Xia, Y., et al., 2008, *Hemojuvelin regulates hepcidin expression via a selective subset of BMP ligands and receptors independently of neogenin, Blood, 111, 5195-204*
64. Koch, P.S., et al., 2017, *Angiocrine Bmp2 signaling in murine liver controls normal iron homeostasis, Blood, 129, 415-419*
65. Babitt, J.L., et al., 2006, *Bone morphogenetic protein signaling by hemojuvelin regulates hepcidin expression, Nat Genet, 38, 531-9*
66. Silvestri, L., A. Pagani, and C. Camaschella, 2008, *Furin-mediated release of soluble hemojuvelin: a new link between hypoxia and iron homeostasis, Blood, 111, 924-31*
67. Silvestri, L., et al., 2008, *The serine protease matriptase-2 (TMPRSS6) inhibits hepcidin activation by cleaving membrane hemojuvelin, Cell Metab, 8, 502-11*
68. Mleczko-Sanecka, K., et al., 2010, *SMAD7 controls iron metabolism as a potent inhibitor of hepcidin expression, Blood, 115, 2657-65*
69. Goswami, T. and N.C. Andrews, 2006, *Hereditary hemochromatosis protein, HFE, interaction with transferrin receptor 2 suggests a molecular mechanism for mammalian iron sensing, J Biol Chem, 281, 28494-8*
70. Schmidt, P.J., et al., 2008, *The transferrin receptor modulates Hfe-dependent regulation of hepcidin expression, Cell Metab, 7, 205-14*
71. Ramey, G., J.C. Deschemin, and S. Vaulont, 2009, *Cross-talk between the mitogen activated protein kinase and bone morphogenetic protein/hemojuvelin pathways is*

required for the induction of hepcidin by holotransferrin in primary mouse hepatocytes, Haematologica, 94, 765-72
72. Ganz, T., 2009, *Iron in innate immunity: starve the invaders, Curr Opin Immunol, 21, 63-7*
73. Rodriguez, R., et al., 2014, *Hepcidin induction by pathogens and pathogen-derived molecules is strongly dependent on interleukin-6, Infect Immun, 82, 745-52*
74. Nemeth, E., et al., 2004, *IL-6 mediates hypoferremia of inflammation by inducing the synthesis of the iron regulatory hormone hepcidin, J Clin Invest, 113, 1271-6*
75. Wrighting, D.M. and N.C. Andrews, 2006, *Interleukin-6 induces hepcidin expression through STAT3, Blood, 108, 3204-9*
76. Wang, R.H., et al., 2005, *A role of SMAD4 in iron metabolism through the positive regulation of hepcidin expression, Cell Metab, 2, 399-409*
77. Verga Falzacappa, M.V., et al., 2008, *A bone morphogenetic protein (BMP)-responsive element in the hepcidin promoter controls HFE2-mediated hepatic hepcidin expression and its response to IL-6 in cultured cells, J Mol Med (Berl), 86, 531-40*
78. Kautz, L., et al., 2014, *Identification of erythroferrone as an erythroid regulator of iron metabolism, Nat Genet, 46, 678-84*
79. Tanno, T., et al., 2007, *High levels of GDF15 in thalassemia suppress expression of the iron regulatory protein hepcidin, Nat Med, 13, 1096-101*
80. Tanno, T., et al., 2009, *Identification of TWSG1 as a second novel erythroid regulator of hepcidin expression in murine and human cells, Blood, 114, 181-6*
81. Suzuki, N., 2015, *Erythropoietin gene expression: developmental-stage specificity, cell-type specificity, and hypoxia inducibility, Tohoku J Exp Med, 235, 233-40*
82. Pak, M., et al., 2006, *Suppression of hepcidin during anemia requires erythropoietic activity, Blood, 108, 3730-5*
83. Taylor, M., et al., 2011, *Hypoxia-inducible factor-2alpha mediates the adaptive increase of intestinal ferroportin during iron deficiency in mice, Gastroenterology, 140, 2044-55*
84. Mastrogiannaki, M., et al., 2009, *HIF-2alpha, but not HIF-1alpha, promotes iron absorption in mice, J Clin Invest, 119, 1159-66*
85. Peyssonnaux, C., et al., 2007, *Regulation of iron homeostasis by the hypoxia-inducible transcription factors (HIFs), J Clin Invest, 117, 1926-32*
86. Haase, V.H., 2010, *Hypoxic regulation of erythropoiesis and iron metabolism, Am J Physiol Renal Physiol, 299, F1-13*
87. Liu, Q., et al., 2012, *Hypoxia-inducible factor regulates hepcidin via erythropoietin-induced erythropoiesis, J Clin Invest, 122, 4635-44*
88. Mastrogiannaki, M., et al., 2012, *Hepatic hypoxia-inducible factor-2 down-regulates hepcidin expression in mice through an erythropoietin-mediated increase in erythropoiesis, Haematologica, 97, 827-34*
89. Maurer, E., M. Gutschow, and M. Stirnberg, 2012, *Matriptase-2 (TMPRSS6) is directly up-regulated by hypoxia inducible factor-1: identification of a hypoxia-responsive element in the TMPRSS6 promoter region, Biol Chem, 393, 535-40*
90. McMahon, S., et al., 2005, *Hypoxia-enhanced expression of the proprotein convertase furin is mediated by hypoxia-inducible factor-1: impact on the bioactivation of proproteins, J Biol Chem, 280, 6561-9*
91. Marro, S., et al., 2010, *Heme controls ferroportin1 (FPN1) transcription involving Bach1, Nrf2 and a MARE/ARE sequence motif at position -7007 of the FPN1 promoter, Haematologica, 95, 1261-8*
92. Aydemir, F., et al., 2009, *Iron loading increases ferroportin heterogeneous nuclear RNA and mRNA levels in murine J774 macrophages, J Nutr, 139, 434-8*
93. Liu, X.B., et al., 2005, *Regulation of hepcidin and ferroportin expression by lipopolysaccharide in splenic macrophages, Blood Cells Mol Dis, 35, 47-56*

94. Yang, F., et al., 2002, *Regulation of reticuloendothelial iron transporter MTP1 (Slc11a3) by inflammation, J Biol Chem, 277, 39786-91*
95. Deschemin, J.C. and S. Vaulont, 2013, *Role of hepcidin in the setting of hypoferremia during acute inflammation, PLoS One, 8, e61050*
96. Guida, C., et al., 2015, *A novel inflammatory pathway mediating rapid hepcidin-independent hypoferremia, Blood, 125, 2265-75*
97. Peyssonnaux, C., et al., 2006, *TLR4-dependent hepcidin expression by myeloid cells in response to bacterial pathogens, Blood, 107, 3727-32*
98. Schubert, T.E., et al., 2012, *Hypoferraemia during the early inflammatory response is dependent on tumour necrosis factor activity in a murine model of protracted peritonitis, Mol Med Rep, 6, 838-42*
99. Zhang, D.L., et al., 2009, *A ferroportin transcript that lacks an iron-responsive element enables duodenal and erythroid precursor cells to evade translational repression, Cell Metab, 9, 461-73*
100. Sham, R.L., et al., 2005, *Autosomal dominant hereditary hemochromatosis associated with a novel ferroportin mutation and unique clinical features, Blood Cells Mol Dis, 34, 157-61*
101. Fernandes, A., et al., 2009, *The molecular basis of hepcidin-resistant hereditary hemochromatosis, Blood, 114, 437-43*
102. Altamura, S., et al., 2014, *Resistance of ferroportin to hepcidin binding causes exocrine pancreatic failure and fatal iron overload, Cell Metab, 20, 359-67*
103. Bridle, K.R., et al., 2003, *Disrupted hepcidin regulation in HFE-associated haemochromatosis and the liver as a regulator of body iron homoeostasis, Lancet, 361, 669-73*
104. Feder, J.N., et al., 1996, *A novel MHC class I-like gene is mutated in patients with hereditary haemochromatosis, Nat Genet, 13, 399-408*
105. Papanikolaou, G., et al., 2004, *Mutations in HFE2 cause iron overload in chromosome 1q-linked juvenile hemochromatosis, Nat Genet, 36, 77-82*
106. Nemeth, E., et al., 2005, *Hepcidin is decreased in TFR2 hemochromatosis, Blood, 105, 1803-6*
107. Roetto, A., et al., 2003, *Mutant antimicrobial peptide hepcidin is associated with severe juvenile hemochromatosis, Nat Genet, 33, 21-2*
108. Sham, R.L., et al., 2009, *Hereditary hemochromatosis due to resistance to hepcidin: high hepcidin concentrations in a family with C326S ferroportin mutation, Blood, 114, 493-4*
109. Pietrangelo, A., 2004, *The ferroportin disease, Blood Cells Mol Dis, 32, 131-8*
110. Origa, R., et al., 2007, *Liver iron concentrations and urinary hepcidin in beta-thalassemia, Haematologica, 92, 583-8*
111. Kattamis, A., et al., 2006, *The effects of erythropoetic activity and iron burden on hepcidin expression in patients with thalassemia major, Haematologica, 91, 809-12*
112. Finberg, K.E., et al., 2008, *Mutations in TMPRSS6 cause iron-refractory iron deficiency anemia (IRIDA), Nat Genet, 40, 569-71*
113. Kim, A., et al., 2014, *A mouse model of anemia of inflammation: complex pathogenesis with partial dependence on hepcidin, Blood, 123, 1129-36*
114. Zaritsky, J., et al., 2009, *Hepcidin--a potential novel biomarker for iron status in chronic kidney disease, Clin J Am Soc Nephrol, 4, 1051-6*
115. Andrews, N.C., 2004, *Anemia of inflammation: the cytokine-hepcidin link, J Clin Invest, 113, 1251-3*
116. Herriges, M. and E.E. Morrisey, 2014, *Lung development: orchestrating the generation and regeneration of a complex organ, Development, 141, 502-13*
117. Kling, M.A., 2011, *A review of respiratory system anatomy, physiology, and disease in the mouse, rat, hamster, and gerbil, Vet Clin North Am Exot Anim Pract, 14, 287-337, vi*

118. Karrer, H.E., 1956, *The ultrastructure of mouse lung; some remarks regarding the fine structure of the alveolar basement membrane, J Biophys Biochem Cytol, 2, 287-92*
119. Burri, P.H., 2006, *Structural aspects of postnatal lung development - alveolar formation and growth, Biol Neonate, 89, 313-22*
120. Rock, J.R. and B.L. Hogan, 2011, *Epithelial progenitor cells in lung development, maintenance, repair, and disease, Annu Rev Cell Dev Biol, 27, 493-512*
121. Whitsett, J.A. and T. Alenghat, 2015, *Respiratory epithelial cells orchestrate pulmonary innate immunity, Nat Immunol, 16, 27-35*
122. Ganesan, S., A.T. Comstock, and U.S. Sajjan, 2013, *Barrier function of airway tract epithelium, Tissue Barriers, 1, e24997*
123. Hussell, T. and T.J. Bell, 2014, *Alveolar macrophages: plasticity in a tissue-specific context, Nat Rev Immunol, 14, 81-93*
124. Wong, A.P., A. Keating, and T.K. Waddell, 2009, *Airway regeneration: the role of the Clara cell secretory protein and the cells that express it, Cytotherapy, 11, 676-87*
125. Suresh, K. and L.A. Shimoda, 2016, *Lung Circulation, Compr Physiol, 6, 897-943*
126. Reid, L., 1965, *The angiogram and pulmonary artery structure and branching (in the normal and with reference to disease), Proc R Soc Med, 58, 681-4*
127. Hislop, A. and L. Reid, 1978, *Normal structure and dimensions of the pulmonary arteries in the rat, J Anat, 125, 71-83*
128. Low, F.N., 1952, *Electron microscopy of the rat lung, Anat Rec, 113, 437-49*
129. Townsley, M.I., 2012, *Structure and composition of pulmonary arteries, capillaries, and veins, Compr Physiol, 2, 675-709*
130. Rawlins, E.L. and B.L. Hogan, 2008, *Ciliated epithelial cell lifespan in the mouse trachea and lung, Am J Physiol Lung Cell Mol Physiol, 295, L231-4*
131. Popatia, R., K. Haver, and A. Casey, 2014, *Primary Ciliary Dyskinesia: An Update on New Diagnostic Modalities and Review of the Literature, Pediatr Allergy Immunol Pulmonol, 27, 51-59*
132. Hovenberg, H.W., J.R. Davies, and I. Carlstedt, 1996, *Different mucins are produced by the surface epithelium and the submucosa in human trachea: identification of MUC5AC as a major mucin from the goblet cells, Biochem J, 318 (Pt 1), 319-24*
133. Thornton, D.J., K. Rousseau, and M.A. McGuckin, 2008, *Structure and function of the polymeric mucins in airways mucus, Annu Rev Physiol, 70, 459-86*
134. Knowles, M.R. and R.C. Boucher, 2002, *Mucus clearance as a primary innate defense mechanism for mammalian airways, J Clin Invest, 109, 571-7*
135. Roy, M.G., et al., 2014, *Muc5b is required for airway defence, Nature, 505, 412-6*
136. Evans, M.J. and C.G. Plopper, 1988, *The role of basal cells in adhesion of columnar epithelium to airway basement membrane, Am Rev Respir Dis, 138, 481-3*
137. Evans, M.J., et al., 1989, *The role of basal cells in attachment of columnar cells to the basal lamina of the trachea, Am J Respir Cell Mol Biol, 1, 463-9*
138. Rock, J.R., et al., 2009, *Basal cells as stem cells of the mouse trachea and human airway epithelium, Proc Natl Acad Sci U S A, 106, 12771-5*
139. Hong, K.U., et al., 2004, *Basal cells are a multipotent progenitor capable of renewing the bronchial epithelium, Am J Pathol, 164, 577-88*
140. Singh, G. and S.L. Katyal, 1997, *Clara cells and Clara cell 10 kD protein (CC10), Am J Respir Cell Mol Biol, 17, 141-3*
141. Stripp, B.R., et al., 2002, *Clara cell secretory protein deficiency alters clara cell secretory apparatus and the protein composition of airway lining fluid, Am J Respir Cell Mol Biol, 27, 170-8*
142. Mango, G.W., et al., 1998, *Clara cell secretory protein deficiency increases oxidant stress response in conducting airways, Am J Physiol, 275, L348-56*

143. Chen, L.C., et al., 2001, *Cutting edge: altered pulmonary eosinophilic inflammation in mice deficient for Clara cell secretory 10-kDa protein, J Immunol, 167, 3025-8*
144. Harrod, K.S., et al., 1998, *Clara cell secretory protein decreases lung inflammation after acute virus infection, Am J Physiol, 275, L924-30*
145. Reynolds, S.D. and A.M. Malkinson, 2010, *Clara cell: progenitor for the bronchiolar epithelium, Int J Biochem Cell Biol, 42, 1-4*
146. Rawlins, E.L., et al., 2009, *The role of Scgb1a1+ Clara cells in the long-term maintenance and repair of lung airway, but not alveolar, epithelium, Cell Stem Cell, 4, 525-34*
147. Linnoila, R.I., 2006, *Functional facets of the pulmonary neuroendocrine system, Lab Invest, 86, 425-44*
148. Youngson, C., et al., 1993, *Oxygen sensing in airway chemoreceptors, Nature, 365, 153-5*
149. Branchfield, K., et al., 2016, *Pulmonary neuroendocrine cells function as airway sensors to control lung immune response, Science, 351, 707-10*
150. Herzog, E.L., et al., 2008, *Knowns and unknowns of the alveolus, Proc Am Thorac Soc, 5, 778-82*
151. Crapo, J.D., et al., 1982, *Cell number and cell characteristics of the normal human lung, Am Rev Respir Dis, 126, 332-7*
152. Desai, T.J., D.G. Brownfield, and M.A. Krasnow, 2014, *Alveolar progenitor and stem cells in lung development, renewal and cancer, Nature, 507, 190-4*
153. Barkauskas, C.E., et al., 2013, *Type 2 alveolar cells are stem cells in adult lung, J Clin Invest, 123, 3025-36*
154. Goerke, J., 1998, *Pulmonary surfactant: functions and molecular composition, Biochim Biophys Acta, 1408, 79-89*
155. Perez-Gil, J. and T.E. Weaver, 2010, *Pulmonary surfactant pathophysiology: current models and open questions, Physiology (Bethesda), 25, 132-41*
156. Wright, J.R., 2004, *Host defense functions of pulmonary surfactant, Biol Neonate, 85, 326-32*
157. Cerrada, A., et al., 2015, *Pneumocytes Assemble Lung Surfactant as Highly Packed/Dehydrated States with Optimal Surface Activity, Biophys J, 109, 2295-306*
158. Akella, A. and S.B. Deshpande, 2013, *Pulmonary surfactants and their role in pathophysiology of lung disorders, Indian J Exp Biol, 51, 5-22*
159. Williams, G.D., et al., 1999, *Surfactant protein B deficiency: clinical, histological and molecular evaluation, J Paediatr Child Health, 35, 214-20*
160. Sano, H., et al., 1999, *Pulmonary surfactant protein A modulates the cellular response to smooth and rough lipopolysaccharides by interaction with CD14, J Immunol, 163, 387-95*
161. Gardai, S.J., et al., 2003, *By binding SIRPalpha or calreticulin/CD91, lung collectins act as dual function surveillance molecules to suppress or enhance inflammation, Cell, 115, 13-23*
162. LeVine, A.M., et al., 1997, *Surfactant protein A-deficient mice are susceptible to group B streptococcal infection, J Immunol, 158, 4336-40*
163. LeVine, A.M., et al., 1998, *Surfactant protein-A-deficient mice are susceptible to Pseudomonas aeruginosa infection, Am J Respir Cell Mol Biol, 19, 700-8*
164. Fakih, D., et al., 2015, *Protective effects of surfactant protein D treatment in 1,3-beta-glucan-modulated allergic inflammation, Am J Physiol Lung Cell Mol Physiol, 309, L1333-43*
165. Zissel, G., et al., 2000, *Human alveolar epithelial cells type II are capable of regulating T-cell activity, J Investig Med, 48, 66-75*
166. Snelgrove, R.J., et al., 2008, *A critical function for CD200 in lung immune homeostasis and the severity of influenza infection, Nat Immunol, 9, 1074-83*

167. Lo, B., et al., 2008, *Alveolar epithelial type II cells induce T cell tolerance to specific antigen, J Immunol, 180, 881-8*
168. Fehrenbach, H., 2001, *Alveolar epithelial type II cell: defender of the alveolus revisited, Respir Res, 2, 33-46*
169. Johnson, M.D., et al., 2002, *Alveolar epithelial type I cells contain transport proteins and transport sodium, supporting an active role for type I cells in regulation of lung liquid homeostasis, Proc Natl Acad Sci U S A, 99, 1966-71*
170. Bove, P.F., et al., 2010, *Human alveolar type II cells secrete and absorb liquid in response to local nucleotide signaling, J Biol Chem, 285, 34939-49*
171. West, J.B., 2009, *Comparative physiology of the pulmonary blood-gas barrier: the unique avian solution, Am J Physiol Regul Integr Comp Physiol, 297, R1625-34*
172. Vanoirbeek, J.A., et al., 2010, *Noninvasive and invasive pulmonary function in mouse models of obstructive and restrictive respiratory diseases, Am J Respir Cell Mol Biol, 42, 96-104*
173. King, T.E., Jr., A. Pardo, and M. Selman, 2011, *Idiopathic pulmonary fibrosis, Lancet, 378, 1949-61*
174. Organ, L., et al., 2015, *Structural and functional correlations in a large animal model of bleomycin-induced pulmonary fibrosis, BMC Pulm Med, 15, 81*
175. Guth, A.M., et al., 2009, *Lung environment determines unique phenotype of alveolar macrophages, Am J Physiol Lung Cell Mol Physiol, 296, L936-46*
176. Misharin, A.V., et al., 2013, *Flow cytometric analysis of macrophages and dendritic cell subsets in the mouse lung, Am J Respir Cell Mol Biol, 49, 503-10*
177. Zaynagetdinov, R., et al., 2013, *Identification of myeloid cell subsets in murine lungs using flow cytometry, Am J Respir Cell Mol Biol, 49, 180-9*
178. Naessens, T., et al., 2012, *Innate imprinting of murine resident alveolar macrophages by allergic bronchial inflammation causes a switch from hypoinflammatory to hyperinflammatory reactivity, Am J Pathol, 181, 174-84*
179. Zhang, M., et al., 2007, *Defining the in vivo function of Siglec-F, a CD33-related Siglec expressed on mouse eosinophils, Blood, 109, 4280-7*
180. Guilliams, M., et al., 2013, *Alveolar macrophages develop from fetal monocytes that differentiate into long-lived cells in the first week of life via GM-CSF, J Exp Med, 210, 1977-92*
181. Epelman, S., K.J. Lavine, and G.J. Randolph, 2014, *Origin and functions of tissue macrophages, Immunity, 41, 21-35*
182. Hashimoto, D., et al., 2013, *Tissue-resident macrophages self-maintain locally throughout adult life with minimal contribution from circulating monocytes, Immunity, 38, 792-804*
183. Gasson, J.C., 1991, *Molecular physiology of granulocyte-macrophage colony-stimulating factor, Blood, 77, 1131-45*
184. Qiu, C., et al., 2014, *GM-CSF induces cyclin D1 expression and proliferation of endothelial progenitor cells via PI3K and MAPK signaling, Cell Physiol Biochem, 33, 784-95*
185. Robertson, S.A., 2007, *GM-CSF regulation of embryo development and pregnancy, Cytokine Growth Factor Rev, 18, 287-98*
186. Gearing, D.P., et al., 1989, *Expression cloning of a receptor for human granulocyte-macrophage colony-stimulating factor, EMBO J, 8, 3667-76*
187. Hayashida, K., et al., 1990, *Molecular cloning of a second subunit of the receptor for human granulocyte-macrophage colony-stimulating factor (GM-CSF): reconstitution of a high-affinity GM-CSF receptor, Proc Natl Acad Sci U S A, 87, 9655-9*

188. Martinez-Moczygemba, M. and D.P. Huston, 2003, *Biology of common beta receptor-signaling cytokines: IL-3, IL-5, and GM-CSF, J Allergy Clin Immunol, 112, 653-65; quiz 666*
189. Jeong, W., et al., 2014, *Proliferation-stimulating effect of colony stimulating factor 2 on porcine trophectoderm cells is mediated by activation of phosphatidylinositol 3-kinase and extracellular signal-regulated kinase 1/2 mitogen-activated protein kinase, PLoS One, 9, e88731*
190. Doyle, S.E. and J.C. Gasson, 1998, *Characterization of the role of the human granulocyte-macrophage colony-stimulating factor receptor alpha subunit in the activation of JAK2 and STAT5, Blood, 92, 867-76*
191. Watanabe, S., T. Itoh, and K. Arai, 1996, *JAK2 is essential for activation of c-fos and c-myc promoters and cell proliferation through the human granulocyte-macrophage colony-stimulating factor receptor in BA/F3 cells, J Biol Chem, 271, 12681-6*
192. Beck, J.M., V.B. Young, and G.B. Huffnagle, 2012, *The microbiome of the lung, Transl Res, 160, 258-66*
193. Fernandez, S., et al., 2004, *Inhibition of IL-10 receptor function in alveolar macrophages by Toll-like receptor agonists, J Immunol, 172, 2613-20*
194. Morris, D.G., et al., 2003, *Loss of integrin alpha(v)beta6-mediated TGF-beta activation causes Mmp12-dependent emphysema, Nature, 422, 169-73*
195. Reutershan, J., et al., 2005, *Sequential recruitment of neutrophils into lung and bronchoalveolar lavage fluid in LPS-induced acute lung injury, Am J Physiol Lung Cell Mol Physiol, 289, L807-15*
196. Xing, Z., et al., 1993, *Polymorphonuclear leukocytes as a significant source of tumor necrosis factor-alpha in endotoxin-challenged lung tissue, Am J Pathol, 143, 1009-15*
197. Steinmuller, C., et al., 2000, *Local activation of nonspecific defense against a respiratory model infection by application of interferon-gamma: comparison between rat alveolar and interstitial lung macrophages, Am J Respir Cell Mol Biol, 22, 481-90*
198. Tam, A., et al., 2011, *The airway epithelium: more than just a structural barrier, Ther Adv Respir Dis, 5, 255-73*
199. Mahowald, N.M., et al., 2009, *Atmospheric iron deposition: global distribution, variability, and human perturbations, Ann Rev Mar Sci, 1, 245-78*
200. Ghio, A.J., et al., 1999, *Sulfate content correlates with iron concentrations in ambient air pollution particles, Inhal Toxicol, 11, 293-307*
201. Ghio, A.J., et al., 2008, *Particulate matter in cigarette smoke alters iron homeostasis to produce a biological effect, Am J Respir Crit Care Med, 178, 1130-8*
202. Bailie, G.R., et al., 2013, *Oxidative effect of several intravenous iron complexes in the rat, Biometals, 26, 473-8*
203. Cross, C.E., et al., 1994, *Oxidants, antioxidants, and respiratory tract lining fluids, Environ Health Perspect, 102 Suppl 10, 185-91*
204. Ghio, A.J., 2009, *Disruption of iron homeostasis and lung disease, Biochim Biophys Acta, 1790, 731-9*
205. Ghio, A.J., et al., 1998, *Disruption of normal iron homeostasis after bronchial instillation of an iron-containing particle, Am J Physiol, 274, L396-403*
206. Wang, X., et al., 2002, *Iron uptake and Nramp2/DMT1/DCT1 in human bronchial epithelial cells, Am J Physiol Lung Cell Mol Physiol, 282, L987-95*
207. Ghio, A.J., et al., 2003, *DMT1 expression is increased in the lungs of hypotransferrinemic mice, Am J Physiol Lung Cell Mol Physiol, 284, L938-44*
208. Giorgi, G., M.C. Danna, and M.E. Roque, 2015, *Iron homeostasis and its disruption in mouse lung in iron deficiency and overload, Exp Physiol,*
209. Turi, J.L., et al., 2006, *Duodenal cytochrome b: a novel ferrireductase in airway epithelial cells, Am J Physiol Lung Cell Mol Physiol, 291, L272-80*

210. Yang, F., et al., 2005, *Apical location of ferroportin 1 in airway epithelia and its role in iron detoxification in the lung, Am J Physiol Lung Cell Mol Physiol, 289, L14-23*
211. Yang, F., et al., 2002, *Iron increases expression of iron-export protein MTP1 in lung cells, Am J Physiol Lung Cell Mol Physiol, 283, L932-9*
212. Olakanmi, O., et al., 1993, *Iron sequestration by macrophages decreases the potential for extracellular hydroxyl radical formation, J Clin Invest, 91, 889-99*
213. Hirata, T., et al., 1986, *Expression of the transferrin receptor gene during the process of mononuclear phagocyte maturation, J Immunol, 136, 1339-45*
214. Nguyen, N.B., et al., 2006, *Hepcidin expression and iron transport in alveolar macrophages, Am J Physiol Lung Cell Mol Physiol, 291, L417-25*
215. Mateos, F., J.H. Brock, and J.L. Perez-Arellano, 1998, *Iron metabolism in the lower respiratory tract, Thorax, 53, 594-600*
216. Frazier, M.D., et al., 2011, *Hepcidin expression in human airway epithelial cells is regulated by interferon-gamma, Respir Res, 12, 100*
217. Chen, Q.X., et al., 2014, *Silencing airway epithelial cell-derived hepcidin exacerbates sepsis induced acute lung injury, Crit Care, 18, 470*
218. Philippot, Q., et al., 2014, *Increased iron sequestration in alveolar macrophages in chronic obstructive pulmonary disease, PLoS One, 9, e96285*
219. Ghio, A.J., et al., 2012, *Iron accumulates in the lavage and explanted lungs of cystic fibrosis patients, J Cyst Fibros, 12, 390-8*
220. Ghio, A.J., et al., 2003, *Iron and iron-related proteins in the lower respiratory tract of patients with acute respiratory distress syndrome, Crit Care Med, 31, 395-400*
221. Ghio, A.J., et al., 2008, *Iron homeostasis and oxidative stress in idiopathic pulmonary alveolar proteinosis: a case-control study, Respir Res, 9, 10*
222. Lay, J.C., et al., 1999, *Cellular and biochemical response of the human lung after intrapulmonary instillation of ferric oxide particles, Am J Respir Cell Mol Biol, 20, 631-42*
223. Sadeghi, L., V. Yousefi Babadi, and H.R. Espanani, 2015, *Toxic effects of the Fe2O3 nanoparticles on the liver and lung tissue, Bratisl Lek Listy, 116, 373-8*
224. Park, E.J., et al., 2010, *Inflammatory responses may be induced by a single intratracheal instillation of iron nanoparticles in mice, Toxicology, 275, 65-71*
225. Pfaffl, M.W., 2001, *A new mathematical model for relative quantification in real-time RT-PCR, Nucleic Acids Res, 29, e45*
226. Torrance, J.D. and T.H. Bothwell, 1968, *A simple technique for measuring storage iron concentrations in formalinised liver samples, S Afr J Med Sci, 33, 9-11*
227. Galy, B., et al., 2004, *Targeted mutagenesis of the murine IRP1 and IRP2 genes reveals context-dependent RNA processing differences in vivo, RNA, 10, 1019-25*
228. Galy, B., et al., 2008, *Iron regulatory proteins are essential for intestinal function and control key iron absorption molecules in the duodenum, Cell Metab, 7, 79-85*
229. Mall, M.A., et al., 2008, *Development of chronic bronchitis and emphysema in beta-epithelial Na+ channel-overexpressing mice, Am J Respir Crit Care Med, 177, 730-42*
230. Kosanovic, D., et al., 2011, *Therapeutic efficacy of TBC3711 in monocrotaline-induced pulmonary hypertension, Respir Res, 12, 87*
231. Muhlfeld, C., L. Knudsen, and M. Ochs, 2013, *Stereology and morphometry of lung tissue, Methods Mol Biol, 931, 367-90*
232. Jenkitkasemwong, S., et al., 2012, *Physiologic implications of metal-ion transport by ZIP14 and ZIP8, Biometals, 25, 643-55*
233. Altamura, S. and M.U. Muckenthaler, 2009, *Iron toxicity in diseases of aging: Alzheimer's disease, Parkinson's disease and atherosclerosis, J Alzheimers Dis, 16, 879-95*
234. Theurl, I., et al., 2016, *On-demand erythrocyte disposal and iron recycling requires transient macrophages in the liver, Nat Med,*

235. Sica, A. and A. Mantovani, 2012, *Macrophage plasticity and polarization: in vivo veritas, J Clin Invest, 122, 787-95*
236. Kroner, A., et al., 2014, *TNF and increased intracellular iron alter macrophage polarization to a detrimental M1 phenotype in the injured spinal cord, Neuron, 83, 1098-116*
237. Recalcati, S., et al., 2012, *Iron levels in polarized macrophages: regulation of immunity and autoimmunity, Autoimmun Rev, 11, 883-9*
238. Vinchi, F., et al., 2016, *Hemopexin therapy reverts heme-induced proinflammatory phenotypic switching of macrophages in a mouse model of sickle cell disease, Blood, 127, 473-86*
239. Cimino-Mathews, A. and P.B. Illei, 2013, *Cytologic and histologic findings of iron pill-induced injury of the lower respiratory tract, Diagn Cytopathol, 41, 901-3*
240. Filosa, A., et al., 2000, *Evidence of lymphocyte alveolitis by bronchoalveolar lavage in thalassemic patients with pulmonary dysfunction, Acta Haematol, 103, 90-5*
241. Parakh, A., et al., 2007, *Study of pulmonary function tests in thalassemic children, J Pediatr Hematol Oncol, 29, 151-5*
242. Zumerle, S., et al., 2014, *Targeted disruption of hepcidin in the liver recapitulates the hemochromatotic phenotype, Blood, 123, 3646-50*
243. Lakhal-Littleton, S., et al., 2016, *An essential cell-autonomous role for hepcidin in cardiac iron homeostasis, Elife, 5,*
244. Rensen, S.S., P.A. Doevendans, and G.J. van Eys, 2007, *Regulation and characteristics of vascular smooth muscle cell phenotypic diversity, Neth Heart J, 15, 100-8*
245. Mathew, R., et al., 2016, *Hematological disorders and pulmonary hypertension, World J Cardiol, 8, 703-718*
246. Cotroneo, E., et al., 2015, *Iron homeostasis and pulmonary hypertension: iron deficiency leads to pulmonary vascular remodeling in the rat, Circ Res, 116, 1680-90*
247. Benesova, K., et al., 2012, *Hfe deficiency impairs pulmonary neutrophil recruitment in response to inflammation, PLoS One, 7, e39363*
248. Wang, L., et al., 2009, *Selective modulation of TLR4-activated inflammatory responses by altered iron homeostasis in mice, J Clin Invest, 119, 3322-8*
249. Khiroya, H. and A.M. Turner, 2015, *The role of iron in pulmonary pathology, Multidiscip Respir Med, 10, 34*
250. Reid, D.W., et al., 2007, *Increased airway iron as a potential factor in the persistence of Pseudomonas aeruginosa infection in cystic fibrosis, Eur Respir J, 30, 286-92*
251. Damron, F.H., et al., 2016, *Dual-seq transcriptomics reveals the battle for iron during Pseudomonas aeruginosa acute murine pneumonia, Sci Rep, 6, 39172*
252. Carnelli, V., et al., 2003, *Pulmonary dysfunction in transfusion-dependent patients with thalassemia major, Am J Respir Crit Care Med, 168, 180-4*
253. Guidotti, F., et al., 2016, *Pulmonary dysfunction in thalassaemia major: is there any relationship with body iron stores?, Br J Haematol,*
254. Kanj, N., et al., 2000, *Relation of ferritin levels to pulmonary function in patients with thalassemia major and the acute effects of transfusion, Eur J Haematol, 64, 396-400*
255. Bourli, E., et al., 2012, *Restrictive pulmonary dysfunction and its predictors in young patients with beta-thalassaemia major, Pediatr Pulmonol, 47, 801-7*
256. Factor, J.M., et al., 1994, *Pulmonary function abnormalities in thalassemia major and the role of iron overload, Am J Respir Crit Care Med, 149, 1570-4*
257. Piatti, G., et al., 2006, *Lung function in beta-thalassemia patients: a longitudinal study, Acta Haematol, 116, 25-9*
258. Won, S.M., et al., 2011, *Iron mediates endothelial cell damage and blood-brain barrier opening in the hippocampus after transient forebrain ischemia in rats, Exp Mol Med, 43, 121-8*

259. Rodriguez-Capote, K., et al., 2006, *Reactive oxygen species inactivation of surfactant involves structural and functional alterations to surfactant proteins SP-B and SP-C, Biophys J, 90, 2808-21*
260. Sanchez, M., et al., 2007, *Iron-regulatory proteins limit hypoxia-inducible factor-2alpha expression in iron deficiency, Nat Struct Mol Biol, 14, 420-6*

Peer-reviewed article associated with this thesis

EBioMedicine 20 (2017) 230–239

Contents lists available at ScienceDirect

EBioMedicine

journal homepage: www.ebiomedicine.com

Research Paper

Disruption of the Hepcidin/Ferroportin Regulatory System Causes Pulmonary Iron Overload and Restrictive Lung Disease

Joana Neves [a,b,c,d], Dominik Leitz [d,e], Simone Kraut [f], Christina Brandenberger [g], Raman Agrawal [d,e], Norbert Weissmann [f], Christian Mühlfeld [g], Marcus A. Mall [b,d,e,1], Sandro Altamura [a,b,1], Martina U. Muckenthaler [a,b,d,*,1]

[a] Department of Pediatric Hematology, Oncology and Immunology - University of Heidelberg, Im Neuenheimer Feld 350, D-69120 Heidelberg, Germany
[b] Molecular Medicine Partnership Unit, D-69120 Heidelberg, Germany
[c] Graduate Program in Areas of Basic and Applied Biology, Abel Salazar Biomedical Sciences Institute, University of Porto, 4050-343 Porto, Portugal
[d] Translational Lung Research Center Heidelberg (TLRC), German Center for Lung Research (DZL), University of Heidelberg, D-69120 Heidelberg, Germany
[e] Department of Translational Pulmonology, University of Heidelberg, D-69120 Heidelberg, Germany
[f] Justus-Liebig University of Giessen (JLUG), Excellence Cluster Cardiopulmonary System (ECCPS), Universities of Giessen and Marburg Lung Center (UGMLC), German Center for Lung Research (DZL), Germany
[g] Institute of Functional and Applied Anatomy, Biomedical Research in Endstage and Obstructive Lung Disease Hannover (BREATH), German Center for Lung Research (DZL), Hannover Medical School, D-30625 Hannover, Germany

ARTICLE INFO

Article history:
Received 19 January 2017
Received in revised form 27 April 2017
Accepted 28 April 2017
Available online 29 April 2017

Keywords:
Restrictive lung disease
Ferroportin
Hereditary hemochromatosis
Iron Overload
Hepcidin resistance

ABSTRACT

Emerging evidence suggests that pulmonary iron accumulation is implicated in a spectrum of chronic lung diseases. However, the mechanism(s) involved in pulmonary iron deposition and its role in the in vivo pathogenesis of lung diseases remains unknown. Here we show that a point mutation in the murine ferroportin gene, which causes hereditary hemochromatosis type 4 ($Slc40a1^{C326S}$), increases iron levels in alveolar macrophages, epithelial cells lining the conducting airways and lung parenchyma, and in vascular smooth muscle cells. Pulmonary iron overload is associated with oxidative stress, restrictive lung disease with decreased total lung capacity and reduced blood oxygen saturation in homozygous $Slc40a1^{C326S/C326S}$ mice compared to wild-type controls. These findings implicate iron in lung pathology, which is so far not considered a classical iron-related disorder.

1. Introduction

Imbalances of iron homeostasis are implicated in a spectrum of acute and chronic lung diseases (Ghio, 2009; Ghio et al., 2013). In patients with chronic obstructive pulmonary disease (COPD), iron deposits in alveolar macrophages (AM) and the percentage of iron loaded macrophages is associated with increased disease severity (Philippot et al., 2014). On the other hand thalassemia major, a disease characterized by transfusional iron overload, has been associated with impaired lung function (Carnelli et al., 2003; Guidotti et al., 2016; Kanj et al., 2000). However, whether pulmonary iron accumulation contributes to disease onset and progression is poorly understood.

Tissue iron levels must be maintained in such a way that both iron deficiency and iron overload are prevented. Excess free iron generates oxidative stress causing cell damage and tissue injury (Muckenthaler et al., 2017). In the lung, the risk for oxidative stress is exacerbated by its continuous exposure to an atmosphere with high oxygen levels. The mechanisms maintaining lung iron homeostasis are incompletely understood. Like most other cells, lung cells acquire transferrin-bound iron from the plasma. In addition, lung airway epithelial cells take up iron via the divalent metal transporter 1 (DMT1) and sequester it in the iron storage protein ferritin (Ghio, 2009; Wang et al., 2002). Upon iron exposure, pulmonary ferritin levels increase, possibly protecting from oxidative stress (Ghio, 2009; Ghio et al., 1998; Giorgi et al., 2015).

The supply of iron to the lung depends on its systemic plasma availability, which is controlled by the hepcidin/ferroportin regulatory axis (Muckenthaler et al., 2017). Hepatic hepcidin produced in response to increased systemic iron levels binds to the iron exporter ferroportin (FPN) to control its internalization, ubiquitination and subsequent lysosomal degradation (Nemeth et al., 2004; Qiao et al., 2012). In turn, this decreases iron efflux from exporting cells, such as duodenal enterocytes and reticuloendothelial macrophages. Mutations in the iron exporter FPN that confer resistance to hepcidin binding cause hereditary hemochromatosis (HH) type 4, a genetically inherited

* Corresponding author.
E-mail address: martina.muckenthaler@med.uni-heidelberg.de (M.U. Muckenthaler).
[1] Equal contribution.

http://dx.doi.org/10.1016/j.ebiom.2017.04.036

primary iron overload disorder hallmarked by increased systemic iron levels, iron depletion in iron-exporting organs and severe iron deposition in parenchymal tissues (Altamura et al., 2014; Sham et al., 2009; Sham et al., 2005).

Here, we aim to understand whether a disruption in the FPN/hepcidin regulatory system and the subsequent increase in systemic iron levels affect lung iron homeostasis and function. To achieve this goal, we took advantage of a murine disease model of HH type 4, hallmarked by a C326S amino acid substitution in FPN ($Slc40a1^{C326S}$) (Altamura et al., 2014). We show that resistance of ferroportin to hepcidin binding causes pulmonary iron accumulation in defined lung cell types. Homozygous $Slc40a1^{C326S/C326S}$ mice show increased oxidative stress in the lung, restrictive lung disease and decreased blood oxygen saturation, revealing a role of iron in lung pathology.

2. Material and Methods

2.1. Mice

All mice analyzed were maintained on a pure C57BL/6N genetic background (>99.9% congenic). As controls, age- and gender-matched wild-type C57BL/6N mice born and maintained in the same breeding facility were used. Mice were housed in the Heidelberg University animal facility under a constant light-dark cycle and maintained on a standard mouse diet (LASQCdiet Rod18-A - LASvendi) containing 200 ppm iron with ad libitum access to food and water. All mouse breeding and animal experiments were approved by the Regierungspräsidium Karlsruhe (Projects Nr T-81/14, T-66/13, G-41/16, G-39/16).

2.2. Tissue Iron Quantification

Tissue non-heme iron content was measured using the bathophenanthroline method and calculated against dry weight tissue (Torrance and Bothwell, 1968).

2.3. RNA Extraction, Reverse Transcription and qRT-PCR

Total lung RNA was isolated using Trizol (Life technologies) and was reverse transcribed and used in SYBR-green qPCR, as described in (Altamura et al., 2010). mRNA expression was calculated relative to RPL19 and data were analyzed using the ΔΔCt method (Livak and Schmittgen, 2001). The primers used are listed in Supplementary Information.

2.4. Western Blotting

Protein lysates were obtained by homogenizing snap-frozen tissues in RIPA buffer supplemented with protease inhibitors (Roche Diagnostics), as described in (Galy et al., 2004). Protein concentration was determined using the DC protein assay (BioRad). 50 μg of protein were subjected to western-blot analysis with the antibodies listed in Supplementary Information. Western blot images were quantitatively acquired with the Vilber Lourmat Fusion-FX Chemiluminescence system (Eberhardzell). β-actin was used as loading control.

2.5. Lipid Peroxidation - TBARS Measurements

Thiobarbituric acid reactive substances (TBARS) levels were measured in samples of total lung from 36-week old mice using the QuantiChrom TBARS Assay Kit (BioAssay Systems) following manufacturer's instructions.

2.6. Bronchoalveolar Lavage and Differential Cell Count

Mice were anesthetized via intraperitoneal injection of a combination of ketamine and xylazine (120 and 16 mg/kg respectively) and sacrificed by exsanguination. A median sternotomy was performed, the trachea cannulated and the left mainstem bronchus ligated, and the right lung was lavaged with Phosphate Buffered Saline (PBS). Bronchoalveolar lavage (BAL) samples were centrifuged and BAL fluid supernatant was harvested and stored at −80 °C. Total cell counts were determined using a haemocytometer and differential cell counts were determined in cytospin preparations stained with May–Grünwald–Giemsa (Merck).

2.7. Iron Quantification in the Bronchoalveolar Lavage Fluid Supernatant

BAL fluid supernatant was concentrated through Speed-Vacuum. Iron measurements were performed using the SFBC kit (Biolabor) following manufacturer's instructions.

2.8. Measurement of Cytokine Protein Levels in Bronchoalveolar Lavage

Cytokine protein levels (IL6, IL1β and TNFα) were determined in BAL fluid supernatants applying Multiplex bead-array based technology. Measurements were performed on a BioPlex200 System using the Bio-Plex Pro Cytokine Reagent Kit and Bio-Plex Pro Mouse Cytokine sets (Bio-Rad) according to manufacturer's instructions. Cytokine protein levels are given as picograms in total BAL fluid supernatant.

2.9. Lung Function Measurements

Mice were anesthetized via intraperitoneal injection of Na^+-pentobarbital (80 mg/kg), tracheostomized and placed on the FlexiVent system (SCIREQ, Montreal, QC, Canada) for measurements of pulmonary function. Mice were then paralyzed with pancuronium bromide injected intraperitoneally (0.8 mg/kg) to avoid breathing artefacts during the measurement. Mice were ventilated at a frequency of 150 breaths/min, with a tidal volume of 11 mL/kg and a positive end expiratory pressure of 3 cm H_2O to prevent alveolar collapse. Pressure-volume curves, total lung capacity, pulmonary compliance and elastance were measured as previously described in (Mall et al., 2008) and (Vanoirbeek et al., 2010). All perturbations were performed until at least three acceptable measurements were reached.

2.10. Blood Oxygen Saturation

Oxygen saturation was determined using a noninvasive pulse oximeter for laboratory animals (MouseOx® Plus, Starr life science) following manufacturer's instructions. Arterial blood oxygen saturation was analyzed in conscious mice exposed to room air with a thigh clip sensor. The oxygen saturation was measured when pulse waves were stable and regular in order to obtain valid values.

2.11. Stereology of Lung Tissue

Lungs from 36 week old mice were instilled via the trachea with 1.5% paraformaldehyde, 1.5% glutaraldehyde in 0.15 M Hepes buffer at hydrostatic pressure of 25 cm and stored in the same solution at 4 °C until further processing. The lungs were embedded in glycol methacrylate according to standard protocol (Muhlfeld et al., 2013) and 1.5 μm thick sections were cut. Light microscopy was performed using a Leica DM6000B microscope (Leica, Wetzlar, Germany) attached to a computer with the newCAST stereology software (Visiopharm, Horsholm, Denmark). Design-based stereology was used to quantify the volume of the lung parenchyma and non-parenchyma as described in (Muhlfeld et al., 2013).

2.12. Erythropoietin (Epo) Measurements

Plasma Epo levels were determined using a mouse Epo ELISA kit (R&D systems) following manufacturer's instructions.

2.13. Isolation and Differentiation of Bone Marrow Derived Macrophages (BMDM)

Bone marrow cells were flushed from tibia and femur using ice-cold Hank's balanced salt solution (HBSS) and filtered through a 70 μm cell strainer (BD biosciences). Cells were seeded at a density of 350,000 cells/cm^2 in RPMI1640-Glutamax medium (Life Technologies) supplemented with 10% of heat-inactivated fetal bovine serum (Hyclone, Thermo scientific), 1% Penicillin/streptomycin (Gibco) and 10 ng/mL M-CSF (Peprotech). After 4 days, non-adherent cells were removed by HBSS washing and the medium was replaced daily until cell harvesting (6 days after seeding). Before harvesting, BMDM were treated overnight with 75 μM of iron-nitrilotriacetate (FeNTA).

2.14. Immunohistochemistry and Immunocytochemistry

Lungs were inflated with 4% neutral buffered formalin (Fischar) to 25 cm of fixative pressure, fixed overnight by immersion in the same solution, dehydrated and paraffin embedded. Lungs were sectioned at 1.5 or 5 μm and mounted on Superfrost Plus slides (ThermoFisher scientific). Lung sections were rehydrated and treated for 10 min with 3% H_2O_2 (Sigma Aldrich) to block endogenous peroxidases. After washing in distilled water, tissue slides were subjected to microwave-mediated antigen retrieval using the Citraplus reagent (Biogenex). After 30 min of cooling, slides were washed 3 times in PBS and subjected to immunorecognition using Vectastain ABC mouse and rabbit kits (Vector Lab, Burlingame, CA, USA) following manufacturer's instructions. BAL cells in cytopsin preparations were fixed in cold acetone (−20 °C) for 10 min, washed in PBS and treated for 10 min with 3% H_2O_2 (Sigma Aldrich) to block endogenous peroxidases. After washing in PBS, cytospin slides were subjected to immunorecognition using the Vectastain ABC rabbit kit (Vector Lab, Burlingame, CA, USA) following manufacturer's instructions. Antibody dilutions and catalog numbers are reported in Supplementary information. Isotype antibodies were used at the same concentration as the primary antibodies to control for antibody specificity. Slides were developed using the Vector AEC substrate (Vector lab), rinsed with distilled water, counterstained with Hematoxylin, washed in PBS and mounted using the VectaMount AQ mounting medium (Vector lab). Images were digitally acquired with a Nikon Ni-E microscope (Nikon Center of the University of Heidelberg), using the Nikon NIS-Elements software. Splenic cells in cytospin preparations were subjected to the same protocol as BAL cells in cytospin preparations and used as a positive control for FPN immunocytochemistry.

2.15. DAB-enhanced Perls' Stain

Lungs were inflated with 4% neutral buffered formalin (Fischar) to 25 cm of fixative pressure, fixed overnight by immersion in the same solution, dehydrated and paraffin embedded. Lungs were sectioned at 1.5 or 5 μm and mounted on Superfrost Plus slides (ThermoFisher scientific). Lung sections were rehydrated and stained for 10 min with a potassium ferrocyanide/HCl solution (Sigma Aldrich). After washing in distilled water, slides were treated with 3,3-diaminobenzidinetetrahydrochloride (DAB) (Sigma Aldrich). Slides were washed again in distilled water, counterstained with Hematoxylin, washed in PBS, dehydrated and mounted using the Eukitt quick-hardening mounting medium (Sigma Aldrich).

2.16. Perls' Stain

BAL cells in cytopsin preparations were stained with potassium ferrocyanide/HCl solution (Sigma Aldrich), washed in distilled water and counterstained with Fast Red (Sigma Aldrich). Images were digitally acquired with a Nikon Ni-E microscope, using the Nikon NIS-Elements Viewer software.

2.17. Hematoxylin and Eosin Stain

Paraffin lung sections were rehydrated and stained for 6 min with Mayer's Hematoxylin (Sigma Aldrich). Slides were washed in water, rinsed in HCl/EtOH, washed again in water and stained for 1 min with Eosin Y (Sigma Aldrich). Slides were dehydrated and mounted using the Entellan new mounting medium (Merck).

2.18. Masson Goldner Trichrome Stain

Paraffin lung sections were rehydrated and stained with Masson Goldner Trichrome Staining Kit (Carl Roth) following manufacturer's instructions.

2.19. Analysis of Lung Collagen Content

Paraffin lung sections (3 μm) were stained with 0.1% Sirius red solution as previously described (Kosanovic et al., 2011). The degree of fibrosis was calculated by the analysis of the total amount of collagen in the left lung (Leica Microsystem, Wetzlar, Germany). For evaluation of the percentage of collagen, the collagen positive areas (red fibers) were determined in a minimum of 300 images per animal.

2.20. Flow Cytometry Analysis

Cells obtained from BAL were stained with CD45.2, CD11c and SiglecF antibodies for 30 min on ice (antibody dilutions and catalog numbers are reported in Supplementary information). To measure oxidative stress, BAL cells and BMDM were incubated for 30 min at RT with 5 μM CellROX Green reagent (ThermoFisher). After washing, cells were analyzed by flow cytometry using the BD LSRFortessa Cell Analyzer.

2.21. Statistical Analyses

Data are shown as mean ± SEM. Statistical analyses were performed using Prism v6 (GraphPad Software, La Jolla, CA). Two-tailed, Student's *t*-test was used and *p*-values < 0.05 (*), <0.01 (**), <0.001 (***) and <0.0001 (****) are indicated.

3. Results

3.1. Iron Levels are Increased in the Lung of Slc40a1^{C326S} Mice

Slc40a1^{C326S} mice, a disease model of HH type 4, is hallmarked by increased systemic iron levels, iron deposition in parenchymal tissues and iron depletion in iron exporting organs (Altamura et al., 2014). We now analyzed lung tissue of male and female heterozygous Slc40a1$^{wt/C326S}$ and homozygous Slc40a1$^{C326S/C326S}$ mice and demonstrate that iron accumulates in an age- and genotype-dependent manner (Fig. 1A).

Under physiological conditions, elevated cellular iron levels inactivate the iron-responsive element/iron-regulatory protein (IRE/IRP) system. This causes degradation of the transcripts encoding for the iron importers divalent metal transporter 1 (DMT1) and transferrin receptor 1 (TfR1) and allows for the translation of the iron storage protein ferritin light chain (FtL) and ferritin heavy chain (FtH) as well as for the iron exporter FPN (Anderson et al., 2012; Muckenthaler et al., 2008). Accordingly, mRNA and protein expression of TfR1 and mRNA expression of the IRE-containing transcript of DMT1 are decreased in iron loaded lungs of Slc40a1$^{wt/C326S}$ and Slc40a1$^{C326S/C326S}$ mice (Fig. 1B, C, D), while FtL protein expression is increased (Fig. 1D). Furthermore, FPN expression shows a genotype-specific increase both at mRNA and protein levels (Fig. 1D, E).

Excess of iron generates reactive oxygen species (ROS) that will damage proteins, lipids and DNA (Altamura and Muckenthaler, 2009; Papanikolaou and Pantopoulos, 2005). Consistently, increased pulmonary iron levels in Slc40a1$^{C326S/C326S}$ mice correlate with increased

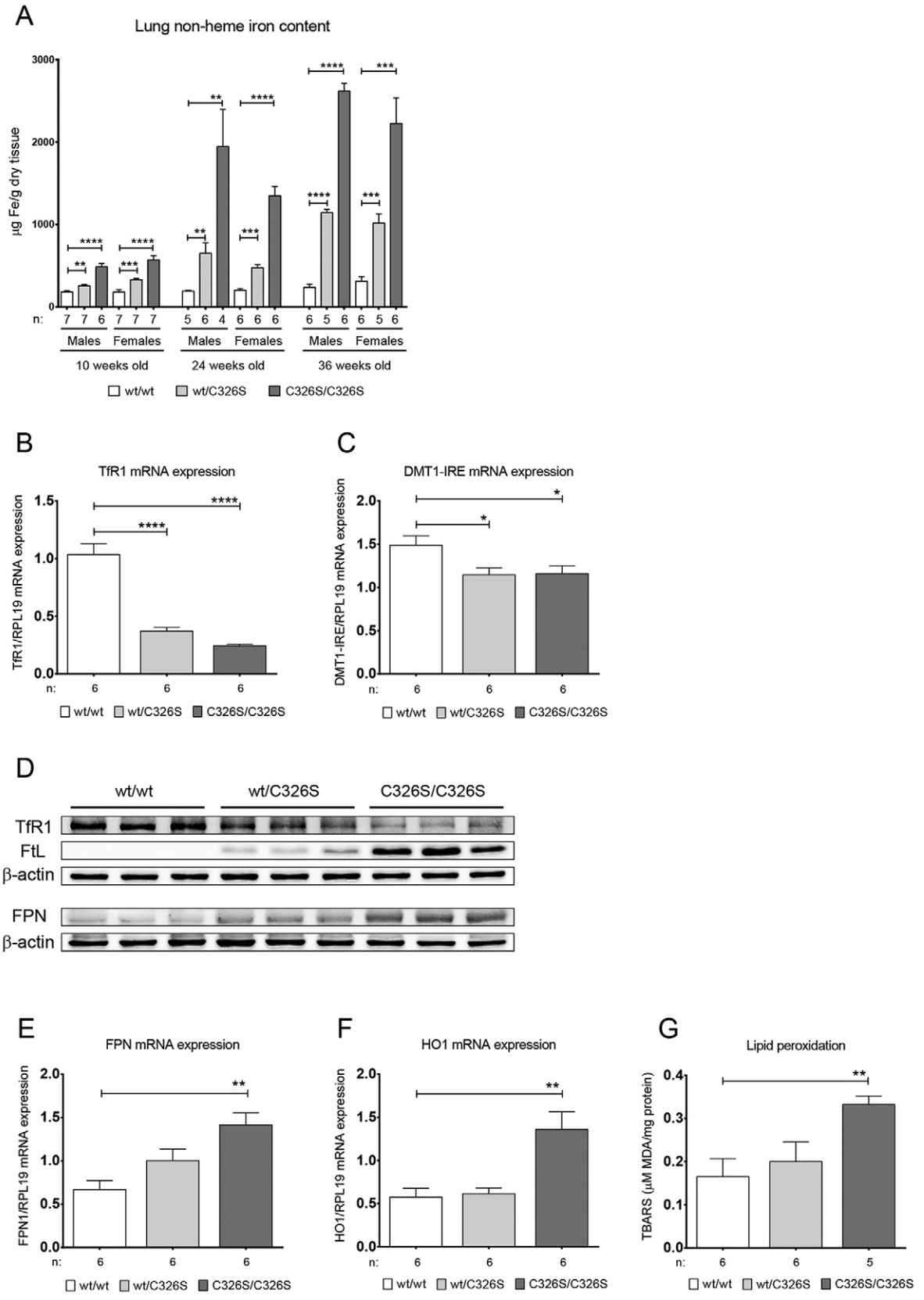

Fig. 1. Slc40a1^{C326S} mice show increased pulmonary iron content. A) Total lung non-heme iron levels measured in male and female 10-, 24- and 36-week old mice. B) qRT-PCR analysis of TfR1 mRNA expression in total lung of female 36-week old mice. C) qRT-PCR analysis of DMT1-IRE mRNA expression in total lung of female 36-week old mice. D) Western Blot analysis of TfR1, FtL and FPN protein expression in total lung of female 36-week old mice. β-actin was used as loading control. E) qRT-PCR analysis of FPN mRNA expression in total lung of female 36-week old mice. F) qRT-PCR analysis of HO1 mRNA expression in total lung of female 36-week old mice. G) Lipid peroxidation measured by the TBARS assay in total lung of female 36-week old mice.

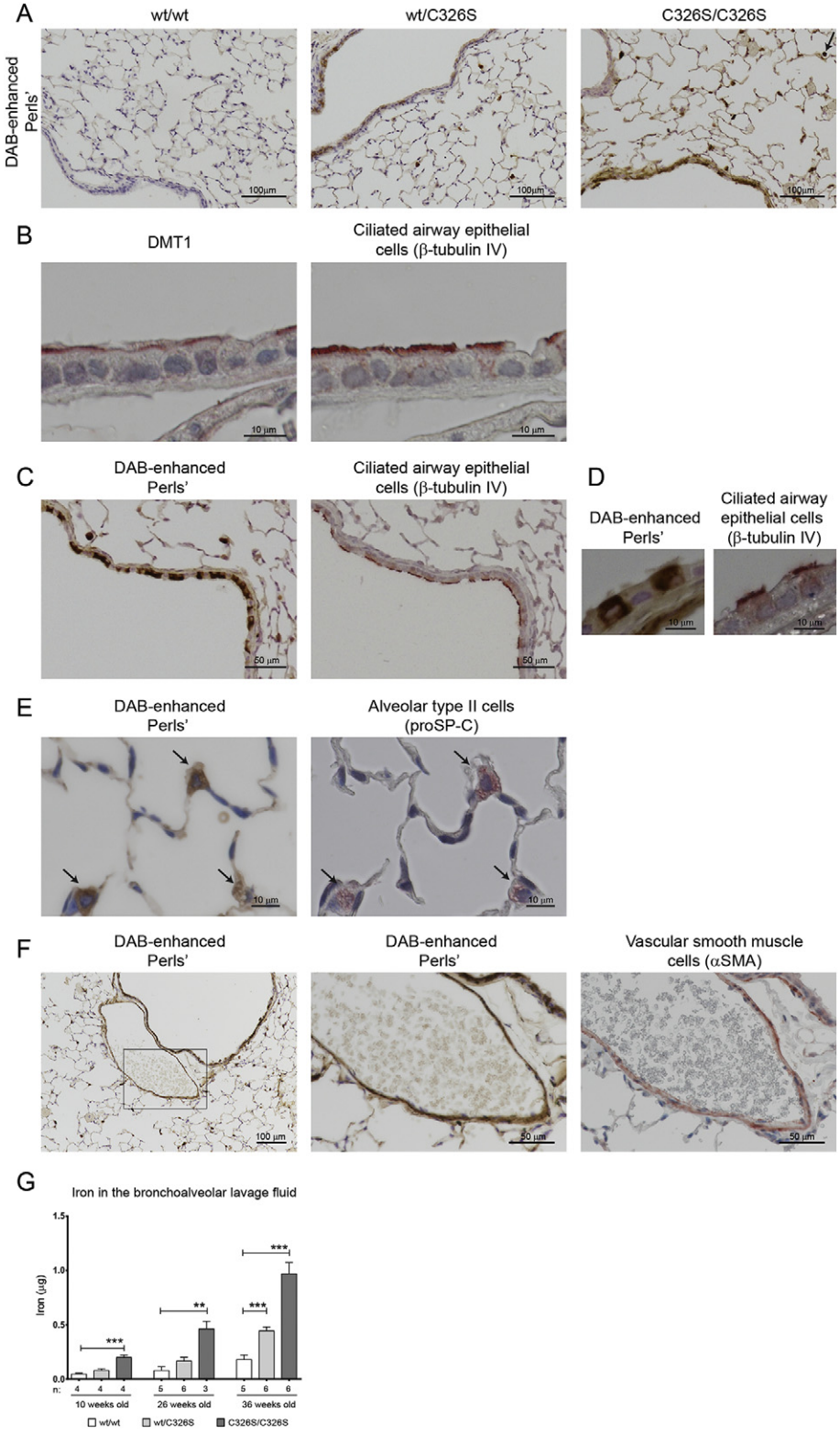

Fig. 2. Iron accumulation in the lung of Slc40a1$^{C326S/C326S}$ mice is restricted to specific cell types. A) DAB-enhanced Perls' staining of lung sections of female 36-week old mice. Arrow shows an alveolar macrophage with strong iron accumulation. B) Immunohistochemistry for DMT1 (left) and β-tubulin IV (right) of consecutive lung sections from wild-type female 36-week old mice. C) DAB-enhanced Perls' staining (left) and immunohistochemistry for β-tubulin IV (right) of consecutive lung sections from Slc40a1$^{C326S/C326S}$ female 26-week old mice. D) Higher magnification of DAB-enhanced Perls' staining (left) and immunohistochemistry for β-tubulin IV (right) of consecutive lung sections from Slc40a1$^{C326S/C326S}$ female 26-week old mice. E) DAB-enhanced Perls' staining (right) and immunohistochemistry against prosurfactant protein C (proSP-C) (left) of consecutive lung sections from Slc40a1$^{C326S/C326S}$ female 36-week old mice. Arrows indicate alveolar type II cells. F) DAB-enhanced Perls' staining (left and center) and immunohistochemistry for alpha smooth muscle actin (αSMA) (right) of consecutive lung sections from Slc40a1$^{C326S/C326S}$ female 36-week old mice. G) Iron levels measured in the bronchoalveolar lavage (BAL) fluid supernatant of 10-, 26- and 36-week old mice.

heme oxygenase 1 (HO-1) mRNA expression, a marker for oxidative stress (Fig. 1F), and with elevated lipid peroxidation (Fig. 1G).

Collectively, our results show that the disruption of the hepcidin/FPN regulatory axis causes iron overload and oxidative stress in the lung.

3.2. Iron Accumulates in Specific Pulmonary Cell Types in Slc40a1^{C326S} Mice

Histological analysis of the lung of Slc40a1^{C326S} mice confirmed the iron overload phenotype and revealed that iron deposition is restricted to specific cell types (Fig. 2A).

Previous reports suggested that airway epithelial cells acquire iron from the airway lumen via DMT1 (Ghio, 2009). In wild-type mice, we detected DMT1 mainly at the apical membrane of ciliated airway epithelial cells (Fig. 2B). In line with this observation, iron was commonly detected in ciliated epithelial cells lining the conducting airways of Slc40a1$^{C326S/C326S}$ mice (Fig. 2C and D). In addition, iron was detected in a subset of another pulmonary epithelial cell type - alveolar type II cells, which line the gas exchanging distal airspaces and produce surfactant proteins such as prosurfactant protein C (Fig. 2E).

Furthermore, vascular smooth muscle cells (SMC) characterized by expression of alpha smooth muscle actin stain for iron (Fig. 2F). Interestingly, vascular SMCs are heterogeneous in regard to iron loading, whereby some show iron overload while others are iron-spared (Fig. S1A). This observation implies that the lung contains at least two populations of vascular SMCs that are hallmarked by differential iron trafficking. Future studies will have to determine whether different populations of vascular SMCs in terms of iron handling may reflect upon their role in maintaining appropriate blood pressure under physiological and/or pathophysiological conditions.

Importantly, increased iron levels were also detected in the bronchoalveolar lavage (BAL) fluid of Slc40a1^{C326S} mice (Fig. 2G).

3.3. Alveolar Macrophages Accumulate Iron in Slc40a1$^{C326S/C326S}$ Mice

Iron accumulation in alveolar macrophages (AM) is a hallmark of certain lung diseases (Ghio et al., 2013; Philippot et al., 2014). Analysis of histological sections of Slc40a1$^{C326S/C326S}$ mice revealed severe iron accumulation in AM (Fig. 2A arrow). We next analyzed the cellular fraction of the BAL by differential May-Grünwald-Giemsa stain and showed that AM were the predominant cell type in the BAL fluid of wild-type and Slc40a1$^{C326S/C326S}$ mice (Fig. 3A, Fig. 3B). Interestingly, the total number of cells in the BAL fluid of Slc40a1$^{C326S/C326S}$ mice was increased, which is explained by an increase in AM (Fig. 3B), a finding confirmed by flow cytometry (Fig. 3C) (Misharin et al., 2013). In both wild-type and Slc40a1$^{C326S/C326S}$ mice, >90% of the immune cells in the BAL fluid correspond to AM (CD45.2^{+} CD11c^{+} SiglecF^{+}) (Fig. 3D). Perls' staining of cytospin preparations revealed severe iron overload in AM of Slc40a1$^{C326S/C326S}$ mice (Fig. 3E). This iron retention phenotype distinguishes AM from hepatic Kupffer cells or splenic reticuloendothelial macrophages in Slc40a1$^{C326S/C326S}$ mice, which are iron depleted (Altamura et al., 2014). It is of note that in the same cell preparations of Slc40a1$^{C326S/C326S}$ mice we also detected iron spared AM (Fig. 3E, arrow), indicating that the population of AM in Slc40a1$^{C326S/C326S}$ mice is heterogeneous regarding iron handling. A heterogeneity in iron accumulation in AM of Slc40a1$^{C326S/C326S}$ mice is possibly explained by a differential expression of FPN (Fig. 3F).

We previously showed that macrophage iron overload results in oxidative stress, which triggers a pro-inflammatory status (Vinchi et al., 2016). We next investigated the degree of oxidative stress in AM as well as the pulmonary inflammatory status in Slc40a1$^{C326S/C326S}$ mice. By applying the CellROX green as ROS reporter, we failed to detect differences in oxidative stress in AM between wild-type and Slc40a1$^{C326S/C326S}$ mice (Fig. S2A). A lack of oxidative stress in iron-loaded AM may be explained by an adaptation to chronic iron accumulation. By contrast, acute iron treatment of bone marrow derived macrophages (BMDM) triggers the formation of oxidative radicals (Fig. S2A). Despite increased numbers of AM in Slc40a1$^{C326S/C326S}$ mice (Fig. 3B), and consistent with a lack of oxidative stress in AM, we failed to detect differences in mRNA and protein levels of inflammatory cytokines (IL1β, IL6 and TNFα) in total lung or in the BAL supernatant, respectively (Fig. S2B, S2C). These observations indicate that increased pulmonary iron levels did not cause pulmonary inflammation in Slc40a1$^{C326S/C326S}$ mice.

3.4. Slc40a1$^{C326S/C326S}$ Mice Show Restrictive Lung Disease and Decreased Blood Oxygen Saturation

Although no differences in lung structure were observed by histological analysis (Fig. S3A-D), we next investigated whether Slc40a1$^{C326S/C326S}$ mice show alterations in lung function. Functional measurements in 36-week old Slc40a1$^{C326S/C326S}$ mice revealed classical signs of restrictive lung disease, such as decreased total lung capacity and decreased lung compliance (Fig. 4A, B). Consistently, Slc40a1$^{C326S/C326S}$ mice show increased pulmonary elastance, thus revealing elevated lung rigidity (Fig. 4C). This observation was confirmed by exposing the mice to fixed air pressures (Flexivent) as shown in the pressure-volume curve (Fig. 4D). We excluded the possibility that the observed differences between wild-type and Slc40a1$^{C326S/C326S}$ mice were due to differences in body size. Despite the fact that aged Slc40a1$^{C326S/C326S}$ mice present with lower body weight most likely due to exocrine pancreatic failure (Altamura et al., 2014), the tibia length, a marker for body size, is comparable to age-matched wild-type mice (Fig. S4A). Furthermore, we detected a decrease in total lung capacity already in 26-week old Slc40a1$^{C326S/C326S}$ mice, which at this age still don't show differences in body weight as well as tibia length (Figs. S4, S5). Stereological analysis of the lung shows that the volume of the lung parenchyma is reduced in Slc40a1$^{C326S/C326S}$ mice, without alterations in the volume of the lung non-parenchyma (Fig. 4E, F). These observations indicate that the decrease in total lung capacity of Slc40a1$^{C326S/C326S}$ mice results from a reduction in the volume of the lung parenchyma.

A major function of the lung is to provide optimal diffusion conditions for efficient oxygen exchange between the atmosphere and the blood stream. Aged Slc40a1$^{C326S/C326S}$ mice show a marked reduction in blood oxygen saturation when compared to wild-type mice (Fig. 4G). Systemic hypoxia is mainly sensed by the kidney which responds by producing the erythroid growth factor, erythropoietin (Epo). Consistent with decreased oxygen saturation, plasma Epo levels are increased in Slc40a1$^{C326S/C326S}$ mice (Fig. 4 H). Increased levels of circulating Epo stimulate erythropoiesis in the bone marrow to restore sufficient oxygen delivery to every cell in the organism. In line with these findings, we observed higher levels of red blood cells, hemoglobin and hematocrit in Slc40a1$^{C326S/C326S}$ mice (Table S1) (Altamura et al., 2014).

4. Discussion

Respiratory diseases are frequently associated with alterations in pulmonary iron homeostasis (Ghio, 2009). Patients with acute respiratory distress syndrome, pulmonary alveolar proteinosis, cystic fibrosis and COPD show higher levels of iron in the lung when compared to healthy individuals (Ghio et al., 2003; Ghio et al., 2012; Ghio et al., 2008; Philippot et al., 2014). So far, the mechanism(s) leading to pulmonary iron accumulation and the role of iron in the development of lung diseases remain unexplored.

Here, we show that the genetic disruption of the regulatory system maintaining systemic iron homeostasis causes age-dependent and genotype-specific pulmonary iron accumulation, increased lipid peroxidation, and gene responses consistent with pulmonary iron overload and oxidative stress; TfR1 and DMT1-IRE expression is decreased and FtL and FPN levels are increased. Elevated FPN protein levels likely result from a combination of transcriptional responses, derepression of FPN

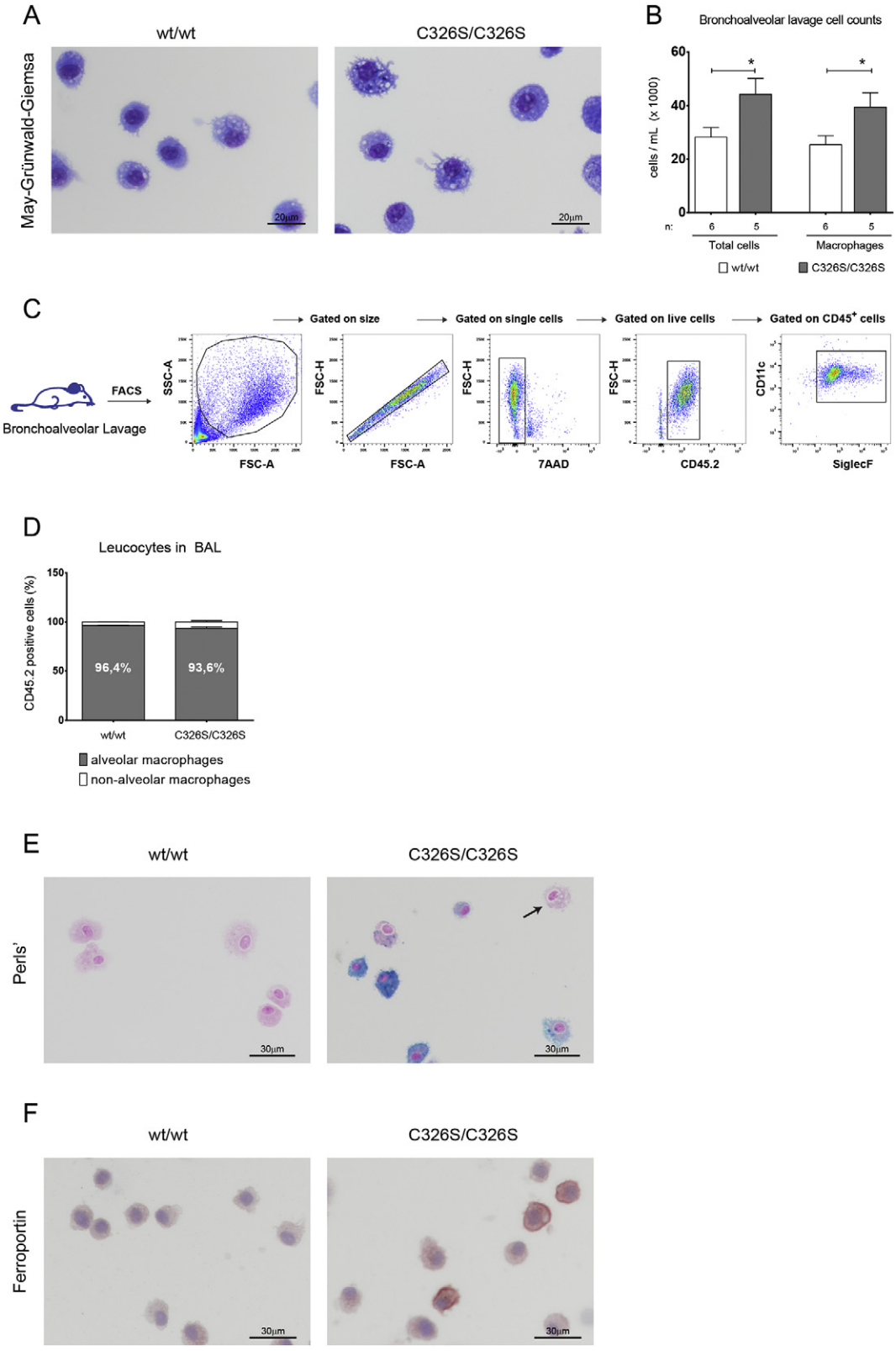

Fig. 3. Alveolar macrophages in Slc40a1$^{C326S/C326S}$ mice show iron deposition. A) May-Grünwald-Giemsa of cytospin preparations of AM obtained from the BAL of male 26-week old mice. B) Total cell count and AM cell count of the BAL fluid of male 26-week old mice. C) Gating strategy used to identify the cells present in the BAL fluid of wild-type and Slc40a1$^{C326S/C326S}$ mice by FACS analysis. D) Percentage of AM (CD11c^{+} SiglecF^{+}) present in the leukocyte fraction (CD45.2^{+}) in the BAL fluid of male 24-week old mice. E) Perls' stain of cytospin preparations of cells isolated from the BAL fluid of male 24-week old mice. Arrow points to an iron spared AM. F) Immunocytochemistry for ferroportin in cytospin preparations of cells isolated from the BAL fluid of male 24-week old mice.

translation via the IRE/IRP system and the hepcidin-resistant phenotype that post-translationally stabilizes the FPN protein (Altamura et al., 2014; Anderson et al., 2012).

Our finding that increased systemic iron levels result in iron accumulation in the lung is supported by a previous study in which intraperitoneal injection of iron-saccharate increased iron levels in the lung

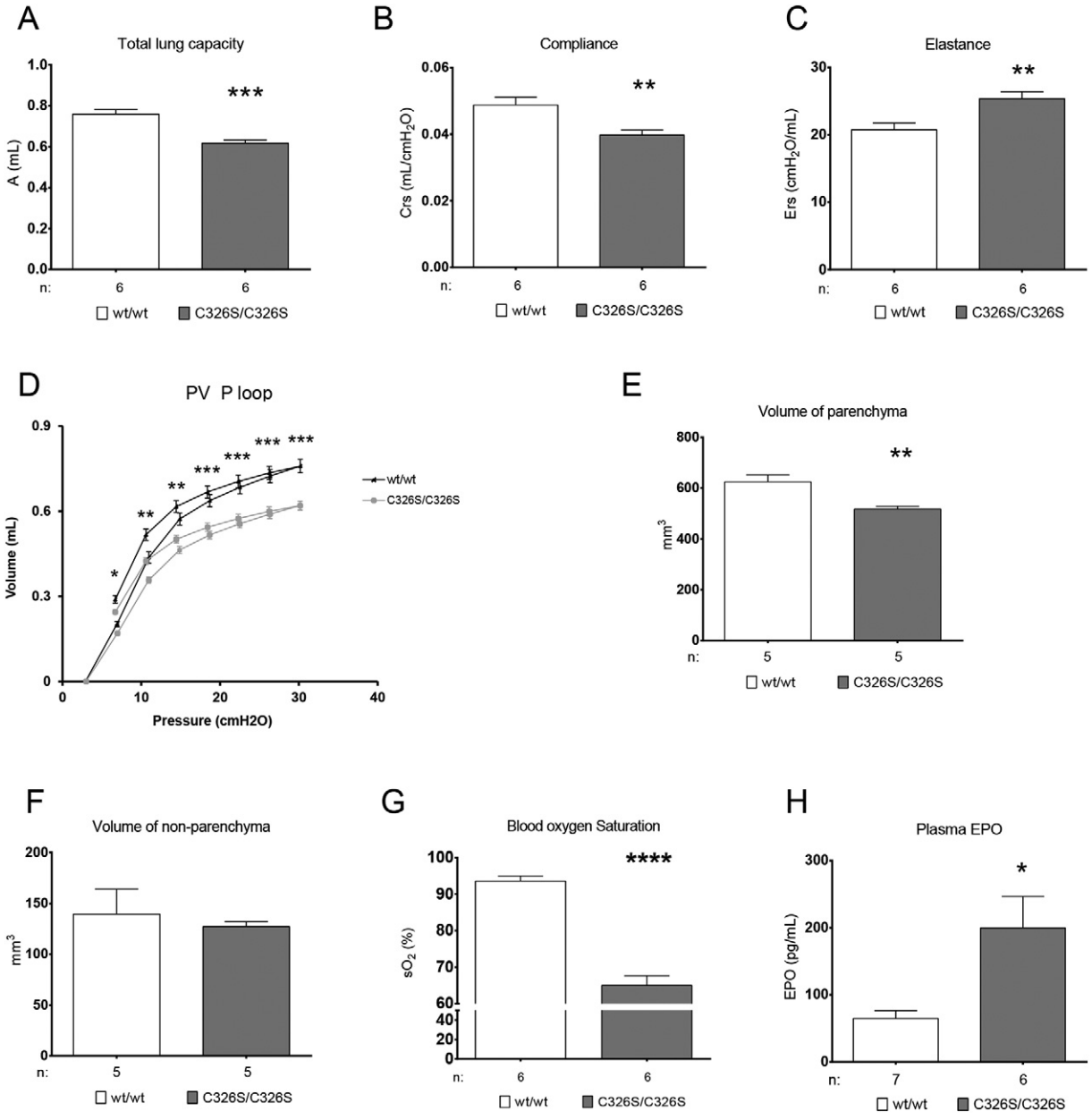

Fig. 4. Impaired lung function and reduced blood oxygen saturation hallmark Slc40a1$^{C326S/C326S}$ mice. (A–D) Lung function measurements performed in female 36-week old mice. A) Total Lung Capacity; B) Dynamic Compliance; C) Elastance; D) Pressure-Volume (PV) curve with controlled pressure applied. E) Volume of lung parenchyma measured in female 36-week old mice. F) Volume of lung non-parenchyma measured in female 36-week old mice. G) Blood oxygen saturation measured in female 36-week old mice. H) Epo levels measured in the plasma of female 36-week old mice.

(Giorgi et al., 2015). While in this study, iron accumulated predominantly in AM, we demonstrate that in addition ciliated airway epithelial cells, alveolar type II cells and vascular SMCs can load iron in Slc40a1$^{C326S/C326S}$ mice. The differences observed in these two mouse models of iron overload may be explained by an acute versus chronic iron overload, by different iron sources or possible local consequences of the disrupted FPN/hepcidin system.

We further show that iron accumulation in Slc40a1$^{C326S/C326S}$ mice does not trigger pulmonary inflammation. However, the availability of free iron in the lung may determine the outcome of pulmonary infections (Khiroya and Turner, 2015). For example, increased pulmonary iron levels are related to the persistence of *Pseudomonas aeruginosa* infection in cystic fibrosis patients (Reid et al., 2007). Moreover, during *Pseudomonas aeruginosa* infection, the murine host up-regulates the expression of proteins involved in iron-sequestration (Damron et al., 2016), highlighting the known competition for iron between the host and the pathogen. Since there is a general increase in pulmonary iron levels in Slc40a1$^{C326S/C326S}$ mice, and in particular in extracellular iron in the bronchoalveolar space, we hypothesize that Slc40a1$^{C326S/C326S}$ mice may have an increased susceptibility to bacterial lung infections. However, this concept needs to be tested experimentally in future studies.

Slc40a1$^{C326S/C326S}$ mice present classical signs of restrictive lung disease, with a decrease in total lung capacity and compliance and an increase in pulmonary elastance. A restrictive pattern is commonly associated with pulmonary fibrosis but collagen deposition in the lung of Slc40a1$^{C326S/C326S}$ mice is not significantly increased and therefore cannot explain the strong phenotype. Rodriguez-Capote and colleagues showed that the presence of ROS and the oxidation of surfactant phospholipids and proteins can alter surfactant function (Rodriguez-Capote et al., 2006). It is thus possible that the presence of extracellular iron in the bronchoalveolar space of Slc40a1$^{C326S/C326S}$ mice may affect

surfactant activity, surface tension and lung compliance. However, the mechanism(s) causing the restrictive pattern in Slc40a1$^{C326S/C326S}$ mice still remain to be elucidated.

It is of note that restrictive lung disease is the predominant pulmonary dysfunction in patients with thalassemia major (Carnelli et al., 2003; Guidotti et al., 2016; Kanj et al., 2000). Due to ineffective erythropoiesis and blood transfusion requirements, these patients present with increased systemic iron levels and parenchymal iron overload. We therefore speculate that the pulmonary restrictive pattern in thalassemia major patients may be a consequence of increased systemic iron levels and/or lung iron deposition (Carnelli et al., 2003; Kanj et al., 2000; Parakh et al., 2007).

Slc40a1$^{C326S/C326S}$ mice show a strong decrease in blood oxygen saturation, despite the absence of observable structural changes in the lung. This finding can be caused by 1) a substantial ventilation/perfusion (V/Q) mismatch, 2) a shunt flow of the blood in Slc40a1$^{C326S/C326S}$ mice or 3) by a low cardiac output. With regard to the first hypothesis, the iron deposition observed in a subset of alveolar type II cells may lead to regional impairment of surfactant production, which may in turn cause a partial collapse of gas exchanging units resulting in ventilation/perfusion mismatch and hypoxemia. Second, a shunting of unoxygenated blood across the heart or the lungs might be caused by abnormal iron deposition in vascular smooth muscle cells leading to the respective vascular dysfunction/abnormalities. Third, low cardiac output could also contribute to such a phenotype by causing low venous O_2 and finally low arterial O_2 saturation. Future studies will be necessary to address these possibilities.

The decrease in blood oxygen saturation correlates with increased plasma EPO levels in Slc40a1$^{C326S/C326S}$ mice. Hypoxia is the main physiological inducer of EPO production in the kidney via the hypoxia inducible factor HIF2α/HIF1β heterodimer (Haase, 2010). In Slc40a1$^{C326S/C326S}$ mice iron may also directly increase HIF-2α mRNA translation by inhibiting the binding of IRPs to its 5′ UTR (Sanchez et al., 2007). Increased plasma levels of EPO stimulate erythropoiesis in the bone marrow. Consistently, we detected high levels of red blood cells, hemoglobin and hematocrit in Slc40a1$^{C326S/C326S}$ mice.

We cannot exclude that pathophysiological consequences of iron overload in Slc40a1$^{C326S/C326S}$ mice other than in the lung may contribute to our observations. The restrictive pattern and decreased blood oxygen saturation may be caused by a combination of high iron levels in the lung as well as other impairments triggered by an increase in systemic iron levels and organ iron deposition (Altamura et al., 2014). To date, there is no evidence of lung pathology in human patients with HH type 4. However, this may reflect upon the fact that patients identified with the FPN C326S point mutation were heterozygous (Sham et al., 2005) and clinical iron overload has been controlled by phlebotomy.

Taken together, our results show that a disruption in the hepcidin/FPN regulatory system leads to an age-dependent pulmonary iron deposition in specific lung cell types. Homozygous Slc40a1$^{C326S/C326S}$ mice show restrictive lung disease and decreased blood oxygen saturation. These observations implicate iron in lung pathology, which so far is not considered a classical iron-related disorder. Moreover, we speculate that an impaired lung function may contribute to the premature death observed in Slc40a1$^{C326S/C326S}$ mice (Altamura et al., 2014).

Funding Sources

This work was supported by research funding from the Dietmar Hopp Stiftung (23011208) (M.U.M.), the German Federal Ministry of Education and Research 82DZL00401 and 82DZL004A1 (M.U.M. and M.A.M), the DFG via the Cluster of Excellence REBIRTH (C.M.), BREATH (C.M.), by a fellowship from Fundação para a Ciência e a Tecnologia, Portugal (SFRH/BD/51702/2011) (J.N.) and by the Deutsche Forschungsgemeinschaft SFB1118 (S.A. and M.U.M.).

Conflict of Interest

The authors declare no conflict of interest.

Author Contributions

J.N. designed the project, performed experiments and wrote the manuscript; D.L. performed the blood oxygen saturation measurements and provided expertise in measurements of lung function; S.K. and N.W. provided expertise in lung physiology and performed analysis of lung collagen content; C.B. and C.M. performed the stereological analysis of the lung; R.A. provided expertise in measurements of lung function and bronchoalveolar lavage analysis; M.A.M. designed and supervised the project; S.A. designed and supervised the project, performed experiments and wrote the manuscript; M.U.M. designed and supervised the project and wrote the manuscript.

Acknowledgements

We thank the EMBL Flow Cytometry facility, in particular Malte Paulsen and Diana Ordonez, for technical assistance. We are grateful to Prof. Dr. Ursula Klingmüller and Dr. Katharina Robichon for support in the Luminex experiment. We thank the personal of the animal facility of the Heidelberg University for the mouse housing and care and the Nikon center at the University of Heidelberg for granting us access to their facility. We thank Katja Müdder for technical assistance.

Appendix A. Supplementary data

Supplementary data to this article can be found online at http://dx.doi.org/10.1016/j.ebiom.2017.04.036.

References

Altamura, S., Muckenthaler, M.U., 2009. Iron toxicity in diseases of aging: Alzheimer's disease, Parkinson's disease and atherosclerosis. J. Alzheimers Dis. 16:879–895. http://dx.doi.org/10.3233/JAD-2009-1010.

Altamura, S., D'Alessio, F., Selle, B., Muckenthaler, M.U., 2010. A novel TMPRSS6 mutation that prevents protease auto-activation causes IRIDA. Biochem. J. 431:363–371. http://dx.doi.org/10.1042/BJ20100668.

Altamura, S., Kessler, R., Grone, H.J., Gretz, N., Hentze, M.W., Galy, B., Muckenthaler, M.U., 2014. Resistance of ferroportin to hepcidin binding causes exocrine pancreatic failure and fatal iron overload. Cell Metab. 20:359–367. http://dx.doi.org/10.1016/j.cmet.2014.07.007.

Anderson, C.P., Shen, M., Eisenstein, R.S., Leibold, E.A., 2012. Mammalian iron metabolism and its control by iron regulatory proteins. Biochim. Biophys. Acta 1823:1468–1483. http://dx.doi.org/10.1016/j.bbamcr.2012.05.010.

Carnelli, V., D'Angelo, E., Pecchiari, M., Ligorio, M., D'Angelo, E., 2003. Pulmonary dysfunction in transfusion-dependent patients with thalassemia major. Am. J. Respir. Crit. Care Med. 168:180–184. http://dx.doi.org/10.1164/rccm.200211-1292OC.

Damron, F.H., Oglesby-Sherrouse, A.G., Wilks, A., Barbier, M., 2016. Dual-seq transcriptomics reveals the battle for iron during Pseudomonas aeruginosa acute murine pneumonia. Sci. Rep. 6:39172. http://dx.doi.org/10.1038/srep39172.

Galy, B., Ferring, D., Benesova, M., Benes, V., Hentze, M.W., 2004. Targeted mutagenesis of the murine IRP1 and IRP2 genes reveals context-dependent RNA processing differences in vivo. RNA 10:1019–1025. http://dx.doi.org/10.1261/rna.7220704.

Ghio, A.J., 2009. Disruption of iron homeostasis and lung disease. Biochim. Biophys. Acta 1790:731–739. http://dx.doi.org/10.1016/j.bbagen.2008.11.004.

Ghio, A.J., Carter, J.D., Richards, J.H., Brighton, L.E., Lay, J.C., Devlin, R.B., 1998. Disruption of normal iron homeostasis after bronchial instillation of an iron-containing particle. Am. J. Physiol. 274, L396–L403.

Ghio, A.J., Carter, J.D., Richards, J.H., Richer, L.D., Grissom, C.K., Elstad, M.R., 2003. Iron and iron-related proteins in the lower respiratory tract of patients with acute respiratory distress syndrome. Crit. Care Med. 31:395–400. http://dx.doi.org/10.1097/01.CCM.0000050284.35609.97.

Ghio, A.J., Stonehuerner, J.G., Richards, J.H., Crissman, K.M., Roggli, V.L., Piantadosi, C.A., Carraway, M.S., 2008. Iron homeostasis and oxidative stress in idiopathic pulmonary alveolar proteinosis: a case-control study. Respir. Res. 9:10. http://dx.doi.org/10.1186/1465-9921-9-10.

Ghio, A.J., Roggli, V.L., Soukup, J.M., Richards, J.H., Randell, S.H., Muhlebach, M.S., 2012. Iron accumulates in the lavage and explanted lungs of cystic fibrosis patients. J. Cyst. Fibros. 12:390–398. http://dx.doi.org/10.1016/j.jcf.2012.10.010.

Ghio, A.J., Roggli, V.L., Soukup, J.M., Richards, J.H., Randell, S.H., Muhlebach, M.S., 2013. Iron accumulates in the lavage and explanted lungs of cystic fibrosis patients. J. Cyst. Fibros. 12:390–398. http://dx.doi.org/10.1016/j.jcf.2012.10.010.

Giorgi, G., Danna, M.C., Roque, M.E., 2015. Iron homeostasis and its disruption in mouse lung in iron deficiency and overload. Exp. Physiol. http://dx.doi.org/10.1113/EP085166.

Guidotti, F., Piatti, G., Marcon, A., Cassinerio, E., Giuditta, M., Roghi, A., Fasano, V., Consonni, D., Cappellini, M.D., 2016. Pulmonary dysfunction in thalassaemia major: is there any relationship with body iron stores? Br. J. Haematol. http://dx.doi.org/10.1111/bjh.14396.

Haase, V.H., 2010. Hypoxic regulation of erythropoiesis and iron metabolism. Am. J. Physiol. Ren. Physiol. 299:F1–13. http://dx.doi.org/10.1152/ajprenal.00174.2010.

Kanj, N., Shamseddine, A., Gharzeddine, W., Kanj, M., Nasr, T.A., Koussa, S., Jibrail, J., Taher, A., 2000. Relation of ferritin levels to pulmonary function in patients with thalassemia major and the acute effects of transfusion. Eur. J. Haematol. 64:396–400. http://dx.doi.org/10.1034/j.1600-0609.2000.90106.x.

Khiroya, H., Turner, A.M., 2015. The role of iron in pulmonary pathology. Multidiscip. Respir. Med. 10:34. http://dx.doi.org/10.1186/s40248-015-0031-2.

Kosanovic, D., Kojonazarov, B., Luitel, H., Dahal, B.K., Sydykov, A., Cornitescu, T., Janssen, W., Brandes, R.P., Davie, N., Ghofrani, H.A., et al., 2011. Therapeutic efficacy of TBC3711 in monocrotaline-induced pulmonary hypertension. Respir. Res. 12:87. http://dx.doi.org/10.1186/1465-9921-12-87.

Livak, K.J., Schmittgen, T.D., 2001. Analysis of relative gene expression data using real-time quantitative PCR and the 2(-Delta Delta C(T)) method. Methods 25:402–408. http://dx.doi.org/10.1006/meth.2001.1262.

Mall, M.A., Harkema, J.R., Trojanek, J.B., Treis, D., Livraghi, A., Schubert, S., Zhou, Z., Kreda, S.M., Tilley, S.L., Hudson, E.J., et al., 2008. Development of chronic bronchitis and emphysema in beta-epithelial Na+ channel-overexpressing mice. Am. J. Respir. Crit. Care Med. 177:730–742. http://dx.doi.org/10.1164/rccm.200708-1233OC.

Misharin, A.V., Morales-Nebreda, L., Mutlu, G.M., Budinger, G.R., Perlman, H., 2013. Flow cytometric analysis of macrophages and dendritic cell subsets in the mouse lung. Am. J. Respir. Cell Mol. Biol. 49:503–510. http://dx.doi.org/10.1165/rcmb.2013-0086MA.

Muckenthaler, M.U., Galy, B., Hentze, M.W., 2008. Systemic iron homeostasis and the iron-responsive element/iron-regulatory protein (IRE/IRP) regulatory network. Annu. Rev. Nutr. 28:197–213. http://dx.doi.org/10.1146/annurev.nutr.28.061807.155521.

Muckenthaler, M.U., Rivella, S., Hentze, M.W., Galy, B., 2017. A red carpet for iron metabolism. Cell 168:344–361. http://dx.doi.org/10.1016/j.cell.2016.12.034.

Muhlfeld, C., Knudsen, L., Ochs, M., 2013. Stereology and morphometry of lung tissue. Methods Mol. Biol. 931:367–390. http://dx.doi.org/10.1007/978-1-62703-056-4_18.

Nemeth, E., Tuttle, M.S., Powelson, J., Vaughn, M.B., Donovan, A., Ward, D.M., Ganz, T., Kaplan, J., 2004. Hepcidin regulates cellular iron efflux by binding to ferroportin and inducing its internalization. Science 306:2090–2093. http://dx.doi.org/10.1126/science.1104742.

Papanikolaou, G., Pantopoulos, K., 2005. Iron metabolism and toxicity. Toxicol. Appl. Pharmacol. 202:199–211. http://dx.doi.org/10.1016/j.taap.2004.06.021.

Parakh, A., Dubey, A.P., Chowdhury, V., Sethi, G.R., Jain, S., Hira, H.S., 2007. Study of pulmonary function tests in thalassemic children. J. Pediatr. Hematol. Oncol. 29:151–155. http://dx.doi.org/10.1097/MPH.0b013e318033a73d.

Philippot, Q., Deslee, G., Adair-Kirk, T.L., Woods, J.C., Byers, D., Conradi, S., Dury, S., Perotin, J.M., Lebargy, F., Cassan, C., et al., 2014. Increased iron sequestration in alveolar macrophages in chronic obstructive pulmonary disease. PLoS One 9, e96285. http://dx.doi.org/10.1371/journal.pone.0096285.

Qiao, B., Sugianto, P., Fung, E., Del-Castillo-Rueda, A., Moran-Jimenez, M.J., Ganz, T., Nemeth, E., 2012. Hepcidin-induced endocytosis of ferroportin is dependent on ferroportin ubiquitination. Cell Metab. 15:918–924. http://dx.doi.org/10.1016/j.cmet.2012.03.018.

Reid, D.W., Carroll, V., O'May, C., Champion, A., Kirov, S.M., 2007. Increased airway iron as a potential factor in the persistence of Pseudomonas aeruginosa infection in cystic fibrosis. Eur. Respir. J. 30:286–292. http://dx.doi.org/10.1183/09031936.00154006.

Rodriguez-Capote, K., Manzanares, D., Haines, T., Possmayer, F., 2006. Reactive oxygen species inactivation of surfactant involves structural and functional alterations to surfactant proteins SP-B and SP-C. Biophys. J. 90:2808–2821. http://dx.doi.org/10.1529/biophysj.105.073106.

Sanchez, M., Galy, B., Muckenthaler, M.U., Hentze, M.W., 2007. Iron-regulatory proteins limit hypoxia-inducible factor-2alpha expression in iron deficiency. Nat. Struct. Mol. Biol. 14:420–426. http://dx.doi.org/10.1038/nsmb1222.

Sham, R.L., Phatak, P.D., West, C., Lee, P., Andrews, C., Beutler, E., 2005. Autosomal dominant hereditary hemochromatosis associated with a novel ferroportin mutation and unique clinical features. Blood Cells Mol. Dis. 34:157–161. http://dx.doi.org/10.1016/j.bcmd.2004.12.002.

Sham, R.L., Phatak, P.D., Nemeth, E., Ganz, T., 2009. Hereditary hemochromatosis due to resistance to hepcidin: high hepcidin concentrations in a family with C326S ferroportin mutation. Blood 114:493–494. http://dx.doi.org/10.1182/blood-2009-04-216226.

Torrance, J.D., Bothwell, T.H., 1968. A simple technique for measuring storage iron concentrations in formalinised liver samples. South Afr. J. Med. Sci. 33, 9–11.

Vanoirbeek, J.A., Rinaldi, M., De Vooght, V., Haenen, S., Bobic, S., Gayan-Ramirez, G., Hoet, P.H., Verbeken, E., Decramer, M., Nemery, B., et al., 2010. Noninvasive and invasive pulmonary function in mouse models of obstructive and restrictive respiratory diseases. Am. J. Respir. Cell Mol. Biol. 42:96–104. http://dx.doi.org/10.1165/rcmb.2008-0487OC.

Vinchi, F., Costa da Silva, M., Ingoglia, G., Petrillo, S., Brinkman, N., Zuercher, A., Cerwenka, A., Tolosano, E., Muckenthaler, M.U., 2016. Hemopexin therapy reverts heme-induced proinflammatory phenotypic switching of macrophages in a mouse model of sickle cell disease. Blood 127:473–486. http://dx.doi.org/10.1182/blood-2015-08-663245.

Wang, X., Ghio, A.J., Yang, F., Dolan, K.G., Garrick, M.D., Piantadosi, C.A., 2002. Iron uptake and Nramp2/DMT1/DCT1 in human bronchial epithelial cells. Am. J. Phys. Lung Cell. Mol. Phys. 282:L987–L995. http://dx.doi.org/10.1152/ajplung.00253.2001.